INFORMATION TO USERS

This manuscript has been reproduced from the microfilm master. UMI films the text directly from the original or copy submitted. Thus, some thesis and dissertation copies are in typewriter face, while others may be from any type of computer printer.

The quality of this reproduction is dependent upon the quality of the copy submitted. Broken or indistinct print, colored or poor quality illustrations and photographs, print bleedthrough, substandard margins, and improper alignment can adversely affect reproduction.

In the unlikely event that the author did not send UMI a complete manuscript and there are missing pages, these will be noted. Also, if unauthorized copyright material had to be removed, a note will indicate the deletion.

Oversize materials (e.g., maps, drawings, charts) are reproduced by sectioning the original, beginning at the upper left-hand corner and continuing from left to right in equal sections with small overlaps. Each original is also photographed in one exposure and is included in reduced form at the back of the book.

Photographs included in the original manuscript have been reproduced xerographically in this copy. Higher quality 6" x 9" black and white photographic prints are available for any photographs or illustrations appearing in this copy for an additional charge. Contact UMI directly to order.

UMI

RICE UNIVERSITY

CHARACTERIZATION OF ALUMINA MEMBRANES DERIVED
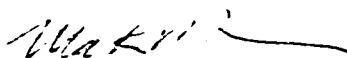FROM ALUMOXANES

by

DIANE AMY BAILEY

A THESIS SUBMITTED
IN PARTIAL FULFILLMENT OF THE
REQUIREMENTS FOR THE DEGREE
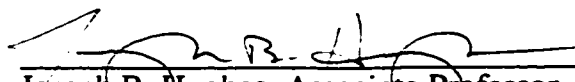MASTER OF SCIENCE

APPROVED, THESIS COMMITTEE

Mark R. Wiesner, Professor, Chair
Department of Environmental Science and
Engineering

Matthew P. Fraser, Assistant Professor
Department of Environmental Science and
Engineering

Joseph B. Hughes, Associate Professor
Department of Environmental Science and
Engineering

Houston, Texas

August, 1998

UMI Number: 1394213

UMI
300 North Zeeb Road
Ann Arbor, MI 48103

Acknowledgments

Abstract

Characterization of Alumina Membranes Derived from Alumoxanes

Diane A. Bailey

Alumoxane-derived membranes are characterized and compared with commercial anodized alumina and polycarbonate track-etched membranes. The alumoxane-derived membranes were produced using two different types of ligands, acetic acid and (methoxyethoxy)acetic acid, or mixes of the two to alter the membrane characteristics. Membranes were studied using scanning electron microscopy, atomic force microscopy, nitrogen adsorption-desorption, cleanwater flux experiments, goniometer measurements, and Zeta-meter measurements to determine membrane morphology, pore size distribution and shape, permeability, hydrophobicity, and surface charge. Alumoxane-derived membranes were found to have a nodular morphology with over 90 % of pores between 5 and 25 nm and permeability ranging from 0.3 to 1.5 nm^2. The two ligands used did not produce large differences in the overall characteristics of the membranes. Alumoxane-derived membranes exhibited similar permeabilities to the commercial membranes tested. Carboxylate-alumoxanes show considerable promise as precursors to membranes and other alumina products.

for this...

Table of Contents

List of Tables

List of Figures

List of Abbreviations

Abbreviations

A-H	Acetic acid
MA-H	Methoxyacetic acid
MEA-H	(Methoxyethoxy)acetic acid
MEEA-H	(Methoxyethoxy) ethoxy] acetic acid
AA	Acetic acid Alumoxane-derived (membrane)
MEAA	(Methoxyethoxy)acetic acid Alumoxane-derived (membrane)
AFM	Atomic Force Microscope
AWWA	American Water Works Association
BET	Brunnauer, Emmet, & Teller Method
BJH	Barret, Joyner, & Halenda Method
CVD	Chemical Vapor Deposition
EPA	Environmental Protection Agency
IUPAC	International Union of Pure and Applied Chemistry
MF	Micro-filtration
UF	Ultra-filtration
NF	Nano-filtration
RO	Reverse Osmosis
MGD	Million Gallons per Day
MWCO	Molecular Weight Cut-Off
PCTE	Polycarbonate Track-Etched Membrane
R	Alkyl Substituent
SEM	Scanning Electron Microscope

Chapter 1

Introduction

1.1.0   Significance of Research

The US Environmental Protection Agency is steadily expanding their scope from pollution abatement and control to include pollution prevention. Recently, the Green Chemistry Program was created to support research and development of novel engineering approaches to pollution prevention or reduction at the source, industrial manufacturing, and processing. The goal is to find alternative chemical pathways that involve less toxic feedstocks, reagents, or solvents and generate fewer toxic products, by-products, or co-products. A number of different processes may exist to manufacture a product, and traditionally the method yielding the best or cheapest product is chosen. These processes need to be re-evaluated on an environmental basis, accounting for external costs such as finite resource consumption, watershed degradation, and public health. Membrane filters are increasingly designed for pollution abatement. Some membranes are manufactured using energy intensive processes that also use strong acids or toxic solvents, particularly for ceramic membranes. Green Chemistry can be used to develop a manufacturing method for membranes that is less environmentally taxing. In this research, we have evaluated a recently developed "green chemistry" pathway for ceramic membrane fabrication and characterized the resulting prototype membrane materials.

1.1.1 Membranes

Membranes have been used commercially for the past half century and are now quite commonly used. They are capable of performing liquid, gas, and solid separations at microscopic levels on an industrial scale. They can replace certain conventional processes saving energy and costs, or concentrate and recover byproducts from wastestreams. Specialized membranes can desalt ocean water making it suitable for consumption, they can remove dyes and other toxic materials from wastewater preventing pollution of waterways, they can separate plasma from blood, they can remove bacteria from milk and other beverages during processing, and in the petrochemical industry they can be used to recover waste oils. The use of membranes in industry is steadily increasing as technology progresses and will play a large role in environmental abatement, such as wastewater treatment. Drinking water treatment is also employing membranes more and more as municipalities shift from groundwater sources to less pristine surface water.

1.1.2 Porous Ceramics

Ceramic materials have a long history of use as containers, from ancient Etruscan cinerary urns to Delft fine china. Though the idea of porous ceramics seems somewhat foreign, the special circumstances of gaseous Uranium Isotope separation processes in the 1940's spurred use of ceramic membranes (Hsieh, 1996). Ceramic membranes can be made with similar separation characteristics to organic polymer membranes, and have some operational advantages. Porous ceramics are typically much more heat-, pH-, and chemical-resistant than are their polymeric counterparts. Alpha-alumina, for example, can withstand temperatures of up to 900 °C and pHs from 0 to 14 without being damaged, while membranes from other types of material may deform, melt, or crack under extreme conditions. The porosity and pore size of ceramics can be controlled by the starting material used, type of processing, and firing time. Because of these special properties,

porous ceramics are commonly used as electronic substrates, catalysts, adsorbents, and also as membranes.

1.2.0   Objectives of Research

The purpose of the following research is to evaluate alumina membranes formed from an environmentally benign process. This new aqueous-based process is less energy intensive than processes currently used to make similar membranes. It also avoids the use of hazardous substances during ceramic processing. The alumoxane-derived membranes formed from this process have potentially valuable and unique characteristics. A detailed analysis of the alumoxane-derived membranes follows, focusing on several key objectives:

- Determination of whether alumoxanes make viable precursors to ultra-filtration membranes;

- Characterization of alumoxane based membranes by pore size and porosity, morphology, hydrophobicity; and permeability;

- Evaluation and comparison of the effects of different alumoxane chemical pathways on membranes; and

- Comparison of alumoxane-derived membranes to other membranes made of similar materials and having similar separation characteristics.

Chapter 2

Literature Review

2.1.0   Membranes

2.1.1   History & Cost

References to filtration processes extend as far back as ancient Chinese and Egyptian civilizations (Cuperus & Smolders, 1991). The French physicist, Nollet, is credited with the discovery of osmosis in 1748, when he observed water diffusing through a pig bladder membrane into alcohol. Over one hundred years later, in 1867, the German chemist, Traube, performed the first filtration experiments using artificial membranes (Conlon, Water Quality and Treatment). Synthetic membranes, however, did not become widely used until the middle part of this century, with the introduction of asymmetric membranes by Loeb and Sourirajan (Loeb, 1981). By the late 1960's, a substantial membrane industry had evolved, and continues to show rapid growth (Hsieh, 1996).

Thus, membranes are relatively recent alternatives to conventional separations including distillation, adsorption, centrifugation, and chemical treatments. The worldwide market for membranes more than quadrupled from $1 billion in 1986 to over $4 billion in 1996 (Hsieh, 1996). Cost is the largest factor in the decision to incorporate membranes, and was originally quite high. However, in the last twenty years membrane costs have decreased considerably. Wiesner *et al.* (1994) compared the cost of ultrafiltration and

nanofiltration membrane treatment to conventional treatment using data from pilot studies of three different potable water sources, and concluded that at that time membranes were cost effective for potable water treatment facilities at least as large as 5 million gallons per day (MGD). More recent experience indicates that membranes are likely to be cost effective options for facilities up to at least 30 MGD. Studies have also shown that membranes can save considerable amounts of energy, a fact that may be of greater importance if energy costs increase in the future. For example, membranes replacing distillation for difficult organic separations, such as olefins, have been shown to save 84 percent in energy costs per year (Hsieh, 1996).

In addition to costs, membranes may provide other advantages over conventional technologies. Membrane modules operate in considerably less space than conventional systems, a significant consideration in urban areas where land is scarce. Also, the modular design of membrane systems permits easy expansion of facilities, allowing utilities to increase capacity incrementally instead of incurring a single "upfront" capital investment. (Dykes & Conlon, 1989).

3.1.2 Membrane Classifications

Membranes can be categorized both by driving force and size of materials separated (Table 2.1).

Table 2.1: Membrane Types (Adapted from Osmonics)

Separation Process	Driving Force (kPa)	Size Range of Removal Capability	Examples of Materials Removed
Microfiltration	Pressure Difference (30 - 300)	0.05 - 0.45 μm	Bacteria, Asbestos
Ultrafiltration	Pressure Difference (50 - 700)	2.5 - 150 nm	Viruses, Carbon Black
Nanofiltration	Pressure Difference (350 - 1000)	8 - 80 Å	Divalent Ions, Pesticides & Herbicides
Reverse Osmosis	Pressure Difference (800 - 8000)	< 500 Molecular Weight	Monovalent Ions & Small Molecules

Microfiltration (MF) membranes have the largest pore size range of the four classifications in Table 2.1. Materials as small as a virus can be removed by ultrafiltration (UF) membranes, which have smaller pores than MF. Nanofiltration (NF) and Reverse Osmosis (RO) can remove molecular materials, and do not always have distinct pores. Separation occurs in large part by differential rates of diffusion. The applications of these membranes are discussed in the next section.

In addition, membranes can be further classified as either symmetric, meaning that the material is homogenous throughout, or asymmetric. In the later case, the membrane consists of a selective skin layer on a more porous support. Membranes can be made from a variety of materials, or mixtures of materials including polymers, ceramics, glass, and metal, depending upon the desired characteristics. They may also be classified on the basis of their geometry (Figure 2.1).
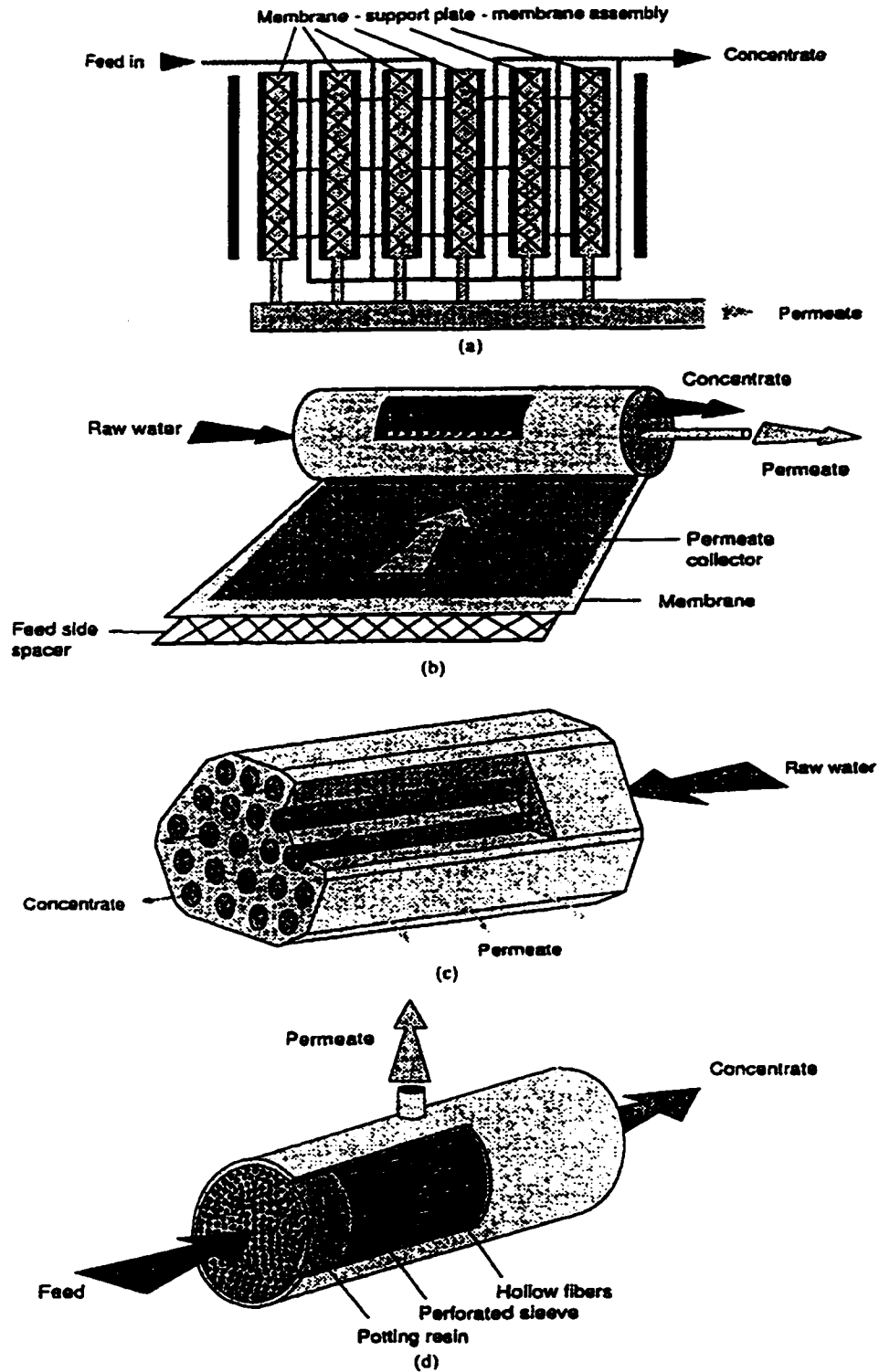
Figure 2.1: Membrane Module Geometries, a) plate and frame, b) spiral module, c) tubular module, d) hollow fiber. (Adapted from Mallevialle *et al.*, 1996)

2.1.3 Applications

There is a wide variety of applications for membrane processes. Table 2.2 lists typical uses for these membranes, which range from drinking water treatment applications to catalyst recovery in petroleum refining operations.

Table 2.2: Applications for different types of Membranes

Membrane Type	Industry	Example of Use
RO	Drinking Water	Desalination of Seawater
RO	Textile	Removal of Dyes from waste water
RO / UF	Pulp & Paper	Treatment of "Black Liquor"
NF	Drinking Water	Removal of Hardness, Treatment of Brackish water, & Nitrate removal
UF	Industrial Waste	Concentration of Oily Waste
UF	Automotive	Recovery of Electrodeposition Paints
UF	Petroleum	Solvent Recovery from Deasphalted Oil
UF	Food & Beverage	Concentration of Skim milk for Production of Cheese & other Dairy
MF / UF	Biotechnology	Clarification of Fermentation Broth in Production of Antibiotics
MF / UF	Semiconductor	Production of Ultrapure Water & Purification of Process Fluids
MF / UF	Petroleum	Catalyst Recovery from Converted Oil
MF	Biomedical	Separation of Blood into Plasma & Cellular Fractions
MF	Food & Beverage	Wine Stabilization & Purification (replacing heat pasteurization)
MF (Ceramics)	Industrial Waste	Separation of Organic Solvents from Water & Treatment of Produced Water from Oil Wells

Membranes have been employed in water treatment plants in areas with brackish water or seawater intrusion problems, namely Florida and California for some 20 years. Dykes and Conlon (1989) have extensively studied the use of RO, NF, and UF in water treatment plants in Florida, and report that membrane plants can be cost effective. The San Jose Water Company in California recently replaced their diatomaceous earth filtration system with MF and is successfully producing high quality water (Gere, 1997). In 1989, more than 4,000 RO plants were operating around the world to produce over one billion gallons per day of drinking water. Although fewer than 30 UF and MF plants existed in 1989, use of these membranes in potable water treatment has increased significantly due to decreasing costs and more stringent regulations on water quality (AWWA, 1992).

Membranes have been used extensively for desalination, softening, removal of organics, and liquid-solid separations. In addition, they have allowed for the use of secondary water sources, some of which are brackish and lower in quality. Trihalomethane precursor control is a concern in drinking water treatment plants that can also be addressed with membranes. Taylor *et al.* (1987) have reported that RO and NF are effective in removing trihalomethane precursors. Coagulation pretreatment before membrane filtration has also been evaluated as a means of removing organic materials and increasing the effectiveness of the membranes (Lahoussine-Turcaud *et al.*, 1990).

Membranes play a significant role in water reclamation. Freeman and Morin (1995) reviewed six different water reuse projects at different stages of completion, all incorporating reverse osmosis. One facility had recently started reclaiming municipal effluent for reuse as irrigation water in San Pasqual, California and is modeled after a long established and well known water reclamation plant in Orange County, Water Factory 21. A second facility in Vero Beach, Florida, has been successfully reclaiming 0.2 million gallons per day (MGD) of municipal effluent for reuse as boiler feed water at a power plant for several years. Mexico City is currently designing a facility to reclaim secondary effluent for specialized agricultural efforts to reforest the region. Livermore, California has been successfully reclaiming water from municipal effluent since the late 1950's for use at a golf course, airport, and highway median strips, as well as for fire water. The city has also pilot tested a new RO facility with MF pretreatment for more irrigation and possibly groundwater recharge. Scottsdale, Arizona is also piloting membranes for a project that will reclaim 40 MGD of municipal effluent for irrigation and ground water recharge. The final case study of Freeman and Morin's review is Chandler, Arizona, which is planning to re-process as drinking water industrial effluent from a semi-conductor chip making facility after underground storage in an aquifer.

One notable water reclamation success has occurred in a tiny border town in Texas. The city of Harlingen added a Reverse Osmosis unit to their domestic wastewater treatment

plant and now supplies a neighboring textile plant with clean process water (Filteau, 1995). The treatment plant is now expanding and will treat the effluent from the textile mill using UF and RO, recycling an extra 2 MGD of dyewastewater along with the 2 MGD of domestic wastewater. Treatment of dye wastewater is not at all uncommon using membranes; RO or Hyperfiltration along with various pretreatments including MF and UF has been researched extensively (Porter & Porter, 1995; Porter & Zhuang, 1996; Buckley, 1992; Porter & Goodman, 1984; Brandon *et al.*, 1981 and Treffry-Goatley *et al.*, 1983).

2.1.4 Chemistry

The focus of this research is the characterization of ceramic ultrafiltration membranes. Ultrafiltration uses pressure to drive fluid through a membrane leaving behind particulates, colloids, and large macromolecules. The separation is largely physical, although chemical phenomena may play a role as well. The surface charge of the membrane, the charge of the species in the fluid to be filtered, the amount of material deposited on the membrane surface, the orientation of the membrane with respect to the flow, the pH, and the temperature all have an impact on ultrafiltration. In some cases the chemical nature and composition of the surface of a membrane may play a role in the performance of the membrane, and can be modified to suit specific waste streams to be filtered. This is particularly true for the case of membrane fouling. Roughly half of the commercial membranes sold today are modified with some type of ligand, enzyme, or catalytic group attached to the surface (Zeman & Zydney, 1996).

Surface charge is an important chemical characteristic of a membrane, closely related to its hydrophilicity (water loving characteristic) or hydrophobicity. Hydrophobic bonding such as may occur between natural organic material (NOM) in water and the surface of hydrophobic membranes can enhance the adsorption of NOM onto the surface and subsequently cause membrane fouling (Lahoussine-Turcaud, 1990). Most ceramic and

organic polymer UF membranes are negatively charged, with a tendency to be hydrophilic. Hydrophilic functional groups include hydroxyls, ethers, carboxyls, sulfonates, and amines, while aliphatic and aromatic hydrocarbon groups are hydrophobic (Zeman & Zydney, 1996). Laîné et al. (1989) found that relatively hydrophilic UF membranes performed much better than hydrophobic membranes for water treatment applications.

Lloyd & Meluch (1985) established an index for membrane material selection based on desired components for separation. Operating temperatures and pH are also important. Fluorocarbon, α-alumina, zirconia, and silver membranes are all capable of operating at pHs from 1 to 14, while the popular cellulose acetate membranes can only operate at pHs between 3 and 7. Industrial waste streams can be quite acidic, while water treatment plants may operate at pH values near 8. Nylon, polyphosphazene, glass, and alpha alumina membranes are capable of operating at temperatures up to 180, 200, 700, and over 900 °C respectively. In contrast, polyimide membranes can only operate at temperatures up to 40 °C, ambient for a very hot summer day. Cellulose acetate membranes are limited to temperatures below 50 °C, which is problematic for processes run under sterile conditions (Hsieh, 1996). Other factors that may be important in membrane material selection include mechanical strength, flammability, optical characteristics, surface roughness, and biological compatibility.

2.1.5 Kinetics & Flux

The capacity of a membrane is determined by its flow properties. Membranes exhibiting the highest flow per area, or flux, for a given pore size range are the most desirable. Darcy's law provides a suitable general description of the flux, J, of very clean water across a macroporous membrane (UF or MF) without any material deposition on the surface or within pores.

$$J = \frac{\Delta P}{\mu R_m} \qquad (1)$$

Where ΔP is the pressure drop across the membrane, μ is the viscosity of pure water, and R_m represents the resistance of the clean membrane. Since R_m is unknown, one can elaborate on Darcy's law by assuming that the membrane is made up of many cylindrical pores and applying Poiseuilles's law.

$$J = \frac{\varepsilon r_{pore}^2 \Delta P}{8 \mu \tau l} \qquad (2)$$

Where ε is surface porosity, r_{pore} is the average or effective pore radius, l represents the length of a pore or thickness of the membrane, and τ is tortuosity. Tortuosity is a factor that relates the actual liquid path through a membrane to the membrane thickness; it can be quite high for polymeric membranes with interconnected pores. Comparing equations (1) and (2), one should note that the resistance of a membrane, R_m, is proportional to $\tau l/\varepsilon r_{pore}^2$. Permeability, k, is also a useful quality for comparing membrane resistance.

$$k = \frac{\varepsilon r_{pore}^2}{8 \tau} \qquad (3)$$

$$J = \frac{k \Delta P}{\mu l} \qquad (4)$$

Thickness is not included in permeability, allowing for comparisons of porous media of different dimensions.

Evaluating the flux and permeability of a membrane can be done by directly measuring the volume of pure water that goes through a membrane of known surface area at a given time under a constant pressure, known as the pure water flux.

$$J = \frac{(Volume\ pure\ water)}{(Membrane\ area)(time)} \qquad (5)$$

Substituting the experimental flux from equation (5) into equation (4), one can calculate permeability, assuming that the pressure and viscosity are known. The pore length can be obtained by measuring the thickness of the membranes or skin layer thickness for symmetric and asymmetric membranes respectively. Equation (2) can be used to check the measured flux. This equation represents the maximum theoretical flux of a membrane, when the tortuosity equals one, indicating perfectly straight pores. The viscosity, length, and pressure are known and pore size and porosity can be measured independently.

Surface porosity and pore size have the largest effect on flux of all the parameters contained in the flux equations. These properties can vary considerably throughout a membrane surface. Fane et al. (1981) report that 50% of the flow passes through 20 - 25% of the pores for a typical UF membrane. Surface porosities and average pore sizes can be measured using Scanning Electron Microscopy (SEM) and the accompanying software, or a number of other techniques discussed in the next section.

Permeate flux is also highly affected by two external factors, concentration polarization and fouling. Concentration polarization is the phenomenon of accumulation of rejected materials near the surface of the membrane. It can increase the resistance to transport of water across the membrane, cause less soluble species to precipitate, and can increase adsorption of organic species on the membrane surface. A reduction of flux through a membrane is referred to as fouling. Fouling can be either reversible, that is

removable via chemical cleaning or backwashing, or irreversible (Wiesner & Chellam, 1992).

Fouling is currently the largest problem associated with the use of UF membranes in water treatment (Laîné et al., 1989). Lahoussine-Turcaud et al. (1990) showed that coagulation pretreatment can reduce short-term reversible fouling, but it does not reduce or slow irreversible fouling. A 1992 American Water Works Association (AWWA) research committee report called for research aimed at understanding processes controlling fouling and rejection in membranes (AWWA, 1992). Tarleton & Wakeman (1994), along with many other researchers since then, have conducted comprehensive reviews of membrane morphology and other factors in an effort to understand flux decline in membranes.

2.1.6 Morphology

The morphology of a membrane refers to the physical structure, including parameters such as membrane thickness, symmetry, and pore size, shape and interconnectivity. Morphology is usually related to the formation mechanism of a membrane (discussed in section 2.2.4) and is classified into four common types: Closed-cellular, open-cellular, lacy, and nodular. Closed-cellular pores are non-intersecting, clearly defined pores. Open-cellular pores are similar, but many of the pores have merged, creating a more open structure. A lacy structure is typical of certain polymers and lacks defined pores. Nodular morphology is a result of tightly packed grains with interstitial spaces acting as pores.

Membrane symmetry is also an important morphological feature. Skin layers are not always desirable. However, gradient anisotropic membranes usually have higher permeabilities and improved flux characteristics. These membranes require special manufacturing processes to create a narrow pore size on one side gradually tapering to a much wider pore size on the other side (Zeman & Zydney, 1996). Although membrane

morphology is important, morphological influence on flux is diminished as particles in the fluid to be filtered approach the pore size of the membrane (Tarleton & Wakeman, 1994).

2.1.7 Pore size, Pore size distribution, Porosity, & Surface area

Membranes may not have a single pore size, but more typically have pores sizes distributed over a range referred to as the pore size distribution. The pore size distribution affects the rate of flux through a membrane profoundly, since flux is proportional to the pore size raised to the fourth power. Single pore sizes reported for membranes are averages of the pore size distributions representing the hydraulic radius of the pores or the effective size above which a given fraction of larger materials will not pass through the membrane. Baltus (1997) illustrated different means of rating pore size by showing that one can distinguish between UF membranes with the same "average pore size" yet different hydraulic and diffusive permeabilities with different solutes. Additionally, the shape of pores and permeation effectiveness also play a large role in transport through a membrane. There are several ways to measure these parameters, related to either permeation (P) or morphology (M) (Table 2.3).

Nakao (1994) reviews methods for determining pore size and pore size distributions of membrane filters. A similar review was done by Kaneko (1994) for adsorbents and catalysts, and most of these methods are useful for inorganic membranes as well. Three size ranges are designated by IUPAC according to pore diameter:

Micropores	< 2 nm
Mesopores	2 nm - 50 nm
Macropores	> 50 nm

Table 2.3 Characterization Methods and Characteristic Parameters
(Adapted from Cuperus and Smolders, 1991)

Method	Characteristic	Remarks	M/P
Gas adsorption-desorption	Pore size distribution BET area	Dry samples	M
Electron Microscopy	Top layer thickness Surface porosity Pore size distribution Qualitative structure analysis	Surface (pore) analysis	M
Flux Measurements	Hydraulic pore radius Pure water flux		P
Rejection / Selective Permeation	Molecular Weight Cut-off value		P
Bubble pressure method Liquid displacement method	Pore size distribution	Active pores	P/M
Mercury Porosimetry	Pore size distribution	Dry samples, measurement of the pore entrance	M
Thermoporometry	Pore size distribution Pore shape	Wetted samples	M
Permporometry	Pore size distribution	Active pores	P/M

Pores can also be classified according to origin and structure. Intraparticle pores are contained within grains or particles of material, for example, inside a single crystal. Interparticle pores are formed as interstitial spaces between agglomerated or aggregated material. Pores are also classified according to accessibility to surroundings. Open pores communicate with the external surface of a membrane, while closed pores do not communicate continuously with the surface. Therefore, closed pores do not contribute to flux through a membrane. Pores are often categorized as being one of five shapes (Figure 2.2), cylindrical, conical, slit shaped, ink bottle, and interstitial. Small angle X-ray scattering and nuclear magnetic resonance imaging, as well as gas adsorption in some cases, can be used to determine pore geometry.
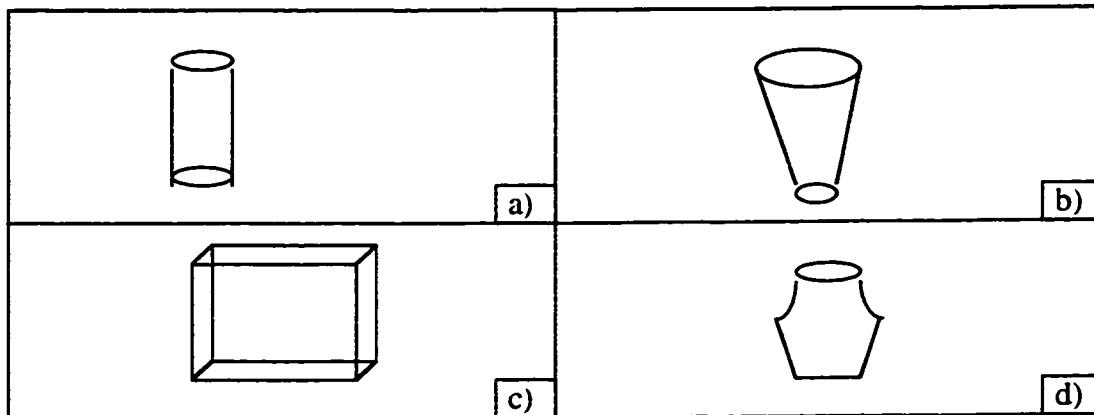
Figure 2.2: Types of Pore Shapes, a) cylindrical, b) conical, c) slit shaped, d) ink bottle

2.1.7.1 BET Theory

The pore size distribution of porous materials can often be determined from controlled adsorption experiments with an adsorbate of known dimensions. This approach is used in BET adsorption studies, typically using nitrogen gas. BET adsorption theory, named for Brunauer, Emmet, and Teller was developed in 1938. The theory assumes monolayer adsorption of gases close to their condensation point (Brunauer *et al.*, 1938). The volume of gas adsorbed into a solid is used to calculate the specific surface area. This method is commonly used to determine specific surface areas for adsorbents, catalysts, and membranes.

The following equation (6) represents the linear form of the BET equation (Hiemenz, 1986).

$$\left(\frac{1}{V_A}\cdot\frac{x}{1-x}\right)=\left(\frac{K-1}{KV_m}\right)\cdot(x)+\left(\frac{1}{KV_m}\right) \qquad \text{where } x=\frac{P_s}{P_o} \qquad (6)$$

Here x is the relative pressure and represents a ratio of the sample pressure (P_s), which is measured, to the saturation pressure (P_o), which is known. K is a constant related to the enthalpy of adsorption and is also known. V_A is the volume adsorbed, which is calculated using the following equation (7).

$$V_A = V_d - (P_s \cdot \text{slope} \cdot \text{intercept}) \qquad (7)$$

V_d is the volume of gas dosed, and the slope and intercept come from Helium measurements of the free space of the sample tube. Finally V_m , the monolayer volume, can be calculated using equation (6), and then used in equation (8) to find the BET surface area.

$$S_{BET} = \frac{V_m \cdot N_A \cdot A_m}{M_v} \qquad (8)$$

S_{BET} is the BET surface area, N_A is Avogadro's number, A_m is the cross sectional area occupied by each adsorbate molecule (commonly assumed to be 0.162 nm^2 for N_2), and M_v is the gram molecular volume (22.414 L) (Coulter SA 3100 User Manual).

2.1.7.2 Nitrogen Adsorption/Desorption

Gas adsorption/desorption is often used to determine pore size distribution in porous materials as well as specific surface area. Nitrogen is the gas most commonly used, however, carbon dioxide, oxygen, argon, and carbon monoxide are also used. Lord Kelvin described the thermodynamics of gas adsorption and desorption on curved surfaces in 1855. The resulting Kelvin equation (9) can easily be applied to small pores of a membrane to find the pore radius.

$$RT \ln\left(\frac{P_s}{P_o}\right) = -2\gamma \frac{V_M}{r_K} \qquad (9)$$

Here, R is the gas constant (8.316×10^7 erg/mole-K), T is the boiling point of the adsorbate

(77.3 K for N_2), γ is the adsorbate surface tension at T (8.855 mN/m or dyne/cm), V_M is

the molar volume (34.6 cm^3/mole for N_2), and r_K is the Kelvin radius.

The Kelvin radius accounts for the open space of the pores excluding the thickness

of the adsorbed monolayer of gas such as N_2. The modified Halsey equation (10) is

commonly used to estimate the adsorbed layer thickness,

$$t = 3.54\left[\frac{5}{\ln(P_o/P_s)}\right]^{\frac{1}{3}} \qquad (10)$$

where t is the adsorbed layer thickness in Angstroms. Finally, the total pore radius, r_p, is

the sum of this thickness and the Kelvin radius.

$$r_p = r_K + t \qquad (11)$$

Note that the total pore radius is a function of the log relative pressure. As the relative

pressure approaches one, accuracy of measurement diminishes; a relative pressure of 0.98,

for example, corresponds to a pore radius of 50 nm. The diameter of the adsorbate is the

lower bound of accuracy. A capillary as small as 16.2 angstroms, the size of a diatomic

nitrogen molecule, would constrict the nitrogen and give unreliable measurements (Gregg

and Sing, 1982).

During adsorption and desorption, the curvatures of the gas-liquid interface are

usually different, condensation and evaporation are not reversible. This produces a

hysteresis of the adsorption-desorption isotherm. The hysteresis curve, in turn, provides

insight to the pore structure, shape, and distribution of a sample (Cuperus and Smolders,

1991). Shortly after the BET method was published, Harkins & Jura (1944) created a

more extensive method for determining the surface area of a solid from adsorption/

desorption isotherms. Barret, Joyner and Halenda (1951) then used this method as a

subroutine in their own method for calculating pore size distribution, and it has become the

widely accepted method known as BJH. They applied a measure of mean pore size based

on the ratio of the total pore volume to the surface area:

$$\bar{d}_P = \frac{4000 \cdot V_P}{A_P} \qquad (12)$$

where mean pore diameter is given in units of nm, V_P is in units of ml/g, and A_P is in m^2/g.

Cranston and Inkley (1957) later developed an alternative to the BJH method,

though a slightly more cumbersome method for deriving pore size distribution from

sorption isotherms. They also identified which branch of the isotherm, adsorption or

desorption yields a more accurate pore size distribution for a range of materials, including

silica gels, silica aluminas, aluminas, and clays. The adsorption branch appears to be

considerably more reliable for most materials, excluding clays. Anderson *et al.* (1988)

compared pore size distributions from adsorption and desorption isotherms and concluded

that desorption curves overemphasize the narrow neck of pores yielding falsely narrow

pore size distributions.

Other methods of calculating pore size distribution have also been proposed.

Neimark (1986) developed a method using percolation theory to calculate pore size

distribution. Seaton (1991) extended this theory to determine the connectivity of porous

solids using percolation theory as well. Burgess *et al.* (1989) also performed an extensive

review of adsorption hysteresis, the factors affecting isotherms, and their proper

interpretation. Gregg and Sing (1982) provide a broad guide to gas adsorption/desorption for surface area and pore size distribution, and have identified various isotherm shapes and types as corresponding to characteristic pore structures.

2.1.8 AFM

Created by Binnig, Quate, and Gerber a little over a decade ago, AFM is a promising means of measuring submicron features of non-conducting surfaces. Samples do not have to be coated with metal and can be measured in liquid or air. AFM images provide detailed topological information on samples and can be processed through software calculating other information, such as grain size, roughness, fractal characteristics, and the size of specific features.

Atomic Force Microscopy uses a cantilever with a sharpened tip to trace the morphological features of a sample. The theory is based on the use of displacement of springs as a measurement of force. The sort of forces involved are on the order of 10^{-9} N and lower (Binnig et al., 1986). Imaging can be done in Tapping or Contact mode, depending on how sturdy samples are. The cantilever tip does not actually touch the sample in Tapping mode, which prevents damaging or altering a soft or fragile sample. The tip oscillates up and down as the sample is moved laterally beneath it. Light from a laser source is deflected off the cantilever and detected by a bi-segmented photodiode. The force on the tip is held constant by a feedback control loop. Changes in the amplitude of the tip displacement are recorded to produce a topographical image map of the sample (Dietz and Hansma, 1992, and Nanoscope® Command Reference Manual, 1995). Figure 2.3 shows a general schematic of an AFM.
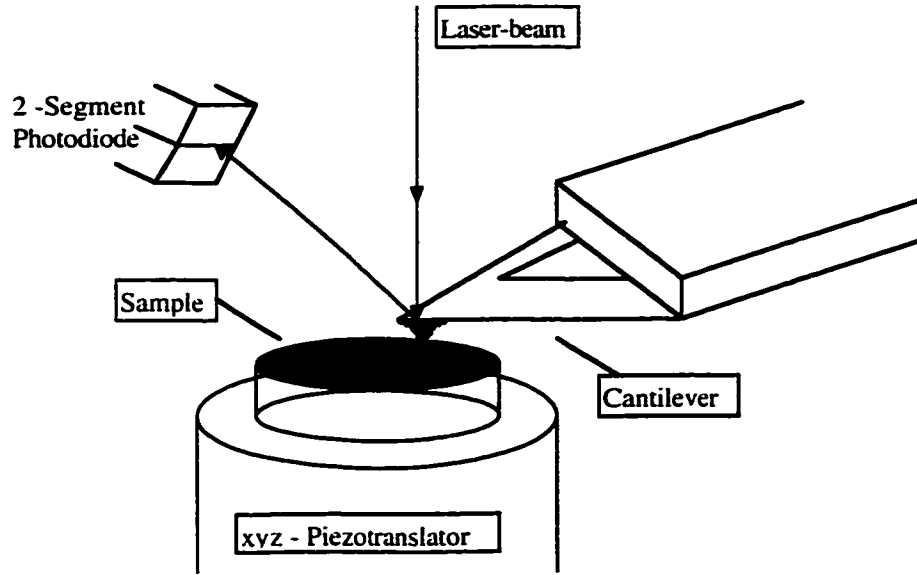
Figure 2.3: General Schematic of AFM

Surface roughness is a useful parameter in evaluating membrane performance.

Cuperus & Smolders (1991) suggest that there is a relation between surface roughness and

fouling of membranes. UF membranes are usually quite rough on a microscopic scale,

often having 'valley'-'hill' differences of 1 - 20 nm, with pores in the valleys. The

roughness not only increases surface area available for adsorption but may provide sites for

colloid deposition and stabilize concentration polarization. Surface roughness

measurements can vary significantly over sample size and location, but specific roughness

measurements from AFM are useful for general comparisons between membranes of

different types (Burger et al, 1994). A measure of average roughness is calculated using

the following equation,

$$R_a = \frac{1}{N}\sum_{i=0}^{N}|z_i - \bar{z}| \qquad (13)$$

where N is the total number of points in the image matrix and $\bar{z}$ is defined by the following equation,

$$\bar{z} = \frac{1}{N}\sum_{i=0}^{N} z_i \qquad (14)$$

where z_i is the height of the ith point over a reference value (Pradanos *et al.*, 1996).

AFM can be used to measure electrokinetic properties in addition to the often measured morphological parameters, such as surface pore size, porosity, and roughness. Larson *et al.* (1997) outlines conditions and measurement techniques for using AFM to find electrokinetic properties. Though AFM is an extremely useful tool in evaluating these characteristics, it should be used qualitatively in concert with other methods. AFM is susceptible to several artifacts discussed in detail by Gruetter *et al.* (1992) and Deckman & Plano (1993) among others.

2.1.9   Reported Membrane Characterizations

Cuperus and Smolders (1991) have done a broad survey of characterization techniques for UF membranes and key characteristics (Table 2.4).

Table 2.4: Characteristics of UF Membranes

Morphology Related Parameters	Performance Related Parameters
Pore Size (distribution)	(pure water) Flux
Pore Shape	Rejection of Solute
Tortuosity	Specific Affinity (for Adsorption)
Surface Porosity	Hydrophobicity
Top Layer Thickness	Charge Density
Surface Roughness	
Surface Area	

2.1.9.1 Membrane Permeability

Permeability can be measured using a liquid, such as water, or a gas. Permeability measurements with gas are usually necessary for membranes with small pores (< 10 nm). Lin and Burggraaf (1991) evaluated ceramic UF membranes using gas permeation techniques. Zaspalis *et al.* (1992) used helium and water permeability measurements to characterize two inorganic UF membranes and derived tortuosities for both as well. Munari *et al.* (1989) measured the permeate fluxes of a variety of liquids through polymeric UF membranes to calculate permeability. Sarrade *et al.* (1994) developed an analytical method based on theoretical models for UF and RO membranes to measure the permeability of two NF membranes. They also recalibrated the model to predict fluxes and rejection rates for NF membranes.

2.1.9.2 Pore Size Distribution, Porosity, and Molecular Weight Cut-off

Nitrogen gas adsorption/desorption appears to be the method of preference for measuring pore size distribution and porosity of ceramic membranes. Anderson et. al. used gas sorption in 1987 to examine the pore size distribution and mean pore size of titania and alumina ceramic membranes. Lin and Burggraaf (1991) used nitrogen sorption to characterize the effects of doping and sintering temperatures on the pore size distributions of alumina composite membranes. Zhang and Ying (1997) also used N_2 adsorption/desorption to measure the effects of niobium doping on the pore size distribution of silica UF membranes. Pradanos *et al.* (1996) successfully used gas sorption to measure the pore size distribution and BET surface area of Polycarbonate track-etched (PCTE) membranes, which are polymeric as opposed to ceramic membranes.

Nitrogen gas sorption is sometimes combined with mercury porosimetry to obtain pore size distribution and porosity. Mercury porosimetry forces mercury, a non-wetting liquid, through a porous sample measuring the pressure required to overcome interfacial

tension incrementally. Leenars *et al.* (1984) and Zaspalis *et al.* (1992) used nitrogen gas sorption and mercury porosimetry to obtain pore size distributions, mean pore sizes and porosities of ceramic UF membranes. Mercury porosimetry, along with Coulter porosimetry was also used by Rocek and Uchytil (1994) to evaluate and compare pore size distributions of ceramic membranes.

Molecular weight cut-off (MWCO) is commonly used to evaluate effective membrane "pore size." It involves measuring flux and rejection rates of various solutes of molecules, such as proteins, that have a known molecular weight. Measuring rejection rates of standard solutes, allows one to estimate a molecular weight cut-off representing the molecular weight of the smallest molecules a membrane can retain. An approximate effective pore size can be estimated from the molecular size of the critical solute at the MWCO. This information allows one to estimate which membranes are appropriate for use on various waste streams. MWCOs for polymeric UF membranes were evaluated by Capannelli *et al.* (1983) and Kim *et al.* (1994) and were also correlated to pore size distribution of the membranes.

Other common pore size characterization techniques include the bubble point method, thermoporometry, and permporometry. The bubble point technique is based on the pressure necessary to overcome capillary pressures in a porous membrane filled with liquid. Thermoporometry is based on microcalorimetric analysis of solid-liquid transformations in porous materials. Permporometry is similar to gas adsorption/desorption, but simultaneously measured flux through a sample with a second liquid or gas. Capannelli *et al.* (1983), Mikulasek and Dolecek (1994), and Jakobs and Koros (1997) used the bubble point or a modified bubble point method to evaluate pore size distributions. Permporometry and thermoporometry were used to measure pore size distribution by Munari *et al.* (1989), Kim *et al.* (1994), Bottino *et al.* (1994), and Xomeritakis *et al.* (1997). Other methods also exist for finding pore size distributions and

porosities; Dalvie and Baltus (1992) performed pressure drop and diffusion experiments to evaluate pore size distributions and porosities of anodized alumina membranes.

2.1.9.3 Microscopy

Atomic force microscopy (AFM) and electron microscopy typically yield information on morphological characteristics of membranes. Recently AFM has been used extensively to characterize membranes by pore size, surface porosity, and roughness. Dietz et. al. determined that AFM was a useful tool for evaluating MF and UF membranes in 1992. Pradanos et al. (1996) and Zeng et al. (1997) used AFM to analyze morphology, roughness, and pore size of Polycarbonate track-etched and composite ceramic UF membranes respectively. Bowen et al. (1996) studied Cyclopore and Anopore membranes extensively with AFM to determine the pore size distributions for each. Guldberg Pederson et al. (1997) used AFM to develop a model for describing the pore size of slip-cast ceramic membranes from measurements of the original particle size. All of these studies can be compared to other conventional characterization techniques as a means of corroborating existing information.

A comparison of AFM and scanning emission microscopy (SEM) imaging for ceramic MF and UF membranes was performed by Bottino et al. (1994). Both methods provide similar information, however, SEM requires samples to be thinly coated with a conducting material, such as gold. Since SEM has been a standard imaging method much longer than AFM, examples in the literature abound (Leenars et al., 1984; Anderson et al., 1988; Lin and Burggraaf, 1991; Dalvie and Baltus, 1992; Zeman and Denault, 1992; Sarrade et al., 1994). Field emission scanning electron microscopy (FESEM) is a newer variation of SEM that allows higher resolution (Kim and Stevens, 1997). Transmission electron microscopy (TEM) offers an even higher resolution down to 0.3 nm, but the field depth is much lower and samples require very tedious preparation. Both Leenars et al.

(1984) and Zhang & Ying (1997) have used TEM to obtain detailed crystal and structural information for inorganic membranes.

2.1.9.4 Surface Charge, Chemical, and Other Methods of Characterization

Surface charge and chemistry have a significant affect on membrane performance. Estimates of zeta potentials or surface charge can be obtained from measurements of electrophoretic mobility or streaming potential. Elimelech *et al.* (1994) estimated zeta potentials of cellulose acetate RO membranes with a streaming potential analyzer, and found that the surface charge of a membrane changes as it is fouled. Lee and Hong (1988) measured electroosmotic flow rates to determine that surface charge of MF membranes is highly dependent on pH and ionic strength, and Sidorova *et al.* (1993) and Nazzal and Wiesner (1994) found similar results. Koh and Anderson (1975) determined that surface charge effects are more important for smaller pore sizes.

Contact angle is usually used as an indicator of hydrophobicity or surface chemistry. Oldani and Schock (1989), Keurentjes *et al.* (1989), Gekas *et al.* (1992), and Zander *et al.* (1996) all used contact angle measurements successfully to compare hydrophobicities of different membranes. Impedance spectroscopy can also be used to characterize membrane surface chemistry (Coster *et al.*, 1992). Other common methods of membrane characterization include x-ray diffraction (XRD), infra-red spectroscopy (IRS), thermal gravimetric analysis (TGA), and nuclear magnetic resonance (NMR) imaging (Zhang and Ying, 1997).

2.2.0 Ceramic Membranes

2.2.1 History and Advantages

The use of organic membranes is much more wide-spread than the use of inorganic membranes. Inorganic membranes, however, have several advantageous characteristics. They are usually quite stable chemically, withstanding organic solvents, chlorine, and pH extremes. They can withstand the high temperatures necessary for sterilization processes such as are common in the food and pharmaceutical industries, and they are resistant to microbial degradation. High pressures can compact some organic membranes lowering permeability, but ceramic membranes usually have a high mechanical strength allowing high pressure operation. The stability towards chemicals, temperature, and microbial degradation imply that ceramic membranes can be more resistant to harsh cleaning treatments and allow for more frequent cleaning compared with organic membranes. Additionally, specialized preparation conditions and precursor ingredients can be employed to further control the separation characteristics. Ceramic membranes, for example, can be doped with a metal or another ceramic material to alter the chemistry or pore size distribution of the membrane (Anderson *et al.*, 1988).

Microporous membranes made of porcelain were studied in the beginning of this century, and in the 1940s, Vycor-type glass membranes became popular for micro-filtration applications. Though still classified, the Manhattan Project of World War II is probably the first large scale application of ceramic membranes. The membranes were used as gaseous diffusion barriers in uranium enrichment processing. Ceramic membranes were separately developed for gaseous diffusion in France in the 1940s and 50s, and the Soviet Union, China, and England also presumably used inorganic membranes for the same purpose, although little has been documented (Hsieh, 1996).

Finally, in the 1970s, the French started applying the same membranes used in uranium isotope separation to liquid phase micro- and ultra-filtration. Currently a wide variety of ceramic membranes are available for food and beverage processes, waste water and water-oil treatments, biotechnology separations, and other specialized applications. In spite of all the advantages of ceramic membranes, they have been rather slow to develop in comparison to organic membranes, in part because it is expensive and difficult to produce crack free ceramic membranes with narrow pore size distributions. Nonetheless, the world market for inorganic membranes, majority of which are ceramic, grew from $12 million in 1986 to $35 million in 1990. These figures do not include usage for uranium isotope separations (Hsieh, 1996).

2.2.2 Special Properties & Uses

Certain membranes are known to have highly specific permselectivities. Dense silver, for example, is highly permselective towards oxygen. Palladium and its alloys have a unique resistance to surface oxidation, and were first found to adsorb large amounts of hydrogen in 1866. Dense refractory metals, such as Nb, V, Ta, Ti, and Zr or alloys and oxides of these metals are selectively permeable to hydrogen. Zirconium, in particular, has been extensively investigated for removal of hydrogen and deuterium from fusion blanket fluids (Hsieh, 1996).

A class of materials known as solid electrolytes has been found to possess selective permeabilities towards certain gases. Table 2.5 lists some crystalline solid and non-crystalline glass electrolytes. Most of these solid electrolytes are either hydrogen or oxygen permselective, but some conduct other ions such as silver, fluoride, sodium, nitrogen, carbon and sulfur. Possible applications for these membranes include: gas sensors, fuel cells, production of hydrogen by electrolysis of water at high temperatures, solid state rechargeable batteries and oxygen and hydrogen pumps (Hsieh, 1996).

Table 2.5: Solid Electrolyte Membranes

Crystalline Solids:	AgI
	β-Al$_2$O$_3$
	Bi$_2$O$_3$
	CeO$_2$
	Li$_3$N
	SrCeO$_3$
	Stabilized ThO$_2$
	Stabilized ZrO$_2$
Non-Crystalline Glasses:	B$_2$O$_3$-Li$_2$O-LiI
	LiNbO$_3$

Although organic solid electrolyte membranes do exist, inorganic membranes have the advantage of tolerance of high temperatures, which facilitates ion transport. In addition, they are less prone to fouling and biological degradation (Hsieh, 1996).

2.2.3 Chemistry/Transport Mechanisms

The chemical, mechanical, and thermal stability of ceramic materials is derived from their compact crystal structure, strong chemical bonding, and high field strengths associated with the small and highly charged cations. Ceramics also have a large free energy and total energy of formation, making them very stable thermodynamically. Generally more acidic ceramics are more resistant to acids and vice versa. Certain chemicals, however, such as hydrogen fluoride, ammonium fluoride, and concentrated hydrochloric and sulfuric acids are quite corrosive to the common metal oxide ceramics. Nonoxide ceramic membranes, on the other hand, are prone to reaction during prolonged

exposure to oxidizing agents. These chemical characteristics are particularly important considering the harsh cleaning procedures often necessary for membranes usually involving strong acids, bases, or peroxides (Hsieh, 1996).

A number of different materials can be used as precursors to ceramic membranes. The most common types of ceramic membranes include alumina, silica, titania, and zirconia. Alumina membranes are the most frequently used ceramic membranes. Silica membranes are known to be highly selective towards hydrogen, and are thermally stable up to 600 °C under gaseous exposure. Titania membranes are less common, however, they exhibit unique catalytic properties and excellent chemical resistances. Zirconia membranes are usually made as composites with silica or other metals and exhibit considerable chemical resistance as well (Hsieh, 1996).

Metal oxide ceramics exist in different phases depending on the chemical path and temperature exposure of the material. The different phases of alumina, alpha (α) and gamma (γ) phases being the most common, exhibit a range of thermal and chemical characteristics. Most aluminas transform to α-alumina above 900 °C, and once alumina is in the α phase, it is thermally stable beyond 1000 °C. In contrast, commercial γ-alumina membranes are typically calcined at 400 - 600 °C and therefore are unstable above 600 °C and less chemically resistant as well. Water can be used to promote phase transitions of alumina at lower temperatures, but this is not always desirable. Leenars et al. (1986) found that one type of alumina membrane had a mean pore size of 4.8 nm and a porosity of 55% when fired at 800 °C (γ phase), but when the firing temperature was increased to 1000°C (α phase), the mean pore size increased significantly to 78 nm and porosity decreased to 41%. Ceramic processing techniques do exist, however, to prevent these types of phase changes (Hsieh, 1996).

The introduction of different oxides can sometimes enhance the stability of ceramics or alter grain growth patterns leading to larger or smaller pores.

"...Addition of MgO reduces abnormal grain growth in Al_2O_3 for reasons that are still in dispute. Oxides of Ti, Mn, Nb, Cu and Ge increase the grain growth rate in alumina. Manganese oxide, ferric oxide and titania have been reported to promote the formation of platelet-shaped or anisotropic grains as a result of differences in the growth rates of the bounding interfaces." (Tartaj and Messing, 1997)

Tartaj and Messing added Fe_2O_3 to Al_2O_3 in varying amounts to change the microstructure of the resulting ceramic. It is also possible to dope membranes with metals to enhance catalytic capabilities. Zhang and Ying (1997) doped silica membranes with Niobium, forming covalently bonded ligands that were well dispersed throughout the silica.

A number of factors in addition to material type affect the chemical and physical characteristics of ceramics. Sintering time and temperature have a significant impact on the pore size, pore size distribution, porosity, and pore structure of a ceramic membrane. Leenars et al. (1984) concluded that pore size tends to increase with firing time and especially with firing temperature, while porosity and surface area decrease with firing temperature. Lin and Burggraaf (1991) report that it is difficult to achieve pore sizes below 50 nm for ceramic membranes with firing temperatures above 1000 °C.

The driving force of the sintering process is a reduction in surface energy. Diffusion and evaporation-condensation mechanisms compete as material transport pathways. Diffusion is the dominant mechanism causing shrinkage and elimination of smaller pores as temperature increases, decreasing the surface area. Tightly packed particles facilitate the sintering process by shortening the diffusion distance for material transport. Grain growth increases, however, with increasing time and temperature, lowering the pore coordination number around small pores and causing instability and ultimately the collapse of the smallest pores. A high pore coordination number, in contrast, corresponds to a large number of grains surrounding or defining a pore, which makes the pore more stable. A crack and pinhole free dense ceramic requires an ideal sinterable

powder made up of fine particles (0.1 - 1.0 μm) with a narrow size distribution and similar shape (Pugh and Bergstrom, 1994).

The chemical nature of ceramic powder is also important and plays a significant role during processing of ceramic membranes. Ceramic powders are usually charged when in aqueous solution. The magnitude and sign of charge is important in determining properties of the sol, such as nonspecific ion or surfactant and polymer adsorption. The dissociation of surface groups in water or the binding of ions to the ceramic powder surface causes a charge, which is then balanced by an equal and opposite charge in the surrounding solution (Pugh and Bergstrom, 1994).

2.2.4 Synthesis Methods

As with polymeric membranes, there are numerous ways to fabricate ceramic membranes. While many of the synthesis methods are still in development, some are patented and already in use commercially. Dense solid electrolyte and non-electrolyte oxide membranes can be synthesized using conventional ceramic or powder metallurgy methods such as pressing, extrusion, slip casting, and chemical vapor deposition (CVD). Most of these methods involve a powder preparation, mixing, calcination and finally, sintering. Methods of producing tortuous pore ceramic membranes vary considerably, and include most commonly pressing, tape casting, extrusion, chemical vapor deposition, and sol-gel processing. Finally, nearly straight-pore ceramic membranes can be formed via anodic oxidation.

2.2.4.1 Dense Solid Electrolyte and Non-electrolyte Oxide Membranes

2.2.4.1a Pressing/Sintering

Disk and plate shaped membranes can be formed with conventional ceramic processing, such as cold pressing (from 2000 to 100,000 psi) or isostatic pressing, which utilizes uniformly distributed hydrostatic pressure from all directions to form denser, more uniform membranes. Usually water is used as a solvent, and lubricants and binders, such as carbowax, polyvinyl alcohol, zirconium oxychloride, or wax are added. As the membranes are heated past 300 °C, the organic binders are burnt out. Solid electrolyte precursor particles are also often mixed or reacted with compatible cementing agents, including substances such as phosphates of zirconium, titanium, zinc, calcium aluminate, and calcium aluminosilicates (Hsieh, 1996).

Sintering temperatures and rates vary depending on the specific membrane being produced. Typically, temperatures are slowly increased to a set sintering temperature and held there for ca. 5 - 10 hours.

2.2.4.1b Extrusion/Sintering

Tubular or rod shaped membranes can be formed by mixing metal oxide precursor powders with certain organic additives to form a paste, known as slip. Plasticizers such as glycerol or rubber solution in an organic solvent can be added to the slip for ease of processing. Other organic additives, such as solvents, dispersants, binders, and viscosity modifiers can be used to help control resulting pore size distribution and morphology. The slip is extruded through a die at high pressure and then sintered (Hsieh, 1996).

2.2.4.1c Slip Casting/Sintering

Tubular membranes can also be slip cast in plaster molds using a slip including stabilized powders and typically polyvinyl alcohol as a binder. Polyvinyl alcohol is used widely in ceramic processing to provide green strength (green referring to any prefired ceramic body). The slip usually has an acidic pH between 3 - 4, and is degassed prior to fabrication to remove any entrapped air, and then cast and fired (Hsieh, 1996).

2.2.4.1d Chemical Vapor Deposition (CVD)

Physical vapor deposition is somewhat impractical for dense non-metal membranes. However, chemical vapor deposition (CVD) has been used successfully to form silica and other oxide membranes. Drying and calcining are not necessary for CVD, and denser membranes can be produced. CVD first partially plugs pores of a heated support with a deposit, then gradually builds the deposit into a continuous layer covering the entire surface of the support (Hsieh, 1996).

2.2.4.2 Tortuous Pore Ceramic Membranes

Pressing, extrusion, tape casting, and CVD of tortuous pore membranes are similar to the processes described above for dense solid electrolyte and non-electrolyte oxide membranes. Pressing utilizes high pressures to ensure green body strength and prevent shrinking during heat treatment. Desired pore size distributions are usually achieved by wet or dry milling, screening and blending of the precursor particles. One drawback of conventional pressing techniques is the presence of occasional cracks and pinholes in the membranes produced. Newer techniques addressing this problem are currently under investigation. Extrusion is often a very complicated process, but has the advantage of

simultaneous production of the support and membrane. Tape casting is a convenient way to produce large flat pieces of membranes or support layers, but does not work well for most ceramics other than alumina. CVD can be used to decrease the pore size of existing membranes down to and below 0.5 nm, and is still in developmental stages.

2.2.4.2a Dip and Spin Coating

Dip and spin coating methods are the most practiced techniques of synthesis. The method involves the coating of a support with a slip of controlled pH and particle size, which is dried or calcined to form a porous membrane. Slips are usually pumped or spun over the surface of a support to cover it evenly, taking advantage of capillary and centrifugal forces. Both dip and spin coating can be applied multiple times to produce layered composite membranes, with drying, calcining, and sometimes sintering steps as part of a cyclical process. Intermediate layers can provide smoother surfaces for membrane layer deposits and avoid extra build up of small particles from the membrane layer in the large pores of the support layer (Hsieh, 1996).

2.2.4.2b Sol-gel processing

Sol-gel processes in conjunction with methods such as dip and spin coating, are an emerging family of techniques for preparing microporous ceramic membranes, and are presently used to make many commercial membranes. Generally, sol-gel is a process converting a colloidal or polymeric solution (sol) to a gelatinous substance (gel), using hydrolysis and condensation reactions of alkoxides or salts dissolved in water or organic solvents (Figure 2.4).
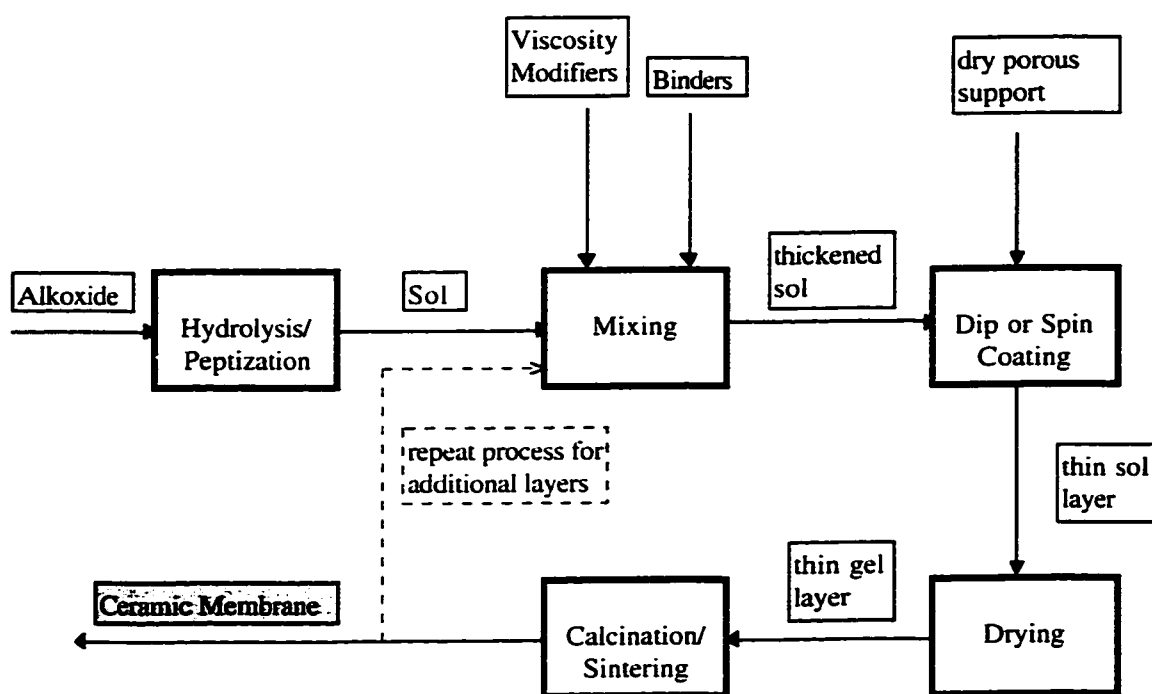
Figure 2.4: The Sol-gel Process

An alkoxide, such as alkoxysilane, undergoes hydrolysis or peptization to form a sol and is mixed with viscosity modifiers and binders to thicken and stabilize the sol. Some commonly used metal oxide precursors include Al tri-sec-butoxide, tetra-ethyl orthosilicate, Ti tetra-isopropoxide, Ti tert-amyloxide, and Zr tert-amyloxide. Nitric acid is commonly used as a peptizing agent as well as HCl, $HClO_4$ or CH_3CO_2H. A porous support is dip or spin coated with the sol, and the resulting gel layer is calcined and/or sintered to form a ceramic membrane. This process can be repeated to form layered membranes. Catalysts can be added either as an additional embedded layer or within the sol itself.

"Among the processes that have been studied extensively, the sol-gel process seems to be by far the most suitable for making thin porous films with macropores (for micro-filtration), mesopores (for ultra-filtration) or nanopores (for nano-filtration), high-purity, and uniform constituent particles in an industrial production environment." (Hsieh, 1996)

2.2.4.3 Anodic Oxidation of Nearly Straight Pore Ceramic Membranes

When aluminum is anodized in certain acid electrolytes, a porous oxide develops which exhibits a remarkably uniform array of cells, each containing a nearly cylindrical pore. Zirconia, theoretically, may also produce membranes through anodic oxidation (Hsieh, 1996). During growth at constant voltage, the barrier-layer thickness remains constant because the electric field oxidizes aluminum at the metal/oxide interface and enhances chemical dissolution at the base of the pores. A geometric model describes how the pore size and pore density are related to the barrier-layer thickness; all three of these parameters are controlled by the voltage. Pore sizes of 10 - 250 nm, pore densities of 10^{12} - 10^{15} m^{-2} and film thicknesses of over 100 μm can be achieved (Furneaux *et al.*, 1989).

Although alumina membranes produced via anodic oxidation have very straight, regular, and tightly packed pores, this method has not yet been applied to large scale processes. There is some difficulty in separating the anodized porous layer with the non-porous barrier layer. Gradual reductions in voltage may lift the membrane off the barrier layer. More typically, an acid etch must be used to dissolve the remaining non-porous aluminum. Additionally, many harsh chemicals are necessary during processing and extensive heat treatments are also necessary to stabilize the membranes.

In conclusion, the methods of ceramic membrane synthesis described in this section are all well suited to specific applications, producing membranes with different characteristics. Table 2.6 compares the smallest pore diameters achievable with the more common processes.

Table 2.6: Ceramic Membrane Synthesis Methods (Adapted from Hsieh, 1996)

Synthesis Method	Membrane Material	Smallest Pore Diameter (nm)
Suspension/Dip coating	Al_2O_3	100
Sol-gel/Dip coating	Al_2O_3, TiO_2, ZrO_2, CeO_2, RuO_2/TiO_2	2.5
Pyrolysis of polymers	SiO_2, molecular sieve C, C, Al_2O_3/cordierite	1
Pore Modifications (CVD)	Al_2O_3/Fe_2O_3, SiO_2/CeO_2, Al_2O_3MgO, TiO_2/V_2O_5, ZrO_2/TiO_2, ZrO_2/Fe_2O_3, Al_2O_3/ZrO_2, Al_2O_3/silicate	0.3
Anodic Oxidation	Al_2O_3, ZrO_2	10

2.3.0 Alumoxanes

2.3.1 History

Alumoxanes are novel materials. They represent a general class of compounds containing "oxo" bridges binding at least two aluminum atoms (Al-O-Al). Alumoxanes were first reported by Adrianov in 1958 (Callender et al., 1997), and were studied extensively in the 1960s as active catalysts for certain polymerization reactions (Pasynkiewicz, 1990). Storr et al. (1967) studied ethylaloxanes $((Et_2Al)_2O)$ and their derivatives as polymerization aids, and found that the compounds were much less volatile than frequently used organoalanes. A series of reports by Bradley et al. in 1971, characterized poly trialkylsiloxanometalloxanes with metal-oxygen-metal bridges including titanium, tantalum, zirconium, and aluminum. The synthesis, structure and reactions of alumoxanes in the context of polymerization catalysis has been reviewed elsewhere in detail (Pasynkiewicz, 1990). Finally, in 1992, Apblett et al. reported other uses for alumoxanes including preceramics, additives in paints and coatings, antiperspirants, supports for metal colloids, and catalysis. They also proposed that siloxy-substituted alumoxanes have a three dimensional cage like structure and a six-coordinate aluminum center analogous to that found in the minerals boehmite and diaspore (shown in the next section, Figure 2.5).

Landry et al. (1995) continued the work of Apblett et al., and developed a synthesis

method for alumoxanes from boehmite and carboxylic acids. Using a number of different

organic acids (RCO_2H) to produce carboxylatoalumoxanes ($[Al(O)_x(OH)_y(O_2CR)_z]_n$, they

found that the physical properties of the alumoxanes are highly dependent on the alkyl

substituent (R) used. The alumoxanes ranged from insoluble crystalline powders to

powders which readily form solutions or gels in hydrocarbon solvents. Although large

boehmite particles were used to synthesize the alumoxanes, they were found to be

spectroscopicly similar to alumoxanes prepared from small molecule precursors.

Thermolysis of alumoxanes yields alumina, and Karieva et al. (1996) formed

homogenous mixed-metal oxides upon thermolysis of transition metal and lanthanide doped

carboxylate-alumoxanes. This formation of a single phase material is comparable to

traditional sol-gel methodologies, yet alumoxanes are identifiably stable in solid and

solution. The alumoxane precursors also show no tendencies to segregate or polymerize,

and have the capability of aqueous or organic phase processing. Most of the carboxylate

alumoxanes made by Landry et al. (1995) were synthesized in xylene, while Callender et

al. (1997) synthesized four different carboxylate-alumoxanes in aqueous phase. In

addition to being extremely simple, the alumoxane method is fast and economical compared

with the sol-gel and ceramic methods (Table 2.7).

Table 2.7: Comparison of the Alumoxane Method with the Ceramic Method and Sol-Gel Synthesis for the Synthesis of Ternary Aluminum Oxides.
(Adapted from Kareiva et al., 1996)

Method:	alumoxane	sol-gel	ceramic
Methodology	simple	complex	simple
Atomic Mixing	yes	yes	no
Metastable Phases	yes	yes	no
Stability	excellent	poor	infinite
Solubility	readily controlled	difficult to control	none
Proccessability	good	good	poor
Time	<8 hours	>20 hours	days
Cost	low	medium-high	low

2.3.2 Physical & Chemical Properties

Alumoxanes are essentially inorganic polymers, with a core of aluminum and oxygen cage-like repeating units. Ligands, namely organic acids, attach to the core alumoxane at the oxygen sites, bridging two oxygens together. Figure 2.5 shows the structure of boehmite (precursor) and the resulting structure of a carboxylate-alumoxane formed with the addition of organic acid and water.

boehmite   carboxylate-alumoxane
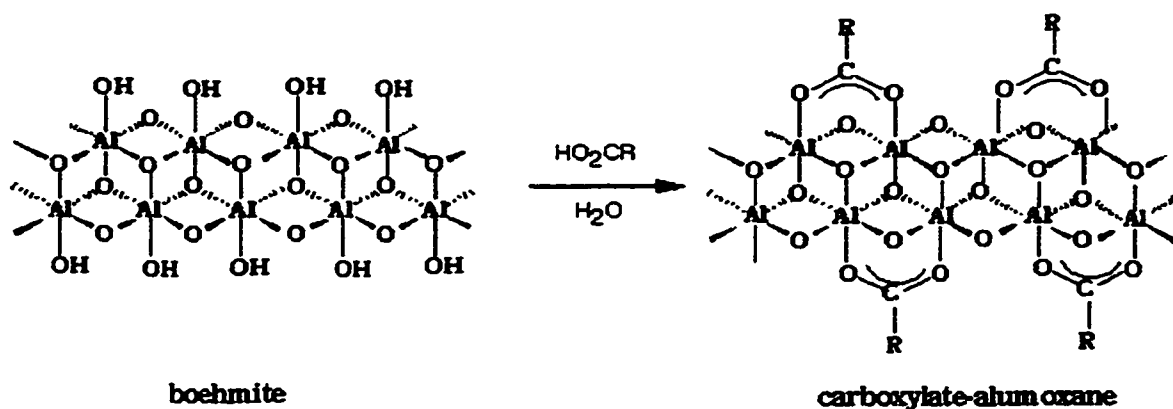
Figure 2.5: Carboxylate-alumoxane

For example, the ligands used in this study are shown in Figure 2.6, and included acetic acid [HO_2CCH_3, A-H], methoxyacetic acid [$HO_2CCH_2OCH_3$, MA-H], (methoxyethoxy)acetic acid [$HO_2CCH_2OCH_2CH_2OCH_3$, MEA-H], and [(methoxyethoxy) ethoxy] acetic acid [$HO_2CCH_2(OCH_2CH_2)_2OCH_3$, MEEA-H].

HO
C
O
acetic acid   (A-H)

HO
C
O
methoxyacetic acid   (MA-H)

HO
C
O
methoxyethoxyacetic acid   (MEA-H)

HO
C
O
methoxyethoxyethoxyacetic acid   (MEEA-H)
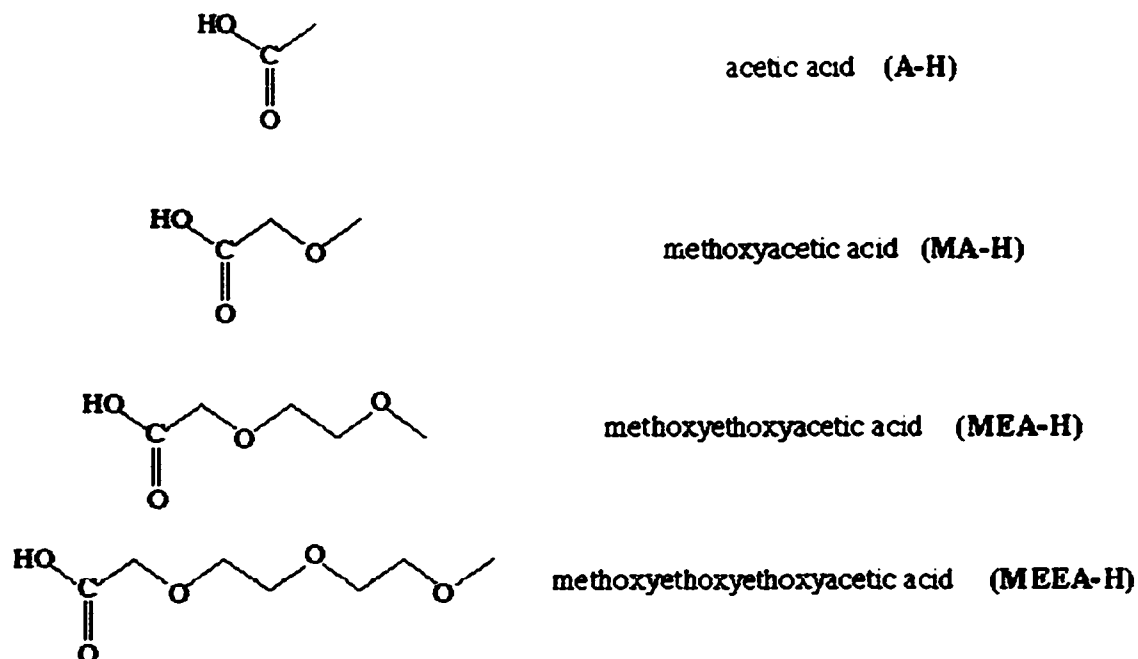
Figure 2.6: Organic Acid Ligands (R groups)

Carboxylate alumoxanes are water soluble and create clear, free flowing colloidal dispersions. Some physical properties for the four selected carboxylate alumoxanes are listed in table 2.8. The gel point represents the mass of alumoxane required to form a solid gel in 1.0 mL of water. Longer chain substituents should show a greater solubility due to hydrogen bonding, but the gel points indicate that the samples have similar solubilities. The refractive index is important in determining potential for use as optical coatings, and falls between that for boehmite and the organic substituents. The dielectric constants of the ligands were significantly lower than that for alumina and close to that of polethylene, suggesting that the electric properties are dominated by the organic part of the alumoxane. Similarly, the hardness of the carboxylate alumoxanes is comparable to organic rather than inorganic materials. The "dec temp" represents the temperature at which the alumoxane decomposes into amorphous alumina. All of the alumoxanes become mixed phase γ-alumina and α-alumina (Corundum) at temperatures above 900 °C, as is common in

alumina transformations. Ceramic yield is highly dependent on the identity of the

carboxylic acid, increasing with decreasing ligand size as would be expected (Callender *et al.*, 1997).

Table 2.8: Selected Physical Properties of the Carboxylate-Alumoxanes
(Adapted from Callender *et al.*, 1997)

Alumoxane	gel point in water (g/ml)	refractive indexes (n_D)	dielectric constant (ε)	hardness V_H (kg mm^2)	dec temp (°C)	ceramic yield (%)
MEEA-alumoxane	0.30	1.5	2.7	2 - 40	370	20
MEA-alumoxane	0.95	1.5	2.5	20 - 40	370	27
MA-alumoxane	0.11			> 40	360	30
A-alumoxane	0.20	1.5	2.5	90	520	76

Finally, in addition to being infinitely stable under ambient conditions, the aqueous

processability of carboxylate alumoxanes implies suitability as binders in traditional ceramic

"green body" processing. Also, the nanoparticle size of the carboxylate alumoxanes allows

full infiltration into microporous materials, which upon firing constitutes an alternative

method of chemical infiltration and surface repair (Callender *et al.*, 1997).

2.3.3 Related Work

Inoue *et al.* have published several works on the structure and synthesis of

aluminum hydroxide and alumina. In 1986, they found that thermal treatment of crystalline

aluminum hydroxide in ethylene glycol forms a compound with the structure of boehmeite

having ethylene glycol bound between the layers. The following year, Inoue *et al.* reported

further on the subject and identified a honeycomb structure and a high surface area as well

as assigning an empirical formula to the compound [$AlO(OCH_2CH_2OH)_x(OH)_y$, where x+y

= 1]. They also reported that larger grain sizes in the gibbsite precursor yielded alumina

with a lower surface area. Inoue *et al.* (1989) then used glycothermal treatment to form

microcrystalline α-alumina from gibbsite. In 1991, they reacted gibbsite with glycols and

aminoalcohols to form organic derivatives of boehmite. They noted that increasing

molecular size of the solvents or particle size of the gibbsite decreased the yield of the

organic derivatives of boehmite. Recently Inoue et al. (1997) studied the organic

derivatives of boehmite further, comparing them to alumoxanes, and suggested a reverse

alkoxide hydrolysis reaction as the formation mechanism (15).

$$>Al-OH + ROH \quad \leftrightarrow \quad >Al-OR + H_2O \tag{15}$$
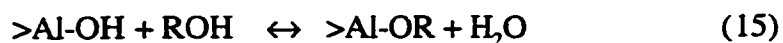
Leenaars et al. (1984) successfully produced alumina membranes with pore sizes

down to 2.5 nm from boehmite sols via aluminum secondary butoxide and water. Zaspalis

et al. (1992) used this same method to produce γ-alumina with narrow pore size

distributions and average pore diameters of 3 nm. They also noted that multiple dippings

can repair defects on membrane surfaces and the addition of polyvinyl alcohol can help

prevent surface defects. Anderson et al. (1988) produced crack-free monoliths of

unsupported γ-alumina membranes with average pore diameters from 1.8 to 5 nm using a

different sol gel process from that which was used by Leenaars et al. (1984) and Zaspalis et

al. (1992). They started the process with aluminum tri-sec-butoxide, 2-butanol and water

forming a sol and let the water evaporate at room temperature to form a thick gel. Lin and

Burggraaf (1991) also used a similar sol-gel process to produce γ-alumina membranes, but

doped the membranes with lanthanum to control the pore size.

2.3.4 Environmental Implications

Although alumina and most other ceramics themselves are environmentally benign,

the manufacturing processes used to create them are not. The alumoxane method of

producing alumina is designed to create as minimal of a stress on the environment as possible. The two most commonly used methods currently used to produce alumina, however, are quite detrimental to the environment. Traditional ceramic processing is energy intensive and involves the use of various binders, solvents, and chemical agents (Callender et al., 1997). A typical slurry composition for this type of processing is shown in Table 2.9, where one should immediately note the presence of chlorinated hydrocarbons as a large percentage of the slurry.

Table 2.9: Typical Composition of a Nonaqueous Tape-Casting Alumina Slurry (Adapted from Callender et al., 1997)

Function	Composition	Volume %
Powder	alumina (Al_2O_3)	27
Solvent	trichloroethylene(TCE)/ethanol	58
Deflocculent	menhaden oil	1.8
Binder	poly(vinyl butyrol)	4.4
Plasticizer	poly(ethylene glycol)/octyl phthalate	8.8

TCE is a toxic chemical that is regulated by the EPA and is known to cause adverse health effects including central nervous system depression, deafness, liver damage, paralysis, respiratory and cardiac arrest and visual effects (Asante-Duah, 1993). Plasticizers, binders and alcohols also create air and water pollution problems since they are pyrolized during the sintering process, or in the case of alcohol, sometimes discharged to waterways exerting high biological oxygen demands (BOD) on the receiving waters (Callender et al., 1997).

The sol-gel process can be environmentally taxing as well, employing strong acids, binders, plasticizers and solvents, and producing sec-butanol. A typical composition of an alumina sol-gel for slipcast filter membranes is shown in Table 2.10.

Table 2.10: Typical Composition of an Alumina Sol-Gel for Slipcast Filter Membranes
(Adapted from Callender *et al.*, 1997)

Function	Composition
Boehmite Precursor	aluminum sec-butoxide, Al[OC(H)MeEt]$_3$, ASB
Electrolyte	HNO$_3$ (0.07 mol/mol of ASB)
Complexing Agent	glycerol (~10 wt %)

This method has potential to produce gaseous pollution from combustion of the binders and plasticizers during sintering and release of NO$_x$ off-gasses from residual nitric acid or nitrate salts. Furthermore, acids and solvents create disposal issues and energy consumption is considerable (Callender *et al.*, 1997). The alumoxane method for producing alumina potentially can eliminate the use of toxic solvents and strong acids through the use of more environmentally benign feedstocks, and can also reduce energy consumption.

2.3.5 Significance

Alumoxanes show potential for fabrication of new ceramic nanofiltration and ultrafiltration membranes with special properties. Oxide and hydroxides of aluminum have a wide range of industrial applications as well, including precursors for the production of aluminum metal catalysts, absorbents, structural ceramic materials, reinforcing agents for plastics and rubbers, antacids, binders and absorbents for the pharmaceutical and cosmetic industries, and as low dialectic loss insulators in the electronic industry. Ternary oxides, such as mullite (Al$_6$Si$_2$O$_{13}$), YAG (Y$_3$Al$_5$O$_{12}$) and β-alumina (NaAl$_{11}$O$_{17}$) can offer distinct advantages over binary aluminum oxides including high temperature shock resistance, high temperature chemical stability and high creep resistance, and potential as interfacial coating for ceramic composites respectively (Callender *et al.*, 1997). We have proposed that alumoxanes can be used as precursors to form ceramic membranes (Callender *et al.*, 1998).

This work is the first effort to characterize alumoxane-derived materials created for this

purpose.

Chapter 3

Materials and Methods

3.1.0   Materials

3.1.1   Preparation of Alumoxane-Derived Membranes

Alumoxane-derived ceramics were prepared by Christopher Jones in the department of chemistry at Rice University. The method of synthesis used is summarized in Figure 3.1.
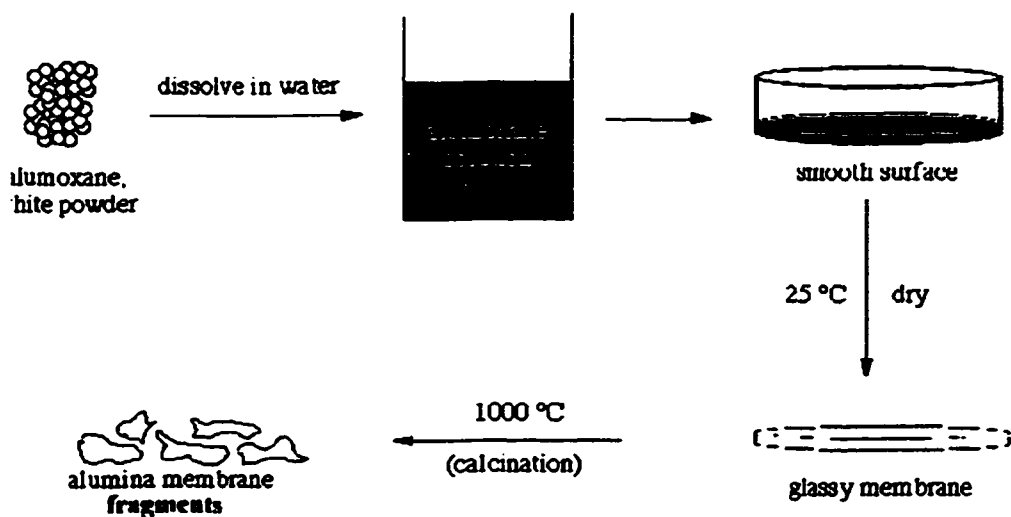
Figure 3.1   Alumoxane based Membrane Synthesis

Powdered pseudo-boehmite was refluxed with an excess of a carboxylic acid in water.

Volatiles of this mixture were vacuumed off and the remainder was washed with Et_2O

draining excess organic acid and leaving a pure alumoxane solution. This solution was

dried on a flat surface. The resulting materials were still water soluble until they were fired

at 1000 °C for approximately 8 hours to yield alumina ceramics (Landry *et al.*, 1995;

Callender *et al.*, 1997). During firing, the carboxylic acid ligands were vaporized and the

repeating structures of the alumoxane were sintered together forming a porous substrate,

which was evaluated as possible membrane material. A more detailed description of the

method used to form each membrane type is contained in appendix A.

Table 3.1 lists the samples used in this study. Acetic acid (A-H) and

(methoxyethoxy)acetic acid (MEA-H) were the organic ligands chosen, and for some

samples were combined chemically, physically, or both chemically and physically.

Chemical mixing of ligands implies that the organic acids were added together to the

boehmite before the alumoxane was formed, while physical mixing implies addition of one

type of alumoxane to another in the aqueous form. We have adopted a three-number

convention for expressing the ratio of ligands added to create a chemical mix and the ratio

of the resulting alumoxanes mixed physically with single-ligand derived alumoxanes:

$$\underbrace{\underbrace{[MEA - Alumoxane; A - Alumoxane]}_{\text{Chemically mixed}} : A - Alumoxane}_{\text{Physically mixed}}$$

A chemical mix in equal proportions, which is physically mixed in an equal proportion is

designated as [1;1]:1, while pure A-alumoxane is designated as [0;0]:1.

Table 3.1: List of Samples Used

Fraction MEAA	Pure Samples	Chemically Mixed Samples	Physically Mixed Samples
0	[0;0]:1 (A-alumoxane)		
0.167		[1;1]:4	
0.2			[1;0]:4
0.25		[1;1]:2	
0.33		[1;1] :1	[1;0]:2
0.4		[1;1]:0.5	
0.5		[1;1]:0	[1;0]:1
0.67			[1;0]:0.5
1	[1;0]:0 (MEA-alumoxane)		

3.1.2 Commercial Membranes for Comparison

Two commercial membranes, a 0.02 μm Anodisc and a 0.015 μm Nuclepore, with reported pore sizes similar to those subsequently determined for the alumoxane based membranes were chosen for comparison. Both types of membranes have straight pores, the former produced by anodization and the later by track-etching. The 0.02 μm Anodisc is asymmetric, with a skin approximately 1μm thick layered on a support 59 μm thick with a mean pore size of 0.2 μm. It is made of alumina, is transparent when wet, and has hexagonal straight pores similar to a honeycomb. The 0.015 μm Nuclepore membrane is a symmetric polycarbonate membrane, which is also transparent, and has a low pore density. These membranes were selected in part as "standards" due to the simple geometry of pores in these membranes and the high degree to which these membranes have been characterized by previous investigators. Table 3.2 lists characteristics of the membranes.

Table 3.2: Characteristics of Anodisc and Nuclepore membranes
(supplied by Manufacturers)

	Anodisc	Nuclepore
Manufacturer	Whatman	Corning
Membrane Material	γ-alumina	Polycarbonate
(Skin) Thickness (μm)	1	6 - 11
Mean Pore Size (nm)	20	15
Porosity (%)	25 - 30	< 15
Pore Density (pores/cm^2)	10^{12}	$1 \times 10^5 - 6 \times 10^8$
Max. Service Temp. (°C)	500	140
pH Resistance	3 -9.5	-
Hydrophilic	yes	yes

3.2.0 Methods

Several different methods were used to characterize the alumoxane based membranes and compare them to the two commercial membranes. Some of the methods overlap in such a way that one type of information may be obtained using several different methods. This was done intentionally as a means of verifying a given method. The focus of this characterization work was on determining membrane pore size, structure, and permeability to water. Simple measures of membrane surface chemistry were also made.

3.2.1 Scanning Electron Microscopy

SEM images come from two different sources and are labeled accordingly. A portion of the SEM imaging was performed on a JEOL JSM 5300 Scanning Microscope by

Christopher Jones in the chemistry department at Rice University. Samples were attached to aluminum studs with graphite paint and sputtered with gold to create a conducting surface. Additional SEM images were supplied by Milton Pierson from the department of Geology at Rice University.

3.2.2 Atomic Force Microscopy

Samples were imaged using a Nanoscope IIIa Scanning Probe Microscope, in tapping mode AFM (Digital Instruments, Santa Barbara, CA). FESP tips were used with a pyramidal shape and end radius of 5 - 10 nm (also from Digital Instruments). Samples were attached to 15 mm magnetic specimen disks (Digital Instruments) with black carbon double sided tape (DI). No other sample preparation was necessary.

Images were taken at scan sizes of 10 μm, 1 μm, and 200 nm. The scan angle was changed occasionally from 0 to 45° to check the integrity of the images. The number of channels used for imaging ranged from one (height image only) to three channels (including height, amplitude, and phase image information). Typical settings used are shown in table 3.3. Images were later processed to obtain roughness, grain size, and section analysis with the accompanying Nanoscope software.

Table 3.3 Typical AFM Settings Used

Scan Controls		Feedback Controls	
Scan Size	200 nm - 10 μm	Integral Gain	0.40 (+/- 0.20)
X offset	0 - 10 μm	Proportional Gain	4.00 (+/- 2.00)
Y offset	0 - 10 μm	Look Ahead Gain	0.00
Scan Angle	0 - 45 °	Setpoint	0.85 - 4.25 V
Scan Rate (Hz)	2	Drive Frequency	71 - 81 Hz
# Samples	256	Drive Amplitude	2 - 10 V
Slow Scan	enabled	Analog 2	0.00 mV
Z-limit	440 V	Phase Offset	50 - 170 °

3.2.3 Nitrogen Gas Adsorption/Desorption

Surface area, pore volume, and pore size distribution were measured by nitrogen adsorption/desorption using a Coulter SA 3100 (Miami, Florida). This machine measures pressure and temperature as nitrogen gas is adsorbed and desorbed from a sample creating an isotherm. Helium was used to measure the freespace in the sample cell. A reference cell was used to compare changes in pressure of the sample cell. The condensation point of nitrogen is 77 K, and the sample and reference cells were immersed in a dewar of pure liquid nitrogen, which was replenished as needed. The resulting isotherm was used to calculate the surface area of the sample based on BET theory, and the pore volume and pore size distribution based on BJH pore theory.

0.1 to 0.5 grams of membrane were broken into small pieces and funneled into the sample cell. The samples were then typically outgassed with a Nitrogen purge at 300 °C for ten hours each before every run. Each sample was outgassed and run at least three times for consistency unless otherwise noted.

Surface area of the sample was reported directly from the machine based on BET calculations; results with correlation coefficients less than 0.996 were discarded. Pore size distributions were also reported directly from the Coulter SA 3100, and were based on both the adsorption and desorption isotherm branches using BJH calculations with a Harkins-Jura subroutine. Average pore sizes were calculated from the adsorption branch using the following equation (16):

$$\bar{d}_P = \Sigma \left[\frac{V_i}{V_T} \cdot d_{P_i} \right] \qquad (16)$$

where $\overline{d_P}$ is average pore size, V_i is the fraction of the total volume (V_T) in the ith pore size range, and d_{P_i} is the average pore size of the ith pore size range. The standard deviation, S, for the average pore size was calculated from equation 17.

$$S = \sqrt{\Sigma\left[\frac{V_i}{V_T}\cdot\left(\overline{d}_P - d_{P_i}\right)^2\right]} \qquad (17)$$

Porosity, ε, was calculated from equation 18:

$$\varepsilon = \frac{V_{pore}}{V_T} \qquad (18)$$

where V_{pore} is the total measured pore volume and V_T (eq. 19) is the volume of the total membrane.

$$V_T = \underbrace{\left(\frac{M_m}{\rho_{bm}}\right)}_{V_{bm}} + V_{pore} \qquad (19)$$

In equation 19, M_m is the membrane mass or sample weight, ρ_{bm} is the density of the bulk membrane material (3.97 for α-alumina), and V_{bm} is the volume of the bulk membrane material. The porosity can also be expressed as a pore number or pore density (N), which is the number of pores per cm^2 of membrane (eq. 20).

$$N = \frac{\varepsilon}{A_{pore}} \qquad (20)$$

3.2.4 Permeability

Permeate flux was measured on membrane samples that were epoxyed to aluminum foil disks with pre-cut holes in the center of known area matching each membrane piece. The membrane pieces typically had an area between 0.5 and 2 cm^2 and a thickness of 100 to 250 μm. Prewetted Glass fiber supports were placed underneath the membranes to prevent cracking. Figure 3.2 shows membrane sample # 66 after it was used. The epoxy was dyed blue so that it could be distinguished from the membrane itself. The round impression surrounding the membrane, visible in Figure 3.2, was formed from the support underneath it.
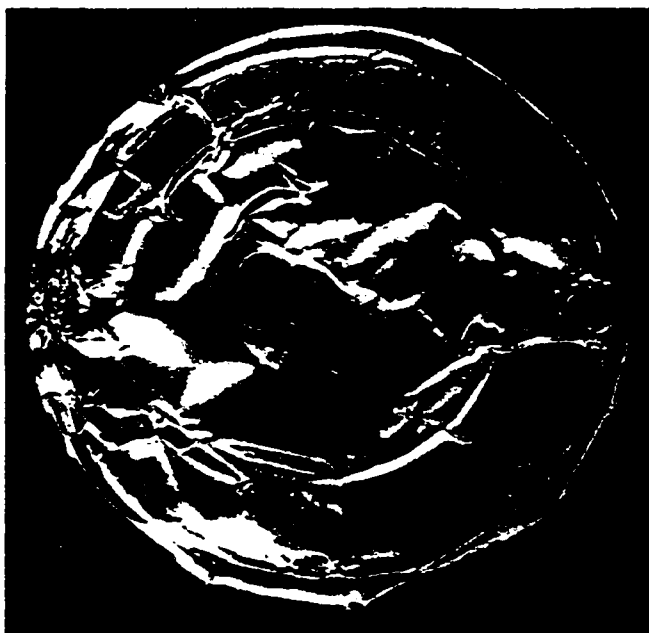
Figure 3.2: Membrane Sample # 66

Permeability measurements were derived from permeate flux measurements using five dead-end filtration cells (Spectrum, Houston, Texas) in parallel. The 400 mL cells were connected to a tank of zero-air for positive pressure. A pressure regulator was used

to set constant pressure for each flux experiment at 10, 20, or 30 psi, and filtrate was collected in beakers and measured volumetrically (Figure 3.3).
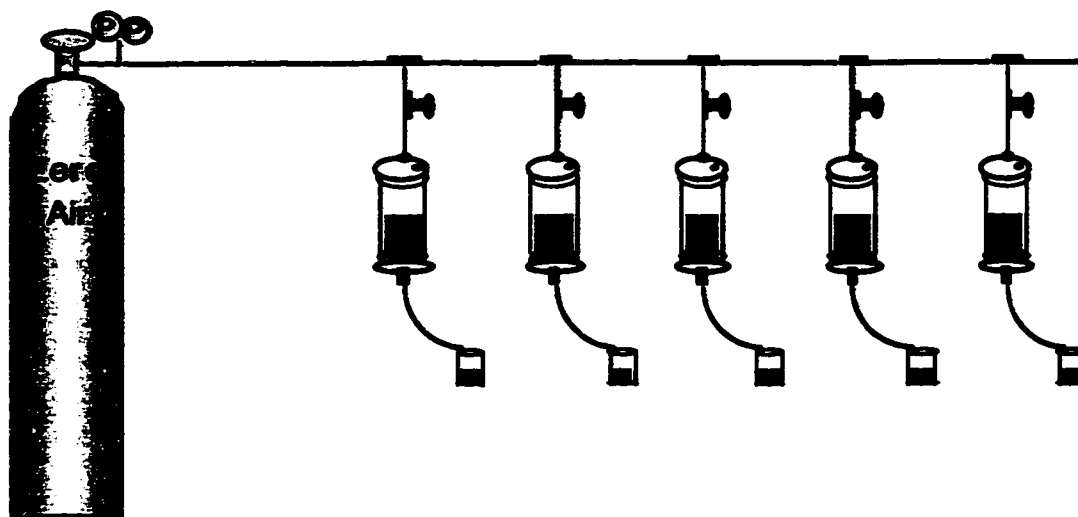
Figure 3.3 Dead-end Filtration Cell Schematic

At the beginning of every experiment, each cell was filled with 200 mL of ultrapure deionized water (Millipore Milli-Q Water System, Jaffrey, NH), and the pressure was set at 10 psi (69 kPa). Permeate was collected at atmospheric pressure, thus, the effective transmembrane pressure was equal to the pressure applied to the filtration cell. Six measurements of the filtrate were taken at 10 psi, usually 4 to 24 hours apart. The pressure was then increased to 20 psi (138 kPa), six more measurements were taken, and the pressure was increased finally to 30 psi (207 kPa) for another six measurements. Volume, time, and area measurements were used to calculate permeate flux (eq.5, sec. 2.1.5). Permeability was then calculated from permeate flux, transmembrane pressure, viscosity of water, and membrane thickness using Equation (4) (section 2.1.5).

3.2.5   Contact angle

Contact angle was measured with a Goniometer. Samples from flux experiments were used, since they were already mounted on a pliable foil. Samples were placed upside-down on top of a glass container full of deionized water, with the sample submerged. An air bubble was placed on the sample surface and ten readings of the contact angle were read for each side of a bubble. Air bubbles occurring naturally on the membranes surface were measured using the same procedure as well.

3.2.6   Surface Charge

Surface charge was determined by measuring electrophoretic mobility with a Zeta-Meter System 3.0 (Zeta-Meter, Inc., Staunton, Virginia). Alumoxane-derived membranes (1;1:1 sample) were crushed with a mortar and pestle and combined with sodium chloride to form a 10^{-2} M electrolyte solution. The solution was tested at 4 different pHs, using hydrochloric acid and sodium hydroxide to adjust the pH. Electrophoretic mobility was measured at a voltage of 100, taking a minimum of 5 measurements three times at each pH. Zeta potential, or surface charge, was calculated using the following equation:

$$\zeta = \frac{113,000 \cdot \mu \cdot EM}{\varepsilon_r} \qquad (21)$$

where ζ is the zeta potential in millivolts, μ is the viscosity in poise (0.01P for water at 20 °C), EM is the electrophoretic mobility in μm/s per V/cm, and ε_r is the dielectric constant (80.4 in water at 20 °C).

Chapter 4

Results and Discussion

4.1.0   Introduction

Characterization of alumoxane-derived membranes was performed using scanning electron microscopy, atomic force microscopy, nitrogen adsorption/desorption, flux experiments, and contact angle measurements. In the following sections, Alumoxane-derived membranes formed from different ligands or combinations of ligands are compared qualitatively and quantitatively. Comparative results for anodized alumina and polycarbonate track-etched membranes are also presented.

4.2.0   SEM Images

Scanning electron imagery was performed for alumoxane-based alumina and anodized alumina membrane samples. The images are useful in evaluating the macroscopic structure of the surface of the membrane samples. Cross-sectional images allow further analysis of the pore morphologies of the samples.

4.2.1 Alumina Sample Images

Figures 4.1, 4.2, 4.3, and 4.4 show SEM images of AA, MEAA, a physically mixed sample (1;1:1), and a chemically mixed sample (1;1:0). Though the samples appear to differ considerably from each other, they are actually quite similar. The specks, visible especially in the AA sample (Figure 4.1), are largely attributable to dirt or dust. Striations that can be seen in the AA and MEAA samples (Figures 4.1 & 4.2) are the result of sample preparation, and should not be considered as a characteristic of those particular samples. The AA appears to have slightly finer grains than MEAA, and both display a nodular morphology, which is expected based on the synthesis method of the alumoxane-derived membranes.
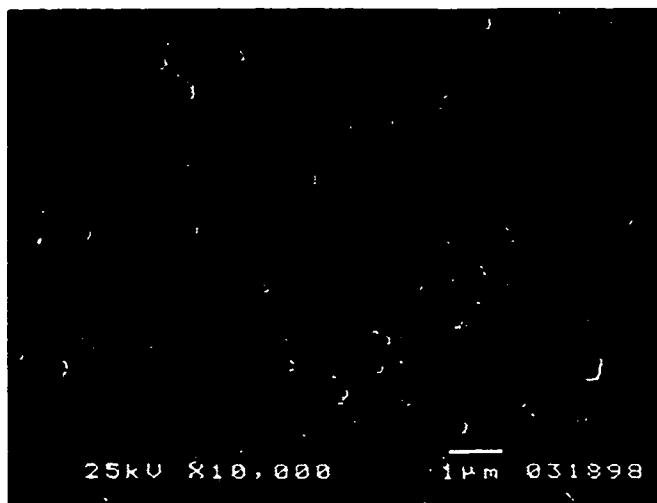
Figure 4.1: SEM Image of AA
(imaged by Christopher Jones, Dept. Chemistry, Rice U.)
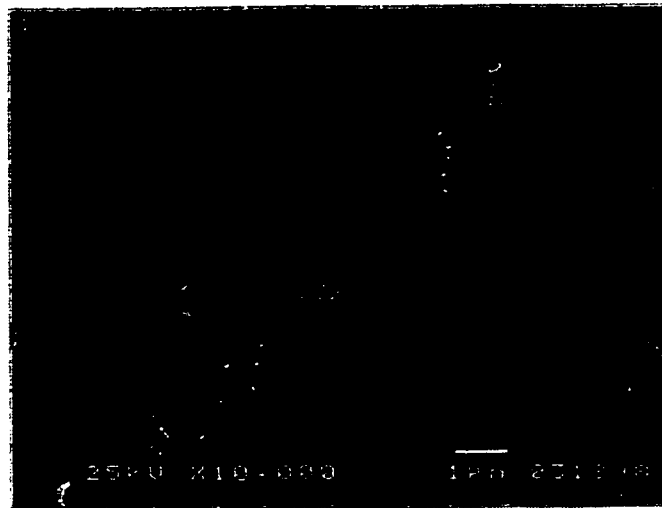
Figure 4.2: SEM Image of MEAA (imaged by C. Jones, Dept. Chemistry, Rice U.)

The physically mixed sample in Figure 4.3 also shows a smooth granular morphology, its two ridges being the result of sample preparation as well. Figure 4.4 shows a chemically mixed sample at twice the magnification of the other three images, hence the grains appear to be twice the size of the others. This image demonstrates the consistency and regularity of the grains of alumoxane-derived alumina.
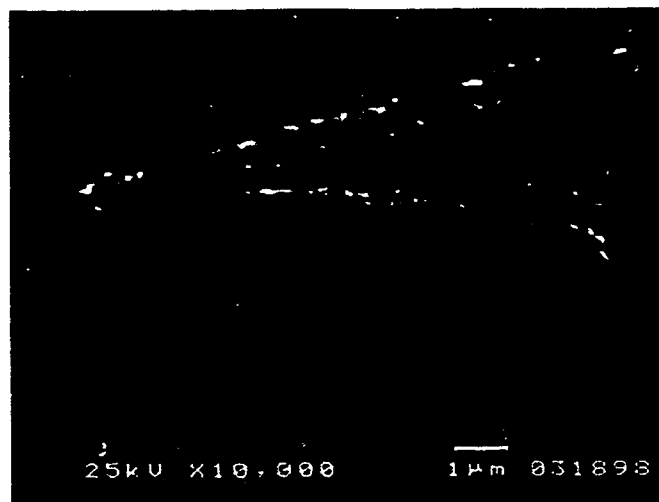
Figure 4.3: SEM Image of Physically Mixed MEAA/AA
(imaged by C. Jones, Dept. Chemistry, Rice U.)
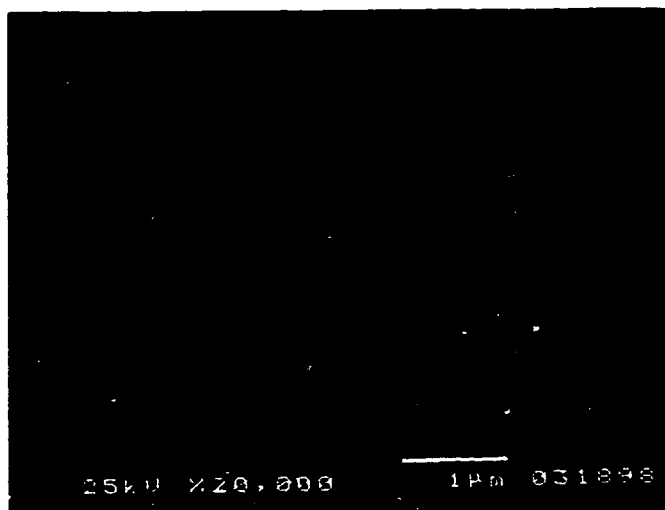
Figure 4.4: SEM Image of Chemically Mixed MEAA/AA
(imaged by C. Jones, Dept. Chemistry, Rice U.)

The support side (0.2 μm pores) of a 0.02 μm anodized alumina membrane is

shown in Figure 4.5.
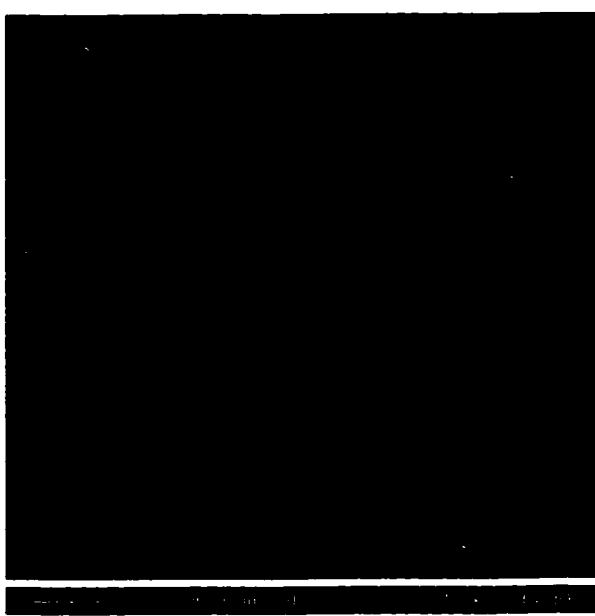
Figure 4.5: SEM Image of the 0.2 μm Support side of a 0.02 μm Anodized Alumina
Membrane (imaged by Milton Pierson, Dept. Geology, Rice U.)

This SEM image appears identical to that shown by the manufacturer for this particular

membrane. The image shows an extremely high pore density. Some of the pores appear to

have merged into larger pores, but they are nearly cylindrical and most are quite close to the rated pore size of 0.2 µm. The high pore density and near-cylindrical shape of the pores result in a higher permeability, improving the performance of these membranes.

Unfortunately, the smaller 0.02 µm pores of the membrane skin itself could not be imaged with this particular scanning electron microscope, due to limited resolution. However, based on the literature, it is anticipated that the pore structure of the 0.02 µm skin is similar to that of the 0.2 µm membrane support.

4.2.2 SEM Cross-Sections

A cross-section of an AA-derived membrane (Figure 4.6) shows that the granular morphology is homogenous throughout the membrane. The tortuosity is highly evident. The thickness of the membrane measured from this image is roughly 180 µm.
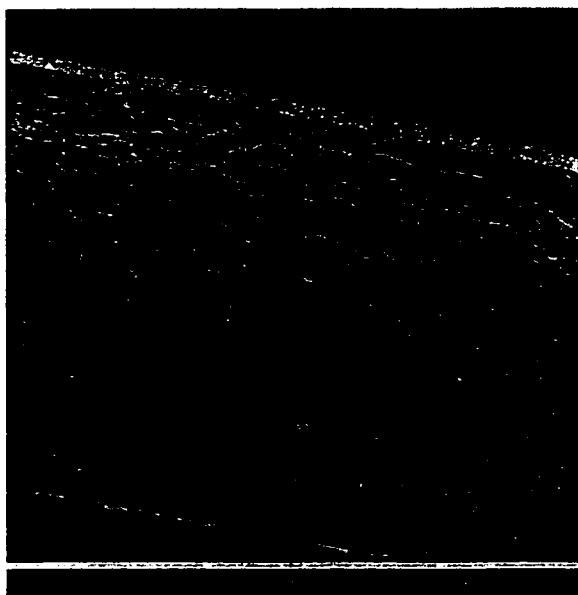
Figure 4.6: SEM Cross-sectional Image of AA
(imaged by M. Pierson, Dept. Geology, Rice U.)

As membrane thickness and pore tortuosity increase, permeate flux is anticipated to decrease (Equation (2), section 2.1.5). The porous openings in this image appear to be on the order of 2 μm. However, it is unclear if these openings are present as isolated chambers within the membrane, or if these are connected, tortuous channels. Data presented in subsequent sections 4.3.1 and 4.5.1 suggest that these are isolated chambers and that the effective porosity of the membrane is defined by the porosity of the intervening material, which appears "solid" at this magnification.

By contrast, the cross-section of the 0.02 μm anodized alumina membrane (Figure 4.7) shows extremely straight pin-like pores.
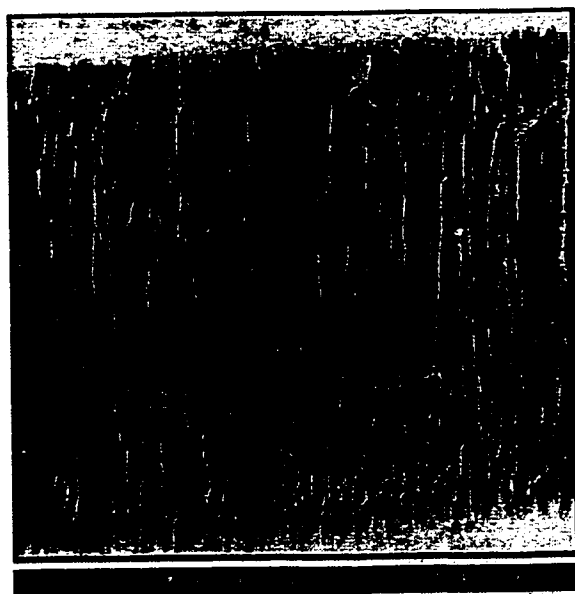
Figure 4.7: SEM Image of 0.02 μm Anodized Alumina Membrane Cross-section (imaged by M. Pierson, Dept. Geology, Rice U.)

The branching of the pores to form the membrane skin layer is obscured in this image, but can be seen in Figure 4.8 for a 0.1 μm anodized alumina membrane. The pores can be seen branching into pores half the size at the top of the image. Though the resolution is quite poor, the membrane skin layer can be estimated as roughly 1 μm thick, as confirmed by literature from the manufacture. This is much thinner than the alumoxane-derived alumina membranes fragments, which ranged in thickness from 100 - 250 μm, and for the

most part is why these membranes have a much higher flux than alumoxane-derived alumina membranes (see section 4.4). One should note however, that thickness can be controlled by membrane processing and anodized alumina membranes go through extensive processing, including use of lasers for cutting, to produce a thin membrane skin layer (Costello, 1997).
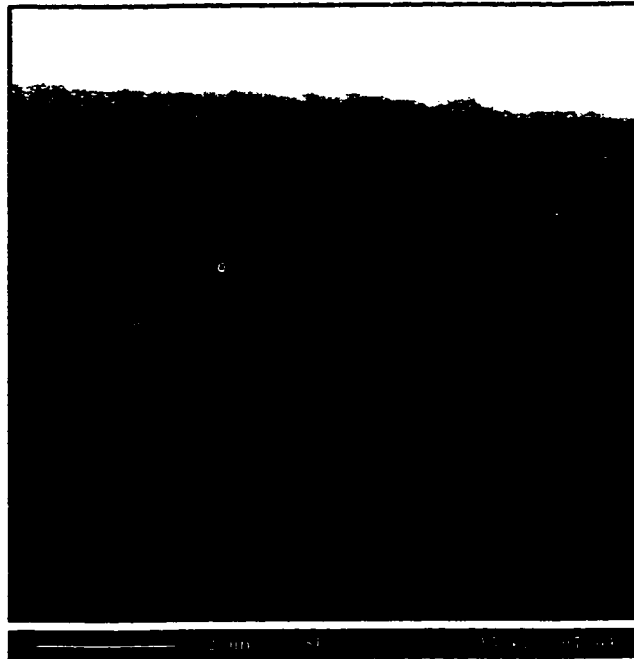
Figure 4.8:   SEM Image of 0.1 μm Anodized Alumina Membrane Cross-section
(imaged by M. Pierson, Dept. Geology, Rice U.)

4.3.0   Atomic Force Microscopy

While SEM images were useful in assessing the qualitative features of the membranes, atomic force microscopy produced detailed topological maps of the microscopic features on the surface of these membranes. AFM images reveal the morphology, pore size, grain size and roughness of membrane sample surfaces. Different

alumoxane based alumina membranes are compared to each other, and are also compared to anodized alumina and PCTE membranes.

4.3.1 Alumoxane Samples

Although some differences between alumoxane-based membranes were observed by AFM, the similarities between membranes made from different alumoxanes are more striking. Many variations between images seemed to be more of a function of the tip used (i.e. old or new) and imaging resolution, than of actual differences between samples. The nodular morphology seen by SEM was also evident in AFM images. This morphology is interpreted as due to of tightly packed grains creating images with peaks and valleys.

4.3.1.a Pre-fired A-alumoxane Membranes

A 10 μm scan of pre-fired A-alumoxane (Figure 4.9) is quite blurry, but shows large granules on the order of 50 nm. The size of A-alumoxane particles in solution was reported by Callender *et al.* (1997) to range from 5 to 65 nm. At 1 μm (Figure 4.10), the grains better reflect the reported particle size, with a surface appearing yet more craggy. The presence of the organic ligand in flexible long chains may cloak, or blur, the features of the alumoxane it is bonded to.

X   2.000 µm/div
Z   50.000 nm/div

view angle
light angle

0 deg
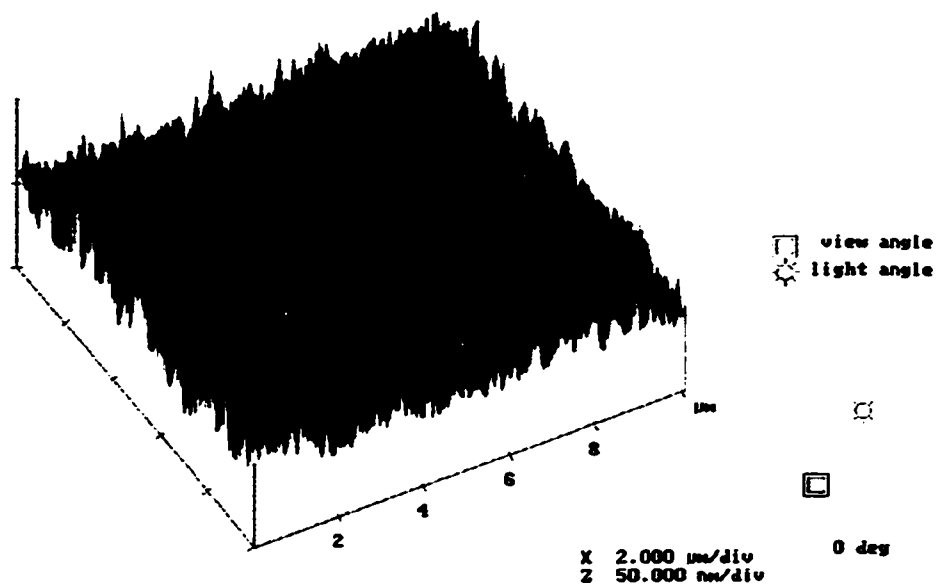
Figure 4.9: 10 µm AFM Scan of Prefired A-alumoxane

X   0.200 µm/div
Z   25.000 nm/div

view angle
light angle

0 deg
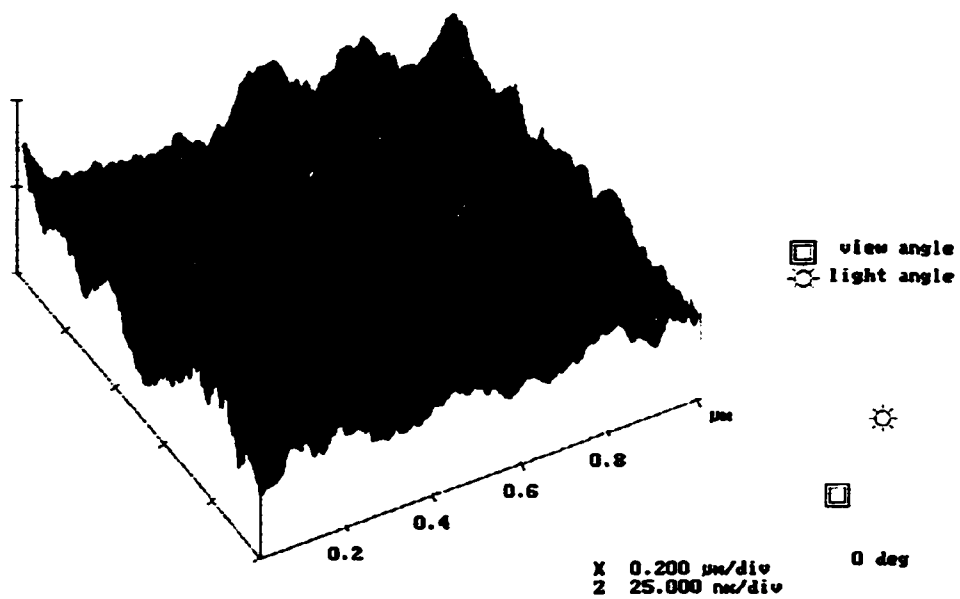
Figure 4.10: 1 µm AFM Scan of Prefired A-alumoxane

4.3.1.b A-alumoxane based Alumina Membranes

A 10 μm image (Figure 4.11) of fired AA shows looks similar to the pre-fired image with grains somewhat sharper and narrower. When the AA is sintered, the peaks seen in the 1 μm scan (Figure 4.12) become much more defined and are smaller than those of the prefired sample. A 200 nm scan of the AA (Figure 4.13) clearly shows surface pore openings between the grains, which may be connected to a network of interstitial spaces. This scale is considerably smaller than the dimension of the possible "pore openings" evident in Figure 4.6. Thus, the features in the 1 μm and 200 nm scans can be attributed to a scale of porosity that likely characterizes the "solid" areas in Figure 4.6.

X 2.000 μm/div
Z 50.000 nm/div

Figure 4.11: 10 μm AFM Scan of AA

NanoScope   Tapping AFM
Scan size   1.000 um
Setpoint   1.265 V
Scan rate   2.001 Hz
Number of samples   256

view angle
light angle

0.8

0.6

0.4

0.2

X 0.200 um/div   0 deg
Z 25.000 nm/div

JL41098.003

Figure 4.12: 1 μm AFM Scan of AA

NanoScope   Tapping AFM
Scan size   200.0 nm
Setpoint   1.065 V
Scan rate   2.001 Hz
Number of samples   256

view angle
light angle

150

100

50

X 50.000 nm/div   0 deg
Z 20.000 nm/div

JL41098.008
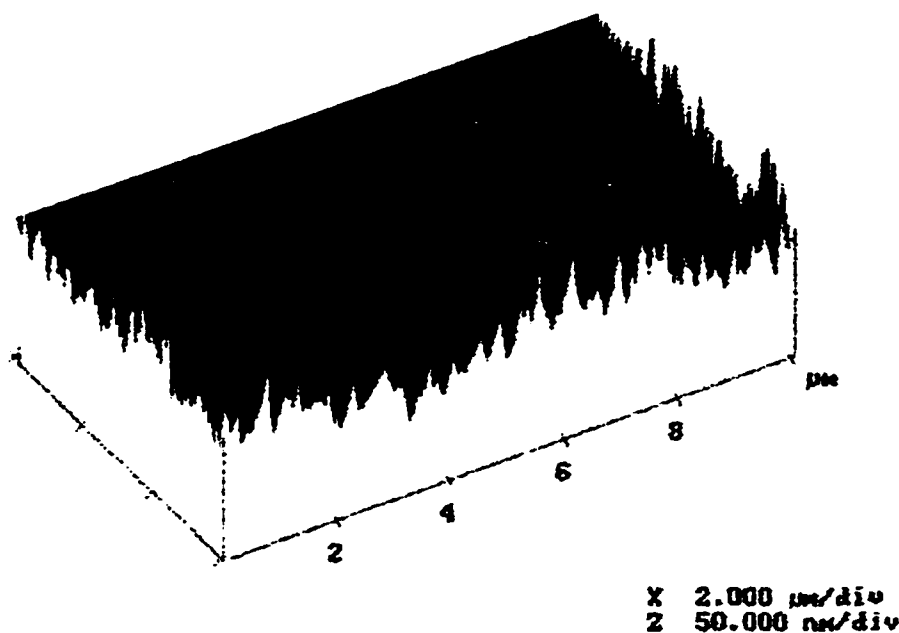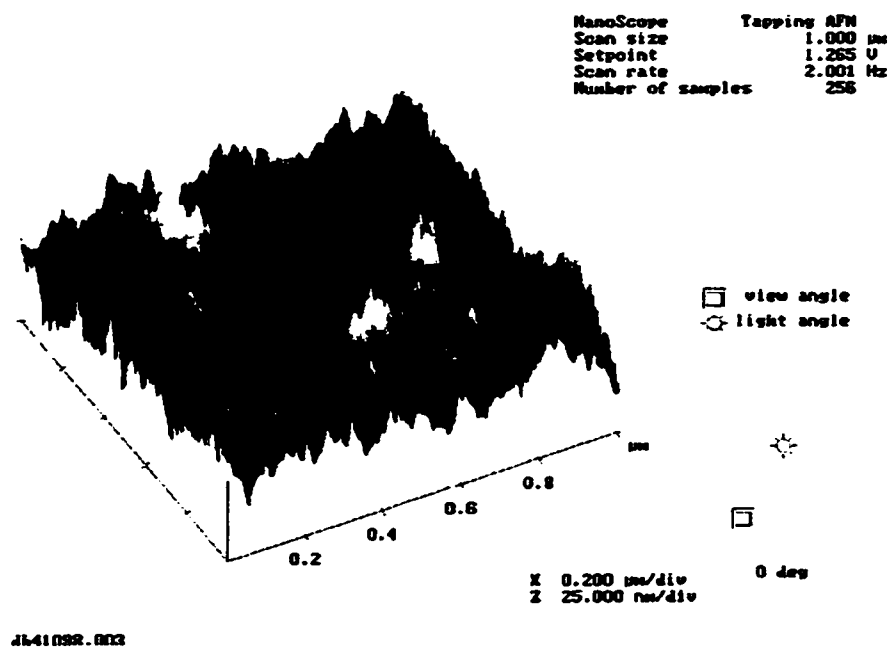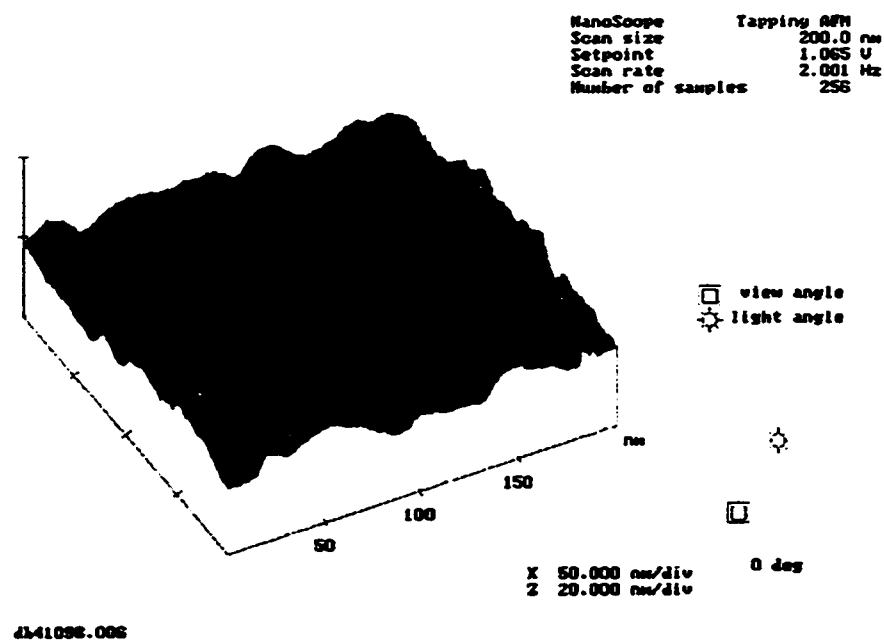
Figure 4.13: 200 nm AFM Scan of AA

4.3.1.c MEA-alumoxane based Alumina Membranes

Though at 10 μm MEAA appears to be identical to AA, a 1 μm scan (Fig 4.14),

while similar to that of AA, shows much smoother peaks. A 200 nm image (Fig. 4.15)

reveals pores that are slightly larger than those in the AA. In light of the BET results for the

two membrane types presented in section 4.4.2, subtle differences between the AFM

images for MEAA and AA appear to reflect slight changes in membrane pore size.

Figure 4.14: 1 μm AFM Scan of MEAA

```
NanoScope          Tapping AFM
Scan size              200.0 nm
Setpoint             0.9852 U
Scan rate            1.969 Hz
Number of samples        256
```

db31898.006
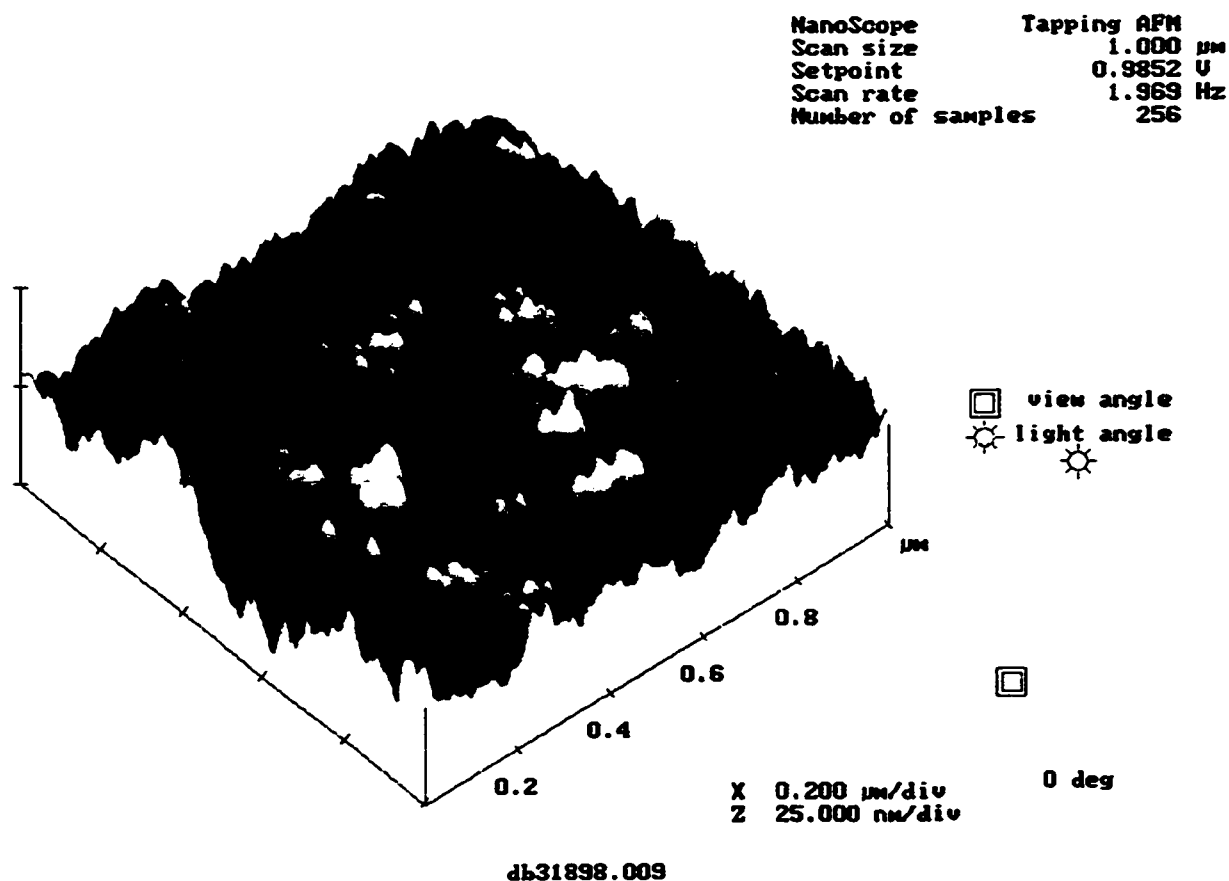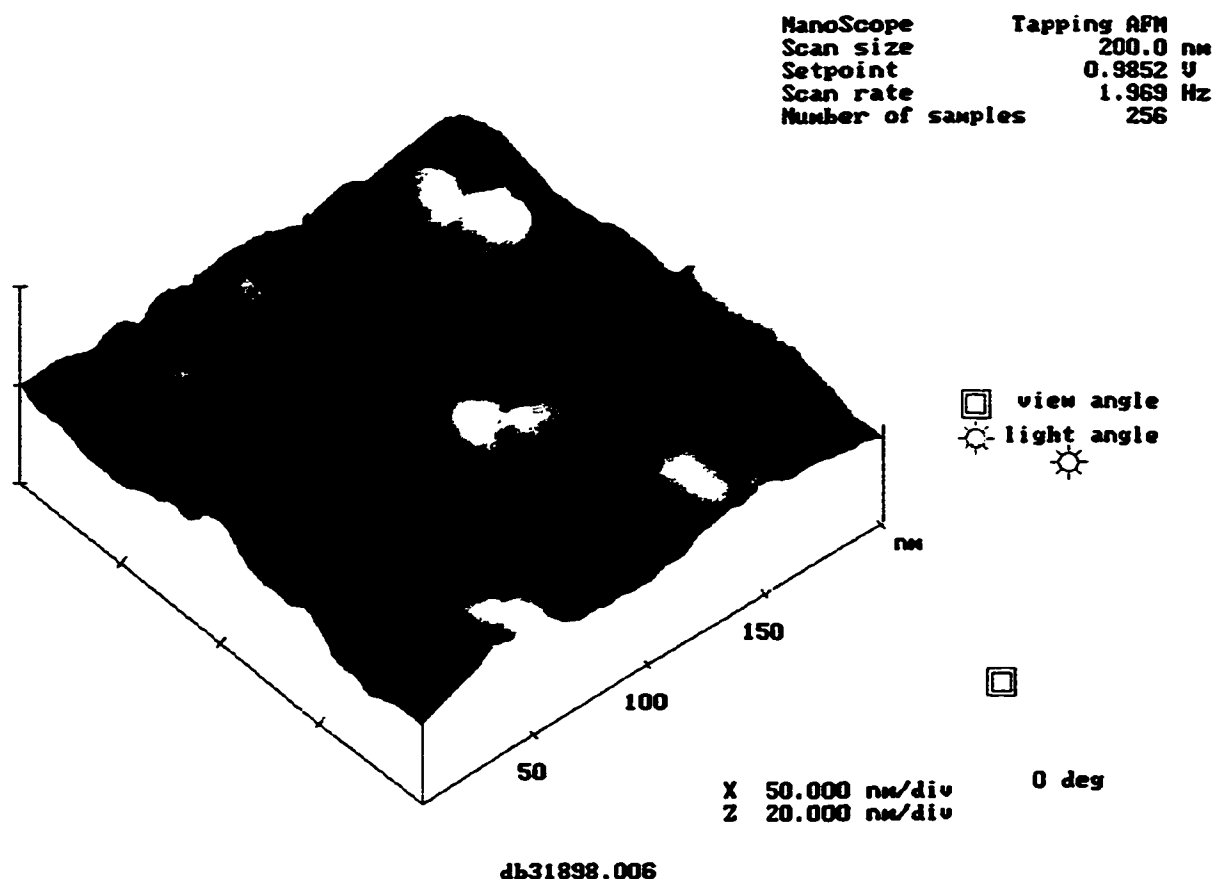
Figure 4.15: 200 nm AFM Scan of MEAA

4.3.1.d Chemically & Physically Mixed Alumoxane Samples

The chemically and physically mixed samples appeared quite similar to one another, but tended toward the MEAA membrane rather than the AA membrane in appearance. At 1 µm fairly smooth peaks are visible. The chemical mix [1;1]:0, for example, is pictured in Figure 4.16 with 1 µm and 200 nm scans virtually indistinguishable from those of MEAA and AA.

a)

b)
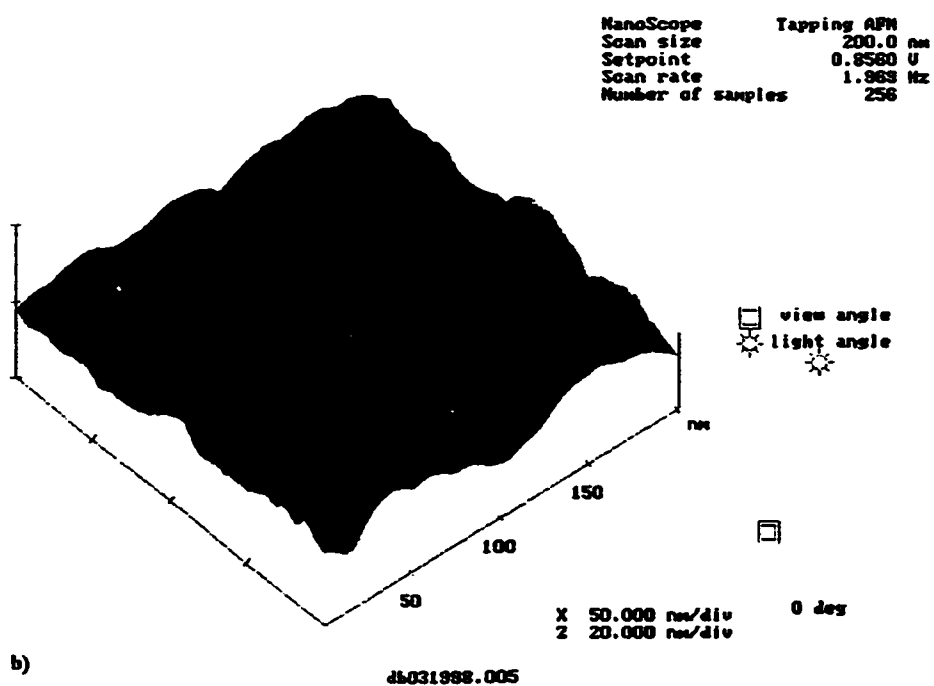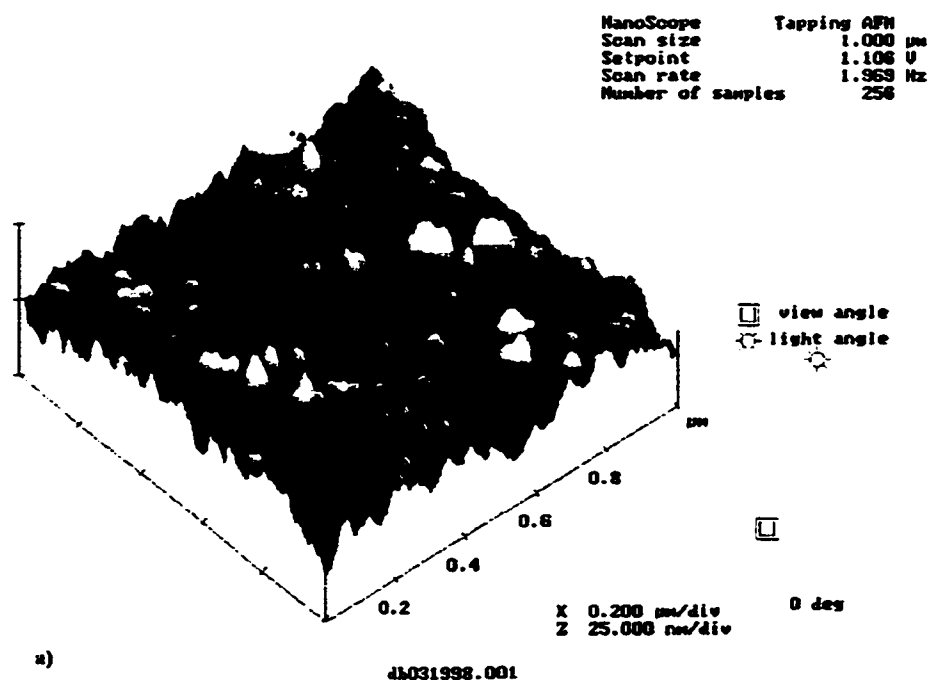
Figure 4.16: AFM Images of the Chemical Mix [1;1]:0 Sample
a) 1 μm Scan, b) 200 nm Scan

4.3.2 Anodized Alumina Samples

AFM images of a 0.02 μm anodized aluminum membrane clearly show the open-cellular pore morphology with a honeycomb structure seen in the SEM images of the previous section. The honeycomb structure of the support side (0.2 μm pores) is easily visible in the 10 μm scan shown in Figure 4.17, and distinct straight pores can be seen at 2 μm (Figure 4.18).
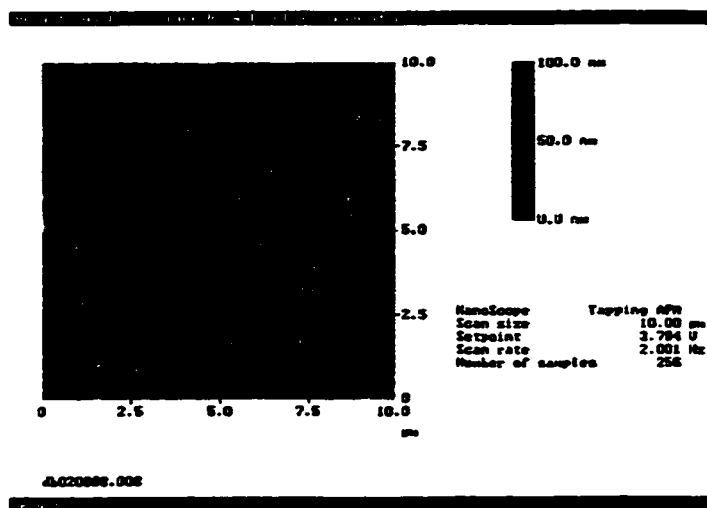
Figure 4.17: 10 μm AFM Image of 0.02 μm Anodized Alumina Membrane Support
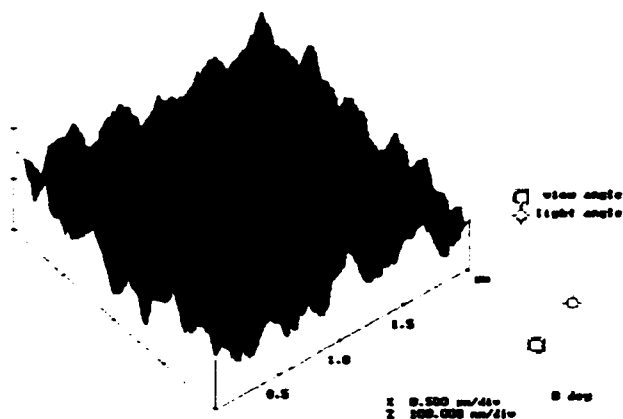
Figure 4.18: 2 μm AFM Image of 0.02 μm Anodized Alumina Membrane Support

The membrane skin layer does not reveal the honeycomb structure until the resolution is increased to 1 µm² (Figure 4.19). One can identify straight, fairly regular pores in this image, and a few pores which have merged, hence the open-cellular designation. The open-cellular structure is illustrated further in Figure 4.20. Here a 200 nm scan of the membrane shows several pores that are connected and several other pores with clearly defined surrounding walls.
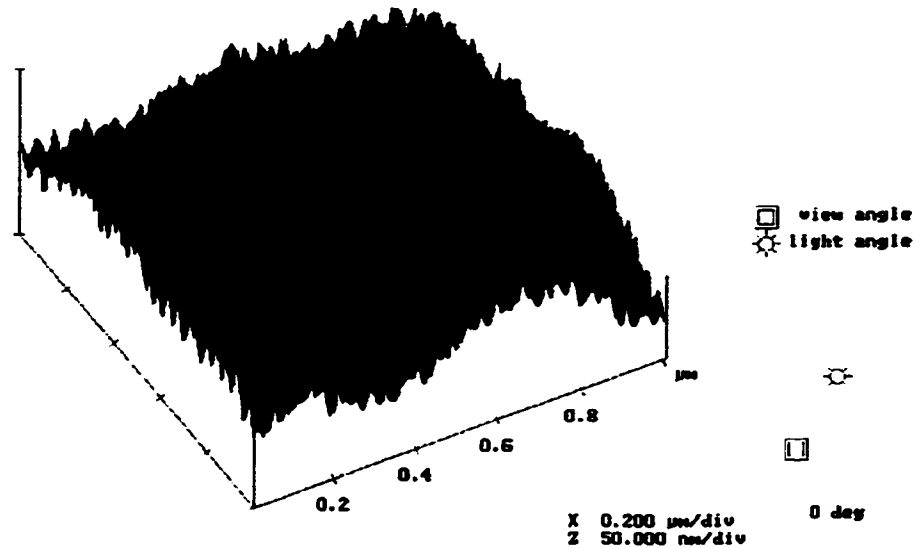
Figure 4.19: 1 µm AFM Image of 0.02 µm Anodized Alumina Membrane (Skin Layer)
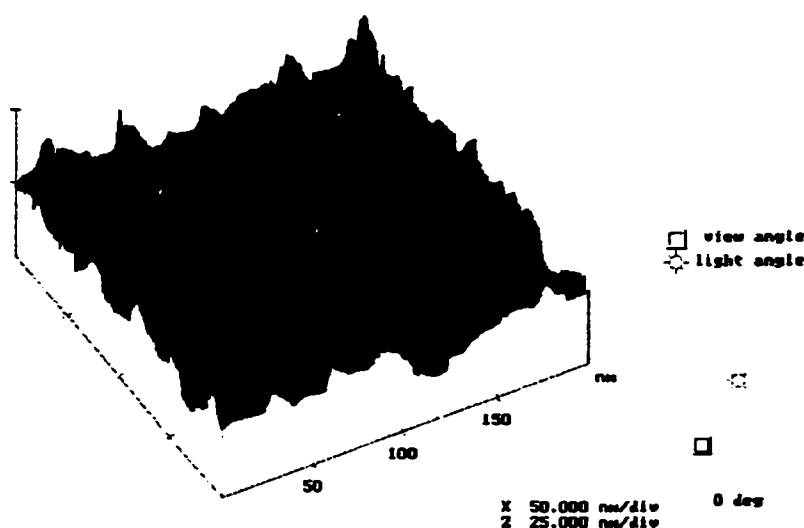
Figure 4.20: 200 nm AFM Image of 0.02 μm Anodized Alumina Membrane (Skin Layer)

This sample, based on several images, has a pore density of roughly 1×10^{10} pores per cm^2 of membrane surface area, which is considerably less than that reported by the manufacturer (1×10^{12} pores/cm^2).

4.3.3 Polycarbonate Track-etched Samples

Though the morphology of the polycarbonate track-etched membranes appears similar to the nodular morphology of the alumoxane-derived membranes, it has in fact a closed-cellular pore structure, resulting from the track-etching process. Figure 4.21 shows a 1 μm scan of the membrane with shallow rounded peaks. A 200 nm scan (Figure 4.22) has a fairly even surface with clearly visible cylindrical pores. It should be noted that the apparent fuzziness of both of these images is attributable to a small amount of noise, which is amplified in flatter samples with narrow height ranges such as these. The pore density of the PCTE membrane, which is roughly 1×10^9 pores/cm^2, is considerably less than that for the anodized alumina sample. Surprisingly, it is significantly higher than the range

reported by the manufacturer (1×10^6-6×10^8 pores/cm^2). Though it is difficult to count the

less clearly defined pores of the alumoxane-derived membranes, the anodized alumina and

PCTE samples both seem to have smaller pore densities.
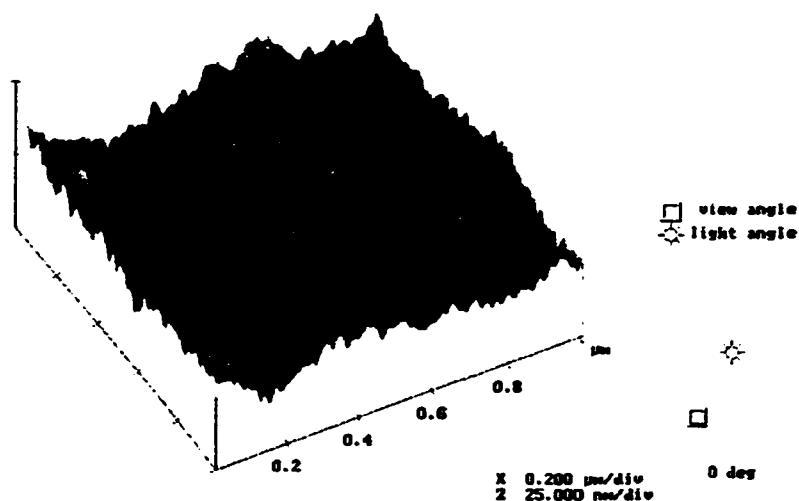
Figure 4.21: 1 μm AFM Image of the 15 nm Polycarbonate Track-etched Membrane
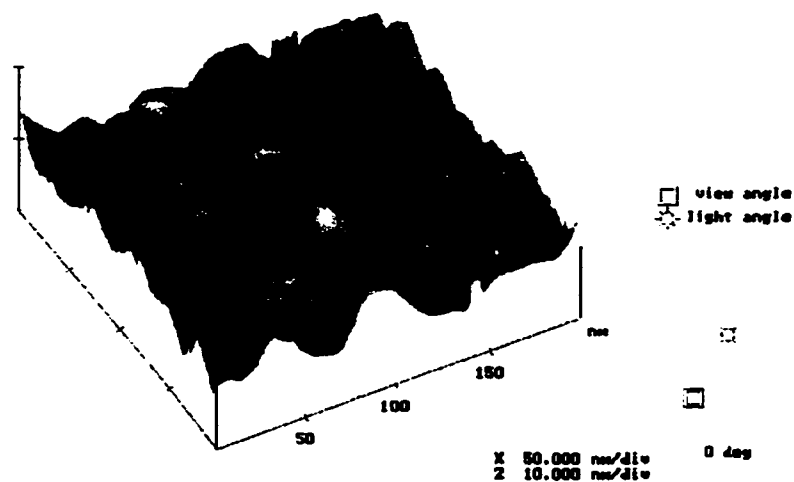
Figure 4.22: 200 nm AFM Image of the 15 nm PCTE Membrane

4.3.4 Section Analysis

A line section of any AFM image can be made with the accompanying AFM software. When a line is drawn on an image, the topology across the line is shown, and cursors can be placed around features, such as pores, showing their size. Some examples of section analysis are shown in Figures 4.23-6, including sections of AA, MEAA, 0.02 μm anodized alumina, and a 15 nm PCTE membrane.

Cursor	Marker	Spectrum	Zoom	Center Line	Offset	Clear

Section Analysis

L	14.844 nm
RMS	0.717 nm
lc	DC
Ra(lc)	0.538 nm
Rmax	2.201 nm
Rz	1.412 nm
Rz Cnt	4

Spectrum

Surface distance	20.894 nm
Horiz distance(L)	18.750 nm
Vert distance	0.262 nm
Angle	0.799 deg
Surface distance	13.954 nm
Horiz distance	11.719 nm
Vert distance	1.016 nm
Angle	4.956 deg
Surface distance	15.723 nm
Horiz distance	14.844 nm
Vert distance	0.362 nm
Angle	1.398 deg
Spectral period	DC
Spectral freq	0 Hz
Spectral RMS amp	0.463 nm

db41098.006

Cursor: fixed   Zoom: 2:1   Cen line: Off   Offset: Off

Figure 4.23: AFM Section Analysis of AA
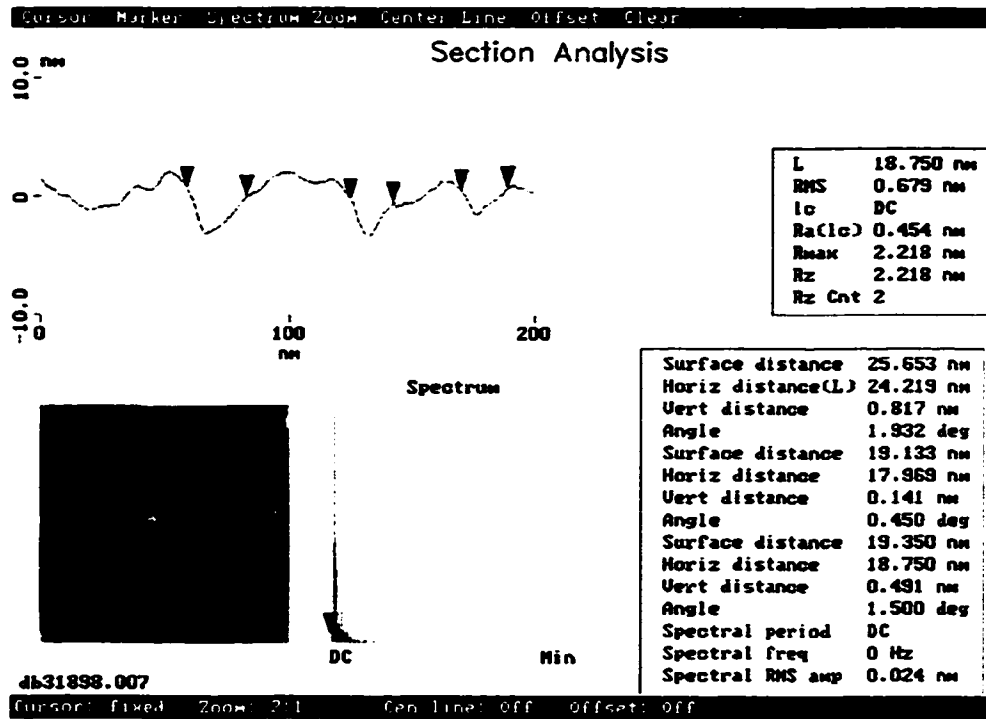
Figure 4.24: AFM Section Analysis of MEAA
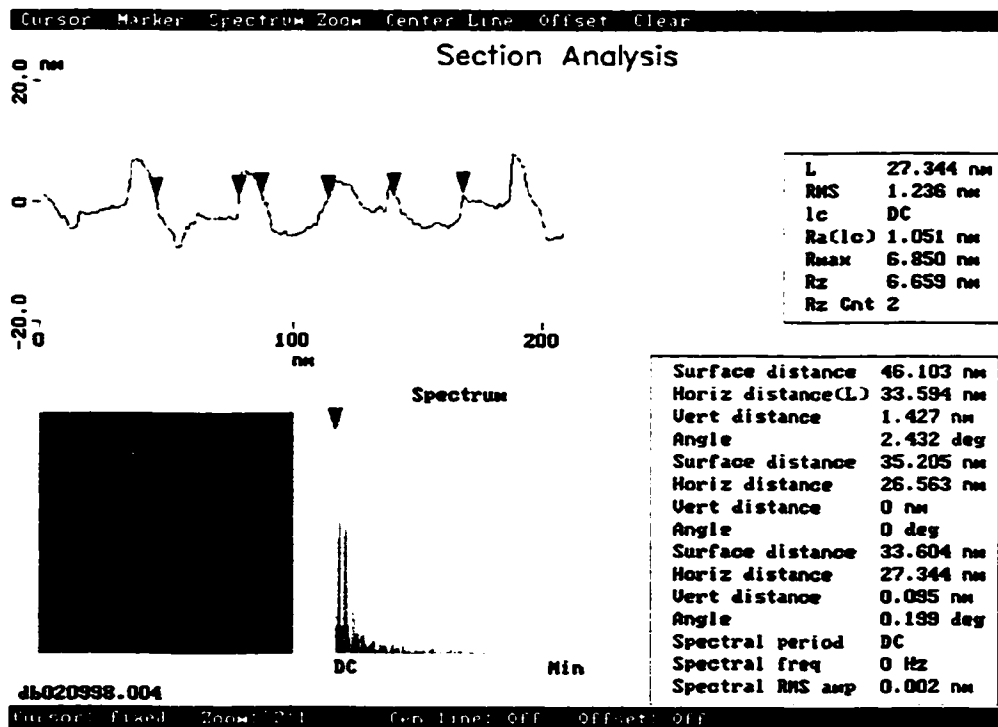
Figure 4.25: AFM Section Analysis of 0.02 μm anodized alumina

Section Analysis

L	29.688 nm
RMS	1.201 nm
Ic	DC
Ra(lc)	0.914 nm
Rmax	4.064 nm
Rz	2.248 nm
Rz Cnt	8

Surface distance	31.242 nm
Horiz distance(L)	29.688 nm
Vert distance	0.092 nm
Angle	0.177 deg
Surface distance	35.022 nm
Horiz distance	33.594 nm
Vert distance	0.053 nm
Angle	0.091 deg
Surface distance	34.405 nm
Horiz distance	29.688 nm
Vert distance	0.025 nm
Angle	0.048 deg
Spectral period	DC
Spectral freq	0 Hz
Spectral RMS amp	0.973 nm

Spectrum

db40198.005

Figure 4.26: AFM Section Analysis of 15 nm PCTE

The AA, MEAA, and PCTE sections have sharp well-like dips indicating pores, while the section of the anodized alumina shows jagged peaks with pores that look like trenches. Table 4.1 lists several pore size approximations from section analysis.

Table 4.1: Approximate Pore Sizes of Samples from AFM

	Approximate Pore Size (nm)	# Pores Measured
AA -Alumoxane	16	6
MEAA -Alumoxane	23	9
0.02 μm Anodized Alumina	30	10
15 nm Polycarbonate Track-etch	27	11

There are relatively few sections taken for each sample, however, the pore sizes serve as a qualitative comparison to those from nitrogen adsorption (section 4.4) and those supplied by manufacturers. Pradanos *et al.* (1996) and Dietz *et al.* (1992) have both indicated that pore size can be considerably overestimated by AFM due to pore entrance geometry and the size of the cantilever tip used. Figure 4.27 illustrates overestimation of pore size due to pore entrance geometry, which is especially problematic in interstitial pores, such as those of alumoxane based membranes.

Interstitial Pore Space

Interstitial Space

Pore Diameter at Opening

Pore Diameter at Neck
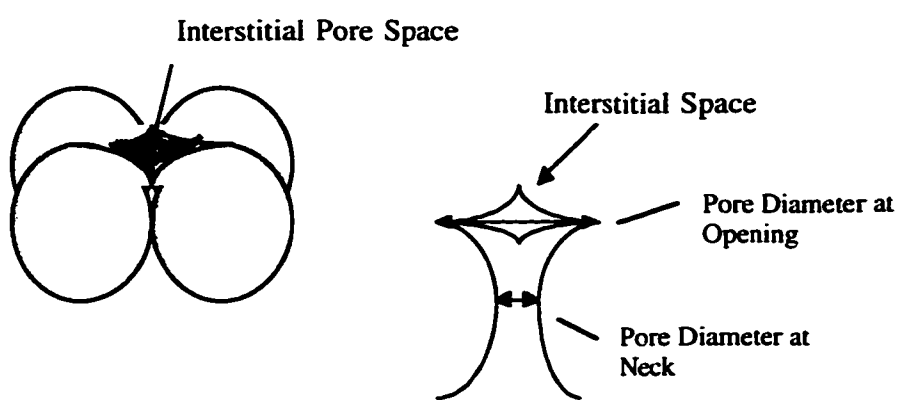
Figure 4.27: Overestimation of Pore Size for Nodular Morphologies

The pore size measured by AFM is actually representative of the pore opening, yet the neck of the pore is ultimately the effective pore size. This may be partially responsible for the larger pore sizes of ca. 16 - 23 nm for the alumoxanes measured from AFM images compared to the pore sizes of ca. 10 - 15 nm from nitrogen sorption measurements (section 4.4). The measurements for the straight pores of the anodized alumina and PCTE membranes should not be affected by this problem. The manufacturers rated pore size, however, is considerably smaller for both membranes: 20 nm rated v. 30 nm measured pore size (by AFM) for anodized alumina and 15 nm rated vs. 31 nm measured pore size (by AFM) for the PCTE sample.

4.3.5 Roughness

Roughness is a highly variable parameter, changing depending on scan sizes and locations. Nevertheless, it serves as a useful comparison tool for different membrane types. Alumoxanes have a roughness of ca. 3-5 nm, that varies little between samples. Roughness of the alumoxane-derived membranes were observed to be slightly less than that of the anodized alumina and slightly more than that of the PCTE membrane. Table 4.2 lists the average roughness of samples from 1 μm scans.

Table 4.2: Average Roughness Measured from 1 μm Scans

	Roughness (nm)	# Scans Measured
AA -Alumoxane	5.2	3
MEAA - Alumoxane	3.2	3
0.02 μm Anodized Alumina	6.5	1
15 nm Polycarbonate Track-etch	2.8	3

As discussed in Section 2.1.8, roughness is important because it can have a large impact on fouling of a membrane. It should be noted that of the alumoxane based membranes, AA is the most rough, however, there is no trend of decreasing roughness with hybrid samples that contain more MEAA than AA. This suggests that roughness is partially resultant of processing methods and is not solely a function of raw materials used.

4.3.6 Artifacts

Extreme care was taken to avoid artifacts in AFM imaging, since they are quite common with this technique. Samples initially showed a corrugated surface, which scaled appropriately with changing scan sizes and angles. The perfectly corrugated images, however, were actually

caused by interference in the detection of the laser beam, and were not at all representative of the samples. Another serious artifact experienced was convolution of the sample with the tip. This occurs when a tip is damaged, misshapen, or simply dulled, and creates images with repeating units of the same size and shape, reflecting the size and shape of the tip, not necessarily the sample surface. An example of this type of artifact is shown in Figure 4.28. The sample, [1;1]:1 alumoxane, shows repeating triangular units because of a damaged tip.

0	10.0 μm 0		5.00 μm
Data type	Height	Data type	Height
Z range	50.0 nm	Z range	50.0 nm

a)   b)
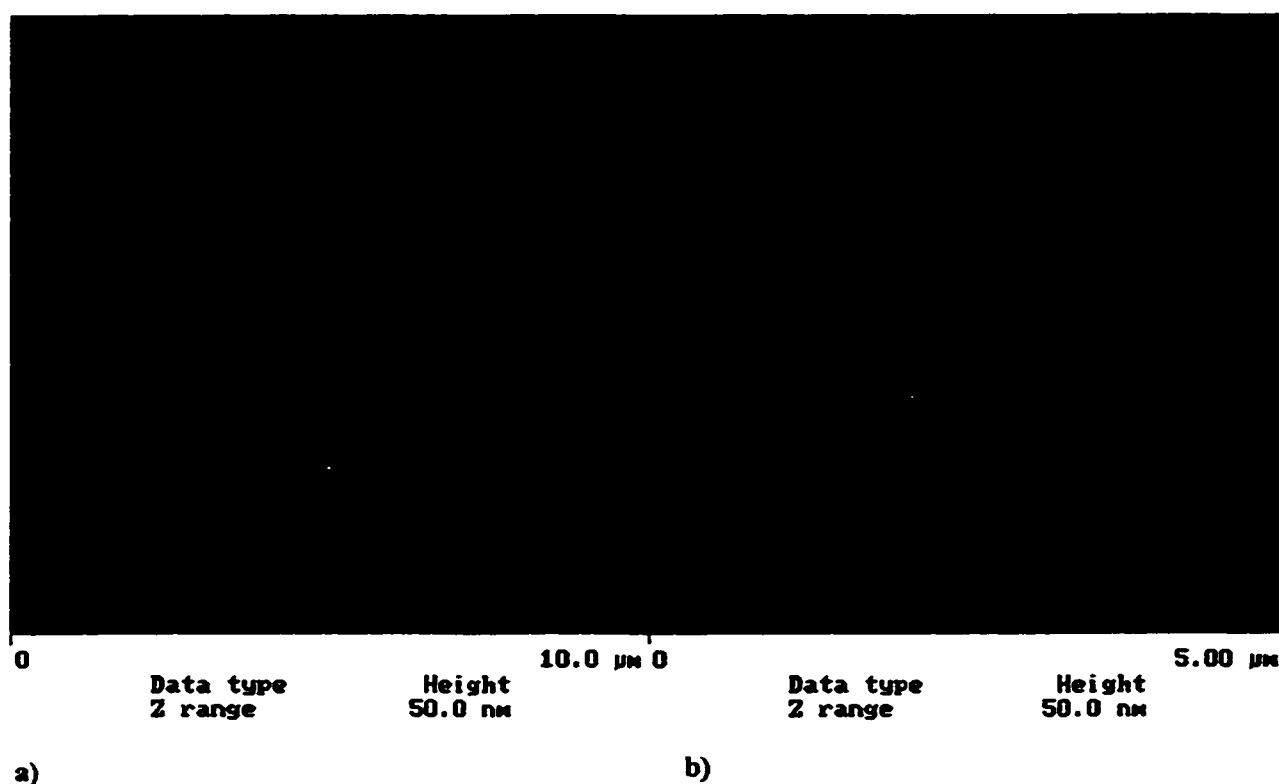
Figure 4.28: An AFM Image artifact on Sample [1;1]:1, a) 10 μm Scan, b) 5 μm Scan

4.4.0 Nitrogen Adsorption/Desorption

Nitrogen adsorption/desorption measurements based on BET theory were performed to obtain total surface area, porosity, pore size distribution and average pore size of PCTE, anodized alumina, and alumoxane-derived membranes. A surface area standard, supplied by the manufacturer of the adsorption apparatus, was used to calibrate the machine. Although this standard could not be used to verify pore size distribution, the BJH method used to derive pore size distribution is partially based on the BET theory used to calculate surface area, hence the standard is acceptable. Because they are well characterized in the literature, PCTE and anodized alumina membranes were examined in an attempt to gain greater confidence in interpreting data. However, the PCTE membranes are extremely thin and therefore did not constitute a large enough sample for accurate measurement. 100 (13 mm) PCTE membranes weigh ca. 0.09 grams; sample size must be 1 - 5 grams for low surface area materials such as this one, which has a reported surface area of ca. 1.5 m²/g (Pradanos et al., 1996). Anodized alumina samples were also problematic because they are asymmetric. The pore size of the support layer, which cannot be separated from the membrane skin, lies outside of the accepted pore size range applicable to BET theory. Based on the mass of material introduced and the appearance of this material in AFM and SEM images, the alumoxane-derived membranes were not considered to be limited by factors that prevented measurement of the PCTE and anodized membranes.

The isotherms produced from the alumoxane-derived membranes were all nearly identical. The characteristic isotherm of this material (Figure 4.29) can be classified as type IV, which is typical of a mesoporous solid. The hysteresis region of the isotherm can be further classified as H1 (IUPAC designation), because of its nearly vertical shape. An H1 designation is common for agglomerates or compacts of spherical particles of uniform size

and packing (Gregg and Sing, 1982). The range of relative pressure that the hysteresis spans is correlated directly to the pore size distribution of the material using the Kelvin equation (Equation (9), section 2.1.7.2). The narrow width of the hysteresis in Figure 4.29 is indicative of a narrow pore size distribution.
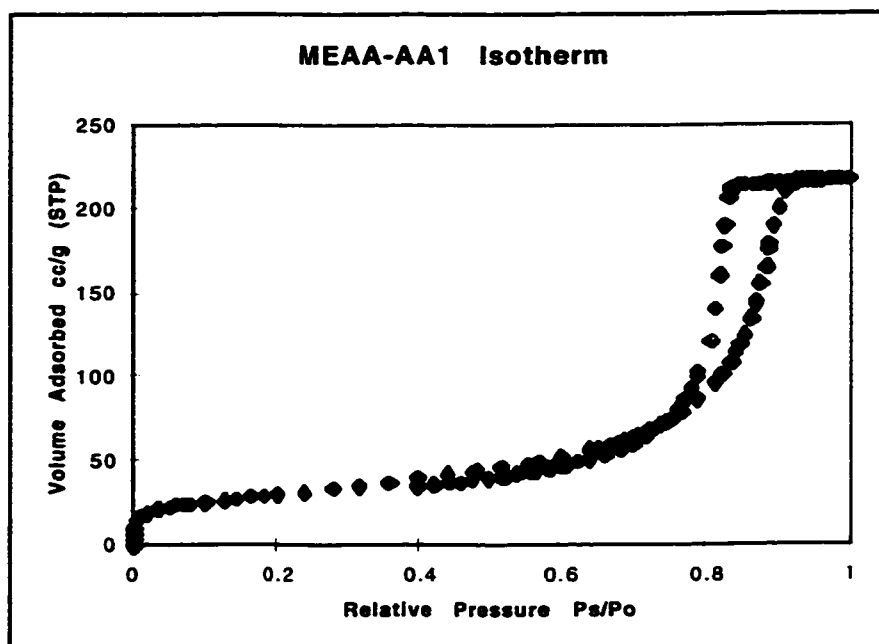
Figure 4.29: Typical Nitrogen Adsorption/Desorption Isotherm for Alumoxane-derived Membranes

4.4.1 Surface Area and Porosity

Surface area and porosity are directly related to each other. Membranes with higher surface areas have higher porosities, which contribute to higher permeabilities. The surface area and porosity of alumoxane-derived membranes are shown in Figure 4.30, with samples represented by their fraction of MEAA (f_{MEAA} = 0 is AA and f_{MEAA} = 1 is MEAA). The surface area of the chemical and physical mixes both increase slightly and then decrease slightly as the fraction of MEAA increases. The third point of the chemical mix series, 1;1:2, has a surface area that stands out as being slightly high. All of the samples, however, are similar on a relative scale, ranging from 114 m^2/g (AA) to 169 m^2/g (1;1:2).

The range of porosity for alumoxane-derived membranes is also quite narrow. Porosity

increases slightly as the fraction of MEAA increases from 54% (AA) to 69% (1;0:0.5).
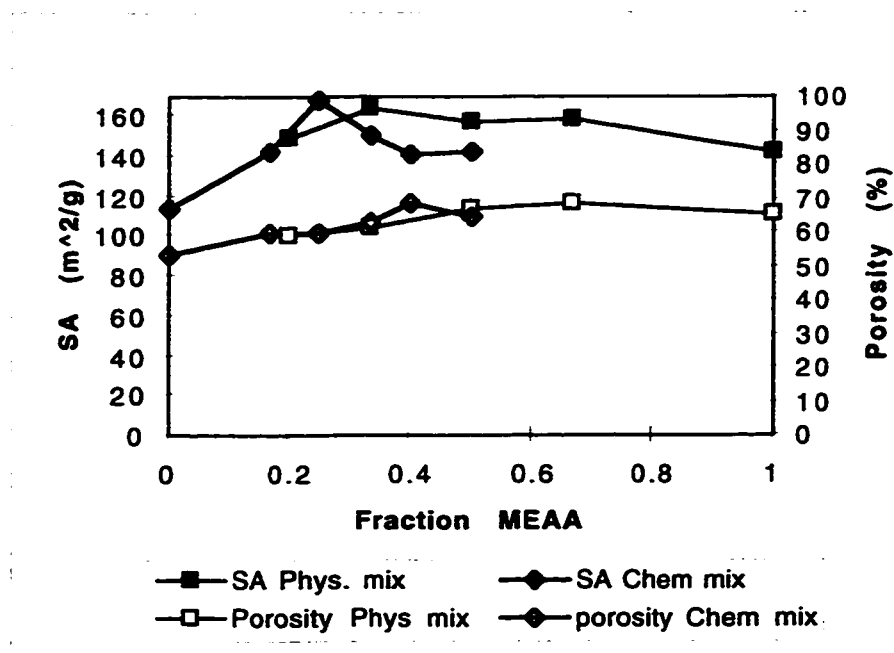
Figure 4.30: Surface Area & Porosity of Alumoxane-derived Membranes

The porosity and surface area of alumoxane-derived, anodized alumina, and PCTE

membranes are listed in Table 4.3. The porosity of the anodized alumina and particularly

the PCTE membranes are considerably less than those for alumoxane-derived membranes.

The surface area of the PCTE membrane is also two orders of magnitude less than that for

the alumoxane-derived membranes. These differences are quite significant. However,

they are typical when comparing straight-pore to tortuous pore membranes. Tortuous pore

membranes, such as the alumoxane based, inherently have a high porosity and surface area;

this improves their permeability, which is lessened by the tortuosity.

Table 4.3: Surface Area and Porosity

Membrane Type	Surface Area (m²/g)	Porosity (%)
Alumoxane-derived	114 - 169	54 - 69
Anodized Alumina	-	25 - 30*
PCTE	1.5**	< 15*

* reported by manufacturer, ** reported by Pradanos *et al.*, 1996

4.4.2 Pore Size Distribution and Average Pore Size

Alumoxane-derived membranes have fairly narrow pore size distributions. All of the chemically and physically mixed samples have distributions falling between that of AA and MEAA (Figure 4.31). Over 90% of the pore volume of MEAA falls between 5 and 25 nm, and over 90% of pore volume in AA is between 5 and 15 nm.
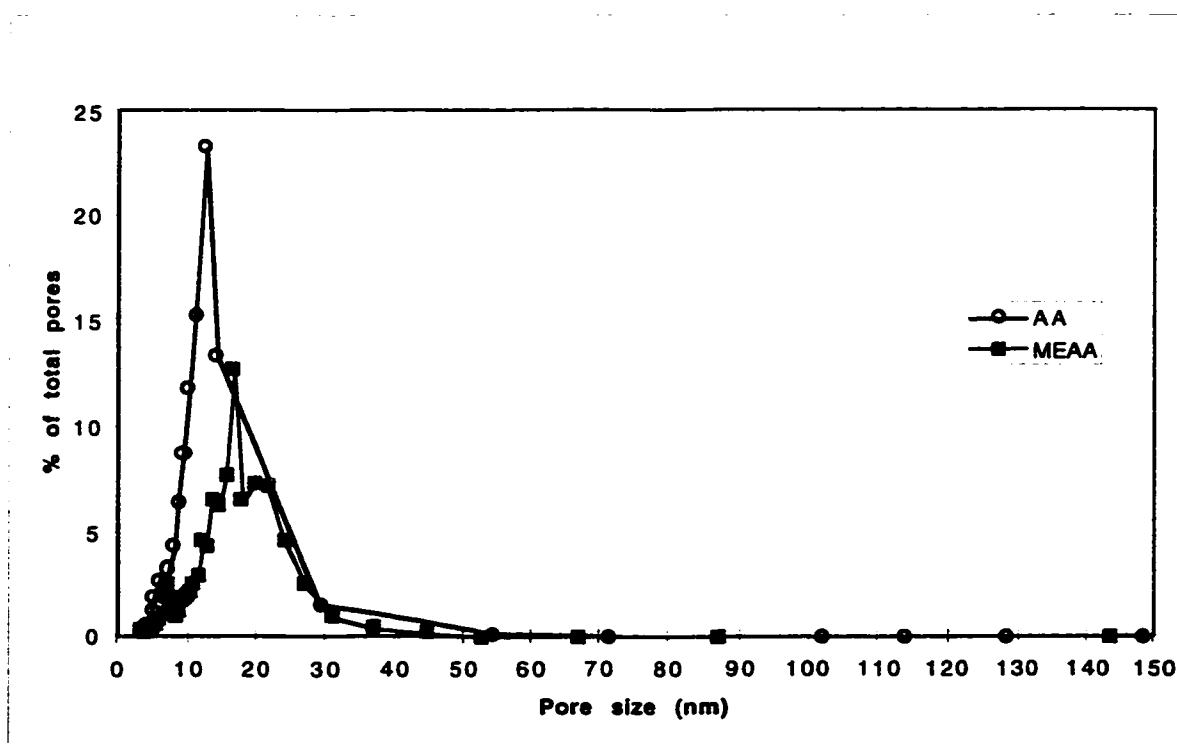
Figure 4.31: Adsorption Pore Volume Distribution for AA and MEAA

The narrow size range of the boehmite precursor particles are predominantly responsible for narrow pore size ranges of the alumoxane-derived particles. The boehmite precursor particles also have the potential to be centrifuged into finer and tighter particle size distributions, thus producing specialized membranes with extremely narrow pore size distributions.

Average pore sizes and standard deviations were calculated from the adsorption branch of the isotherm, which is more reliable for alumina (Cranston and Inkley, 1957). The average pore size ranges from 9.5 nm (1;1:2) to 15.3 nm (1;1:0.5) and standard deviations are quite low, ranging from 4.3 to 8.0 nm (Table 4.4). The prefired AA has an average pore size of 5.5. Because pore sizes increase upon firing, this represents the smallest pore size achievable for this particular boehmite precursor.

Table 4.4: Average Pore Size & Standard Deviation for Alumoxane-derived Membranes

Sample	Fraction MEAA	Avg. Pore Size (nm)	Std. Dev. (nm)
Prefired AA	0	5.5	4.3
AA	0	10.7	4.3
1;1:4	0.167	10.7	7.1
1;0:4	0.2	10.5	8.0
1;1:2	0.25	9.5	6.1
1;0:2	0.33	10.3	6.2
1;1:1	0.33	11.6	5.0
1;1:0.5	0.4	15.3	5.3
1;0:1	0.5	13.3	5.5
1;1:0	0.5	13.8	5.5
1;0:0.5	0.67	14.6	5.4
MEAA	1	15.0	6.3

Figure 4.32 shows the average pore size for each sample by the fraction of MEAA. Pore size clearly increases with increasing MEAA. Samples with fractions of MEAA less than 1/3, as for AA, 1;1:4, 1;0:4, 1;1:2, 1;0:2, and 1;1:1, have average pore sizes close to 10 nm. The 1;1:2 sample, which had an uncharacteristically high surface area, has a lower average pore size than the AA. This could be due to a higher number of very small pores, which increase surface area significantly while lowering average pore diameter. Samples with higher MEAA fractions (greater than 1/3), including 1;1:0.5, 1;1:0, 1;0:1, and 1;0:0.5, have pore sizes closer to that of MEAA. The 1;1:0.5 sample stands out as having a higher average pore size than MEAA. A small number of larger pores present can have a significant impact, raising the average pore size, which is possibly the case with this sample.
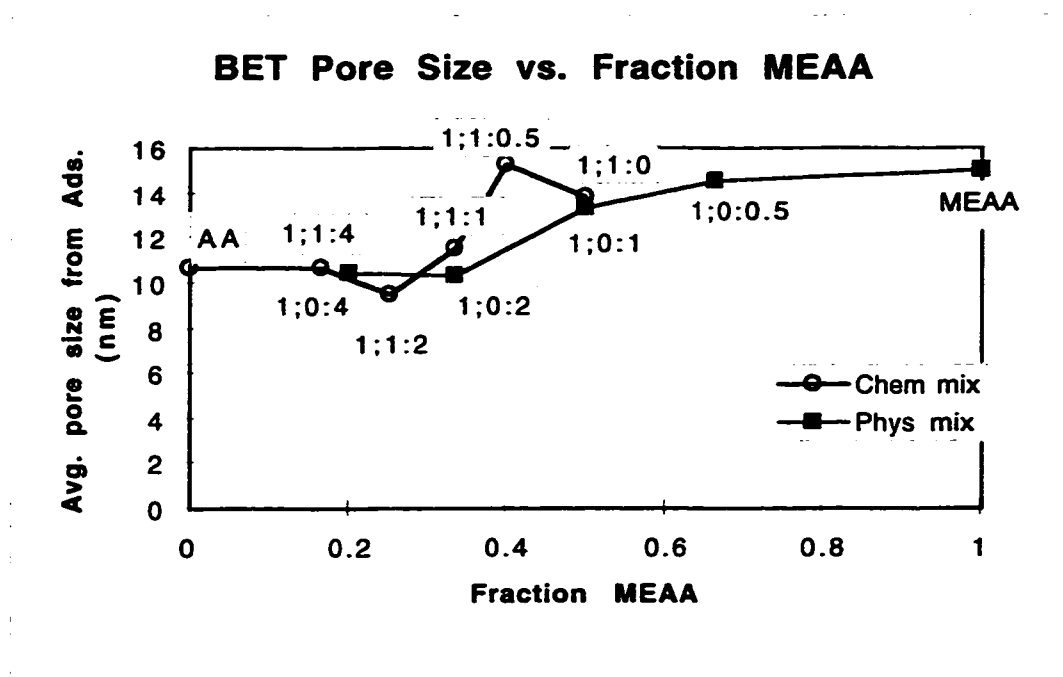
Figure 4.32: Average Pore Size of Alumoxane-derived Membranes

4.5.0   Permeability

Permeability is an extremeiy important membrane characteristic, closely related to the efficiency of transport across the membrane at various driving forces. It determines the capacity of treatment available from a given amount of membrane surface area. Experimental permeabilities were obtained for alumoxane-derived membranes by measuring the passage of ultrapure water across the membrane under an applied transmembrane pressure. Results for alumoxane-derived membranes are compared to experimental permeabilities of commercial membranes, as well as calculated theoretical permeabilities.

4.5.1   Experimental Permeability of Alumoxane-derived Membranes

The permeabilities of alumoxane-derived membranes ranged from 0.3 to 1.5 nm^2. AA and mixed samples containing a majority of AA had lower permeabilities than did membranes derived from MEAA and mixtures with a majority of MEAA. Figure 4.33 shows the permeability for each sample represented by its corresponding fraction of MEAA (f_{MEAA}), where pure AA has an $f_{MEAA} = 0$ and pure MEAA has an $f_{MEAA} = 1$.

The permeabilities of alumoxane-derived membranes follow the same trend as with the average pore sizes calculated from nitrogen adsorption. The chemically and physically mixed samples have nearly identical permeabilities for samples with the same fraction of MEAA, and both generally increased in permeability with increasing fraction of MEAA. Samples with a $f_{MEAA} < 0.4$ have permeabilities close to 0.4 nm^2, while samples with a $f_{MEAA} > 0.4$ have permeabilities ranging from 0.5 to 1.5 nm^2. Two samples, [1;1]:0.5 and [1;0]:0.5 with $f_{MEAA} = 0.4$ and 0.67 respectively, are slightly out of line with the rest of the data. Their permeabilities, however, are not outside the range for alumoxanes, and may be somewhat high and low (respectively) due to experimental error. The calculated average

pore size of the [1;1]:0.5 sample, listed in the previous section, was also disproportionately high, which has a significant impact on permeability. Small increases in pore size cause larger increases in permeability, since permeability is proportional to pore size raised to the fourth power.
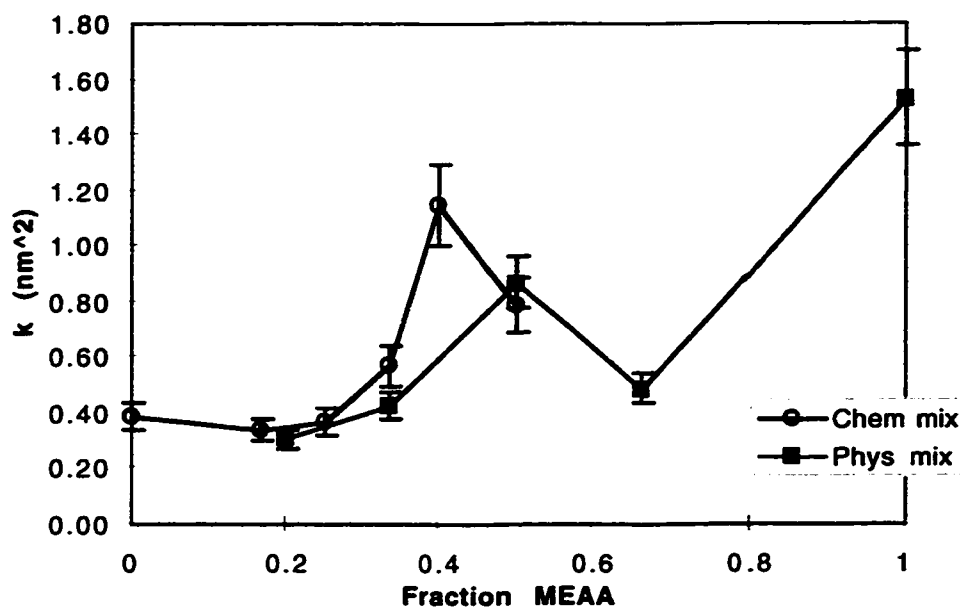
Figure 4.33: Permeability as a Function of the fraction of MEAA

4.5.2   Permeability of Commercial Membranes

Experimental permeabilities of commercial membranes with similar pore sizes to those of alumoxane based membranes are listed in Table 4.5. Anodized alumina membranes have a slightly higher permeability, largely attributable to a low tortuosity caused by their straight pores. The polycarbonate membranes, however, have a much lower permeability than the alumoxane -derived membranes, which is most likely caused by their lower pore density and average pore size. The 100,000 Dalton Cellulose Ester membrane has a permeability of 0.12 nm^2, reflecting its place on the low end of ultra-

filtration. The last two membranes are nano-filtration membranes with permeabilities of 0.05 and 0.003 nm^2, two and three orders of magnitude lower than the alumoxane-derived and anodized alumina membranes.

Table 4.5: Permeability of Alumoxane-derived Membranes and Several Commercial Membranes

Membrane Type	Permeability (nm^2)
Alumoxane-based Alumina	0.3 - 1.5
Anodized Alumina	3.0
Polycarbonate Track-etched	0.05
Cellulose Ester (100,000 D)*	0.12
Cellulose Ester (200 D)*	0.05
Polyamide (~100 D)*	0.003

* Permeabilities from Erin Devitt, Dept. Envir. Sci. & Eng., Rice U.

4.5.3 Theoretical Permeabilities

Experimental permeabilities can be compared to theoretical permeability as a rough indication of the validity of the experimental values, and also as a means of estimating the tortuosity of the membranes. Theoretical permeabilities are calculated based on pore size and pore density from BET results or directly from a manufacturer. For membranes without straight pores such as the alumoxane-derived membranes, the calculated permeability should be larger than that found experimentally, because pore tortuosity is excluded. Therefore, the calculated permeability likely represents an upper bound for a given membrane (Table 4.6).

Permeabilities calculated from measured pore size and density were roughly 6 times larger than experimental permeabilities observed for the alumoxane-derived membranes, indicating a fair amount of tortuosity. PCTE and anodized alumina membranes are both straight pore membranes by design, hence theoretical permeabilities

should be equal to those found experimentally. PCTE membranes have a theoretical permeability 0.1 times larger (10 times smaller) than the experimental permeability, when pore size and density from the manufacturer are considered. When pore size and density measured from AFM images are used, however, the ratio of theoretical to experimental permeability is 2 (in parentheses in the table). The small difference of this ratio (2 instead of the ideal 1) is most likely caused by the variation throughout samples, since AFM images came from a very small area in the middle of only one PCTE membrane sample. PCTE membranes are known to vary significantly from lot to lot (Pradanos *et al.*, 1996), and the manufacturer can only supply ranges for the membrane characteristics.

Table 4.6: Permeability and Associated Errors

Sample type	exp. k (nm^2)	theor. k/ exp. k	Exp Error (%)	% diff. from mean	# of Samples	# of Pressures
1;1:4	0.34	5	9	9	3	7
1;1:2	0.37	5	3 1	3 4	3	3
1;1:1	0.55	4	9	7	3	7
1;1:0.5	1.15	5	1 2	1 0	5	9
1;1:0	0.79	5	1 8	6	1	3
1;0:4	0.31	6	1 7	1 5	3	6
1;0:2	0.43	5	1 8	2 3	3	7
1;0:1	0.87	4	1 3	7	3	7
1;0:0.5	0.49	9	1 0	3	2	6
MEAA	1.53	3	9	6	1	3
AA	0.39	4	1 5	1 0	3	8
15 nm PCTE	0.05	0.1 (2)	9	3 4	3	9
0.02 µm Anodisc	2.93	13 (1)	6	2	2	3

Data in parentheses are based on observed measurements instead of those supplied by the manufacturer.

Theoretical permeability was 13 times larger than experimental permeability for anodized alumina using pore size and density supplied by the manufacturer. The ratio becomes approximately 1, however, when pore size and density measured by AFM are used. The

matching of theoretical and experimental permeabilities for anodized alumina signifies that

permeability experiments and AFM imaging were both producing acceptable results.

4.5.4 Experimental and Other Errors

Experimental error was calculated for each data point relative to the other points in a

single run using the following equation:

$$e = \left[100 \cdot \sum_{i=1}^{n} \left(\frac{\bar{J} - J_i}{\bar{J}} \right) \right]^{1/2}$$
(22)

where e is experimental error, $\bar{J}$ is average flux, J_i is incremental flux for time i, and n is

the number times samples were collected. Figure 4.34, for example, is a plot of the

volume of deionized water flowing through sample # 41 at given time intervals and at a

pressure of 10, 20 and 30 psi.
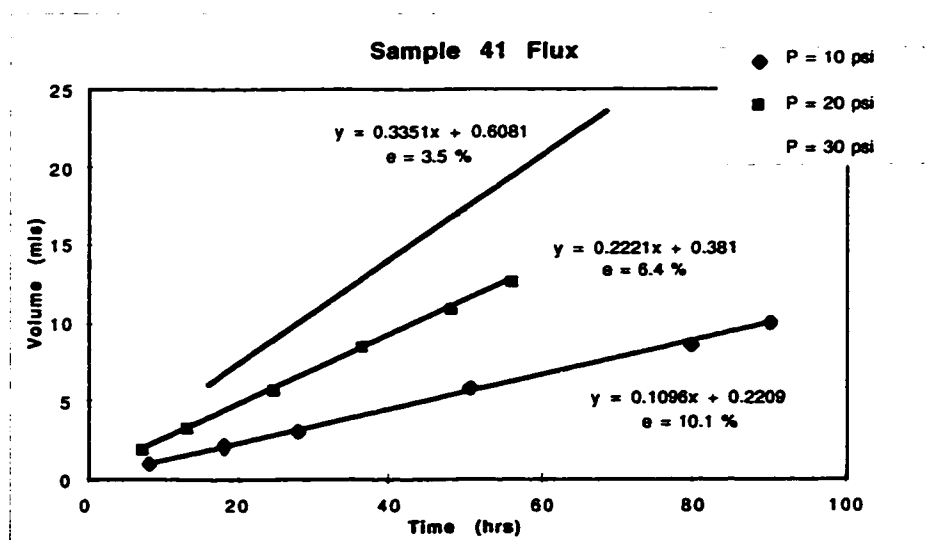
Figure 4.34: Volume per Time Measurements at Three Different Pressures

Average errors for each run are shown on the graph above; the more linear the data are, the smaller the error associated with them. The average experimental errors range from 6 to 31 % and are listed for each sample in column three of Table 4.7.

Errors for each permeability value were also calculated compared to the average permeability of a single type of alumoxane-based membrane. These error values range from 2 to 34 % and are shown in column four of Table 4.7. Columns five and six of Table 4.7 list the number of samples measured and the number of pressures the samples were measured at, respectively. Pure MEAA and the chemical mix [1;1]:0 only have one sample each that was tested over three different pressures. Since the ceramic yield of both of these samples was quite low (27 and 33% respectively), they tended to crumble upon firing leaving membrane fragments too small to test for permeability. One should note however, that agreement at all three pressures for both samples is very high.

There are several sources of experimental error that are likely. Water leakage through the aluminum foil-epoxy-membrane interface was checked by epoxying a piece of aluminum foil to a cut-out in an aluminum-foil disc similar to the method of making the membrane samples. This blank sample did not allow any water through it at pressures up to 30 psi for a one week time period. Water leakage attributable to poor epoxy bonding, however, was detected for several samples, but was quite obvious and those samples were discarded. Other sources of error include human error reading small volumes from volumetric glassware, membrane surface area estimation due to inaccuracy of sealing and irregular shapes of samples, and membrane fouling possibly cause by impurities in the deionized water after handling. Variations in pressure are highly unlikely as contributing to error, since the gas tank regulator was quite accurate and reliable. Comprehensive permeability data, including volumes of water per time for each sample tested, measured surface areas, and associated errors are contained in Appendix B.

4.6.0 Contact Angle

Contact angle is a useful characteristic in evaluating membrane hydrophilicity. Lower contact angles indicate greater hydrophilicity. The alumoxane-derived membranes had contacts angles of approximately 10°, indicating that they are quite hydrophilic. Hydrophilic membranes usually foul less severely than those that are hydrophobic, hence low contact angles are an important membrane performance characteristic. Anodized alumina membranes also have a contact angle of ca. 10° and were listed accordingly as being hydrophilic. The PCTE membrane sample had a contact angle of ca. 25°, which is still fairly hydrophilic. These membranes were listed by the manufacturer as being hydrophilic and capable of being hydrophobic with special treatment for specialized applications.

In comparison, contact angles for some polysulfone and cellulose acetate membranes can be as high as 80° and 45° respectively (Oldani and Schock, 1989). Gekas *et al.* (1992), however, reported contact angles as low as 26° and 14° for polysulfone and cellulose acetate membranes. Contact angles can vary widely for any given material and are affected most by surface roughness and porosity, which themselves vary widely depending on the specific membrane.

4.7.0 Surface Charge

Zeta potentials of the alumoxane-derived membranes were calculated from measured electrophoretic mobility at four different pHs. The changing surface charge, or zeta potential, and electrophoretic mobility with increasing pH are shown in Figure 4.35.
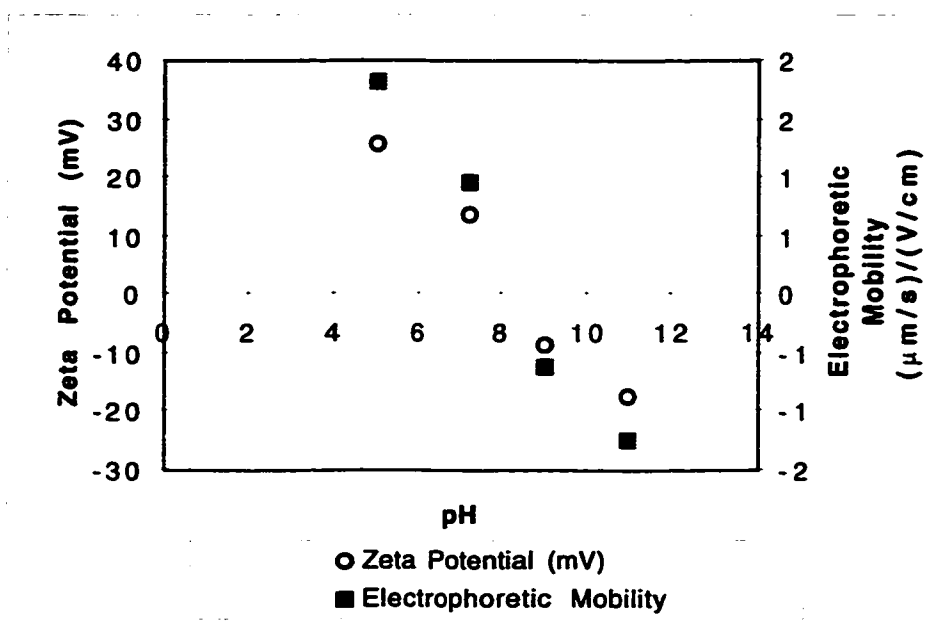
Figure 4.35: Zeta Potential and Electrophoretic MObility v. pH for Alumoxane-derived Membranes

At a pH of 5, the alumoxane-derived membranes have a positive zeta potential between 20 and 30 mV. The zeta potential decreases to ca. 15 near a pH of 7, and between pHs of 7 and 9 the zeta potential becomes negative. At a pH of 9 the zeta potential is approximately -10 and it decreases to -20 near a pH of 11. This graph displays the wide range of the surface charge for these membranes, displaying the amphoteric property of alumina. The iso-electric point, or point of zero charge, can be estimated from Figure 4.30 as existing at pH ~ 8.5. This is fairly close to the well documented IEP of alumina at pH ~ 9.

Chapter 5

Conclusions

The membrane fragments investigated in this study, however, show considerable promise based on several important characteristics, such as permeability, average pore size, and pore size distribution. Because of the simplicity of aqueous processing, the starting material, alumoxane, is highly suitable for making alumina products, namely membranes. In summary, the following conclusions were reached from this research:

- Alumoxanes are a new class of compounds with significant potential as precursors to alumina ultra-filtration membranes.

- Carboxylate-alumoxanes can be cast into membranes with narrow pore size distributions in the range of 5 - 15 nm, which is a difficult range to achieve using conventional techniques. The alumoxane-derived membranes have nodular morphologies with interstitial spaces yielding porosities from 54 to 69%. They are quite hydrophilic and have permeabilities ranging from 0.3 to 1.5 nm^2.

- Though the two ligand precursors studied here did not produce membranes with greatly differing characteristics, there may be nonetheless potential to control pore size through the mixing of other types of alumoxanes that differ more significantly in size (MEEA and MA for example). Altering such processing variables as firing time and temperature used to produce the membranes may be even more effective than ligand precursor selection in controlling membrane characteristics.

- Alumoxane-derived membranes exhibit some performance characteristics similar to those of commercial membranes. Permeabilities of the alumoxane-derived membranes were somewhat lower than those of anodized alumina, but were significantly larger than those of PCTE membranes.

More research is necessary to determine whether alumoxane-derived membranes can be commercially competitive. Engineering issues such as attachment of support, uniformity of membranes, and production of larger and more regularly sized membranes without cracks, must be resolved before alumoxane-drived membranes can be properly evaluated for uses other than laboratory scale.

Chapter 6

Engineering Significance

Alumoxanes are a unique class of materials forming the basis of an alternative alumoxane method of making alumina UF membranes. Aqueous based alumoxanes are a novel approach to minimizing solvent and other toxic material usage in the manufacturing of membranes and other ceramic materials. The low pore sizes of alumoxane-derived membranes can most likely be achieved with a single dip coating, while typical sol-gel routes require progressive dippings to achieve smaller pore sizes. There is also a potential to control pore size distributions using different ligands or mixes of ligands, and the resulting narrow distributions may be capable of high selectivities. Average pore sizes of 10 nm can be achieved at firings of alumoxane-derived membranes up to 1000 °C, which is unusually small for temperatures this high. This is a significant advantage, in that temperatures above 1000 °C produce α-alumina, which exhibits superior chemical resistance characteristics.

The high adsorption surface area and the ability to be doped with other materials make Alumoxane-based membranes good candidates for simultaneous use in catalysis and liquid or gas separations. Amphoteric properties of alumina membranes can also play a significant role in specialized separation operations. The changing surface charge with pH allows controlled rejection of either negative or positive ions in solution. The hydrophilicity of these membranes indicates that they may overcome the acute fouling which leads to additional flux decline for hydrophobic membranes.

Chapter 7

Further Research

Several veins of research stem from this project, that may be beneficial to explore. Specific rejection statistics for different solutions (dextrans, albumin, etc.) would yield much more information on the performance characteristics of the alumoxane-derived membranes. It also naturally follows to perform the same or similar characterization tests on alumoxanes that are slip-casted onto supports, much like commercial membranes. Photocatalysis and gaseous reaction are two strong possibilities for these membranes that are as yet completely unexplored. Finally, following the green chemistry theme, a Lifecycle Assessment of the membranes may prove useful in asserting that the membranes are environmentally benign as claimed.

References

Anderson, Marc A., Mary J. Gieselmann, and Qunyin Xu, (1988) "Titania and Alumina Ceramic Membranes," J. Membrane Science, 39: 243-258.

Apblett, Allen W., Alison C. Warren, and Andrew R. Barron, (1992) "Synthesis and Characterization of Triethylsiloxy-Substituted Alumoxanes: Their Structual Relationship to the Minerals Boehmite and Diaspore," Chem. Mater., 4, 167-182.

Asante-Duah, Kofi, (1993) Hazardous Waste Risk Assessment, Lewis, Boca Raton, Florida.

AWWA Membrane Technology Research Committee, (1992) "Committee Report: Membrane Processes in Potable Water Treatment," J. AWWA, Jan.: 59 - 67.

Baltus, Ruth E., (1997) "Characterization of the Pore Area Distribution in Porous Membranes Using Transport Measurements," J. Membrane Science, 123 (2): 165-184.

Barrett, Elliott P., Leslie G. Joyner, and Paul P. Halenda, (1951) "The Detemination of Pore Volume and Area Distributions in Porous Substances. I. Computations from Nitrogen Isotherms," J. American Chemical Society, 73: 373-380.

Binnig, G., C.F. Quate, and Ch. Gerber, (1986) "Atomic Force Microscope," Physical Review Letters, 56 (9): 930-933.

Bottino, A., G. Capannelli, O. Monticelli et al., (1994) "Porosimetric Characterization of Inorganic Membranes," Separation Science and technology, 29 (8): 985-999.

Bottino, A., G. Capannelli, A. Grosso et al., (1994) "Surface characterization of ceramic membranes by atomic force microscopy," J. Membrane Science, 95: 289-296.

Bowen, W.Richard, Nidal Hilal, Robert W. Lovitt et al., (1996) "Atomic force microscope studies of membranes: Surface pore structures of Cyclopore and Anopore membranes," J. Memb. Sci., 110: 233-238.

Bradley, D.C., J.W. Lorimer, and C. Prevedorou-Demas, (1971) "Metal Oxide Trialkylsilyoxide Polymers. Part VI. Aluminum Oxide Trimtheylsilyloxides," Canadian Journal of Chemistry, 49: 2310-2314.

Brandon, C. A., D. A. Jernigan, J. L. Gaddis et al., (1981) "Closed Cycle Textile Dyeing: Full Scale Renovation of Hot Wash Water by Hyperfiltration," Desalination, 39: 301 - 310.

Brunauer, Stephen, P.H. Emmett, and Edward Teller, (1938) "Adsorption of Gases in Multimolecular Layers," J. Amer. Chem. Society, 60 (1): 309-319.

Buckley, C.A., (1992) "Membrane Technology for the Treatment of Dyehouse Effluents," Wat. Sci. Tech., 25 (10): 203-209.

Burganos, V.N., and S.V. Sotirchos, (1987) "Diffusion in Pore Networks: Effective Medium Theory and Smooth Field Approximation," AIChE Journal, 33 (10): 1678 -1689.

Burger, J., G. Dietler, M. Binggeli et al., (1994) "Aspects of the surface roughness of ceramic bonding tools on a nanometer scale investigated with atomic force microscopy," Thin Solid Films, 253: 308-310.

Burgess, Christopher G.V., Douglas H. Everett, and Stuart Nuttall, (1989) "Adsorption hysteresis in porous materials," Pure & Appl. Chem., 61 (11): 1845-1852.

Callender, Rhonda L., C. Jeff Harlan, Noah M. Shapiro et al., (1997) "Aqueous Synthesis of Water-Soluble Alumoxanes: Environmentally Benign Precursors to Alumina and Aluminum-Based Ceramics," Chemistry of Materials, 9 (11): 2418 - 2433.

Callender, Rhonda L., Christopher D. Jones, Andrew R. Barron, D. A. Bailey, and Mark R. Wiesner, (1998) Chemical Control Over Ceramic Porosity Using Carboxylate-Alumoxanes, U.S. Patent, provisional filing.

Capannelli, G., F. Vigo, and S. Munari, (1983) "Ultrafiltration Membranes -- Characterization Methods," J. Membrane Science, 15: 289-313.

Conlon, W.J., (1990) Water Quality and Treatment, 4th Ed., Ch. 11, McGraw-Hill, Inc., New York.

Costello, Joe, (1997) Whatman Specialty Products, Inc., Fairfield, New Jersey, Personal communication, October 6.

Coster, H.G.L., K.J. Kim, K. Dahlan et al., (1992) "Characterisation of Ultrafiltration Membranes By Impedance Spectroscopy. I. Determination of the Separtat Electrical Parameters and Porosity of the skind and Sublayers," J. Membrane Science, 6 6
(1):   19-26.

Coulter SA 3100 Surface Area Analyzer Reference Manual, (1996) Coulter Corp., Miami, Florida.

Cranston, R.W. and F.A. Inkley, (1957) "The Determination of Pore Structures from Nitrogen Adsoption Isotherms," Adv. Catalysis & Related Subjects, 9: 143-154.

Cuperus, F.P. and C.A. Smolders, (1991) "Characterization of UF Membranes," Advances in Colloid and Interface Science, 34: 135-173.

Dalvie, S.K. and R.E. Baltus, (1992) "Transport Studies with porous Alumina Membranes," J. Membrane Science, 71: 247-255.

Deckman, H.W. and R.J. Plano, (1993) "Artifacts in Atomic Force Microscopy of Nanoporous and Mesoporous Fiducial Samples," presented at the Materials Research Society Symposium, (unpublished).

Dietz, Peter, Paul K. Hansma, Otto Inacker et al., (1992) "Surface pore sturctures of micro- and ultrafiltration membranes imaged with the atomic force microscope," J. Memb. Sci., 65: 101-111.

Dykes, Glenn M. and William J. Conlon, (1989) "Use of Membrane Technology in Florida," Journal of the American Water Works Association, 81 (11): 43 - 46.

Elimelech, M., Chen W.H., and J.J. Waypa, (1994) "Measureing the Zeta (electrokinetic) Potential of Reverse Osmosis Membranes by a Streaming Potential Analyzer," Desalination, 95: 269-286.

Fane, A. G., C.J.D. Fell, and A.G. Waters, (1981) "The Relationship Between Membrane Surface Pore characteristics and Flux for Ultrafiltration Membranes," J. Memb. Sci., 9: 245-262.

Filteau, Gerry, Cloice Whitley, and Ian C. Watson, (1995) "Water Reclamation Fuels Economic Growth in Harlingen, Texas. Reclamation of Municipal Wastewater for Industrial Process Use," Desalination, 103: 31 - 37.

Freeman, Scott D. N. and O.J. Morin, (1995) "Recent Developments in Membrane Water Reuse Projects," Desalination, 103: 19 - 30.

Furneaux, R.C., W.R. Rigby, and A.P. Davidson, (1989) "The formation of controlled-porosity membranes from anodically oxidized aluminum," Nature, 337 (Jan): 147-149.

Gekas, Vassilis, Kenneth M. Persson, Marie Wahlgren et al., (1992) "Contact angles of ultrafitration membranes and their possible correlation to membrane performance," J. Membrane Science, 72: 293-302.

Gere, Andrew R. (1997) "Microfiltration Operating Costs," J. AWWA, 89 (10): 40 - 49.

Gregg, S.J., and K.S.W. Sing, (1982) Adsorption, Surface Area and Porosity, 2nd ed. Academic Press Inc., London.

Gruetter, P., W. Zimmermann-Edling, and D. Brodbeck, (1992) "The Artifacts of Microfabricated Force Sensors for Atomic Force Microscopy," Appl. Phys. Lett., 60: 2741 - 2743.

Guldberg Pedersen, Henrik, Janne Tranto, and Jakob Weiland Hoj, (1997) "Characterization of Multilayer Ceramic Membranes With the Atomic Force Microscope," presented at the 5th Conference and Exhibition of The European Ceramic Society, Verasailles, France, (unpublished).

Harkins, William D. and George Jura, (1944) "Surfaces of Solids. XII. an Absolute Method for the Determination of a Finely divided Crystalline Solid," J. American Chemical Society, 66: 1362-1366.

Harkins, William D. and George Jura, (1944) "XIII. A Vapor Adsorption Method for the Determination of the Area of aSolid without the Assumption of a Molecular Area, a nd the Areas Occupied by Nitrogen and Other Molecules on the Surface of a Solid," J. American Chemical Society, 66: 1366-1373.

Hiemenz, Paul C., (1986) Principles of colloid and surface chemistry, second ed., Marcel Dekker, Inc., New York.

Hsieh, H.P., (1996) Inorganic Membranes for Separation and Reaction, 1 ed. Elsevier, Amsterdam.

Inoue, Masashi, Yasuhiko Kondo, and Tomoyuki Inui, (1986) "The Reaction of Crystalline Aluminum Hydroxide in Ethylene Glycol," Chemistry Letters, 1421-1424.

Inoue, Masashi,Yasuhiko Kondo, and Tomoyuki Inui, (1988) "An ethylene glycol derivative of Boehmite," Inorganic Chemistry, 27: 215-221.

Inoue, Masashi, Hirokazu Tanino, Yasuhiko Kondo et al., (1989) "Formation of Microcrystalline a-alumina by glycothermal treatment of gibbsite," Communications of the American Ceramic Society, 72 (2): 352-353.

Inoue, Masashi, Hirokazu Tanino, Yasuhiko Kondo et al., (1991) "Formation of organic derivatives of boehmite by the reactionof gibbsite with glycols and aminoalcohols," Clays and Clay Minerals, 39 (2): 151-157.

Inoue, Masashi, Hiroshi Kominami, Yasuhiko Kondo et al., (1997) "Organic Derivatives of Layered Inorganics Having the Second Stage Structure," Chem. Mater., 9: 1614-1619.

Jakobs, Egbert and W.J. Koros, (1997) "Ceramic Membrane Characterization Via the Bubble Point Method," J. Membrane Science, 124 (2): 149-159.

Kaneko, Katsumi, (1994) "Determination of pore size and pore size distribution 1. Adsorbents and catalysts," J. Membrane Science, 96: 59-89.

Karieva, Aivaras, Jeff C. Harlan, D. Brent MacQueen et al., (1996) "Carboxylate-Substituted Alumoxanes as Processable Precursors to Transition Metal-Aluminum and Lanthanide-Aluminum Mixed-Metal Oxides: Atomic Scale Mixing via a New transmetalation Reaction," Chemistry of Meterials, 8 (9): 2331-2340.

Keurentjes, J.T.F., J.G. Harbrecht, D. Brinkman et al., (1989) "Hydrophobicity Measurements of Microfiltration and Ultrafiltration Membranes," J. Membrane Science, 47: 333-344.

Kim, K.J., A.G. Fane, R. Ben Aim et al., (1994) "Comparative Study of Techniques Used For Porous Membrane Characterization: Pore Characterization," J. Membrane Science, 87 (1-2): 35-46.

Kim, K.J. and P.V. Stevens, (1997) "Hydraulic and Surface Characteristics of Membranes with Parallel Cylindrical Pores," J. Membrane Science, 123 (2): 303-314.

Koh, W.-H. and J.L. Anderson, (1975) "Electoosmosis and electolyte Conductance in Charged microcapillaries," American Institute of Chemcial Engineers journal, 21 (6): 1176-1188.

Lahoussine-Turcaud, Veronique, Mark R. Wiesner, Jean-Yves Bottero et al., (1990) "Coagulation Pretreatment for Ultrafiltration of a Surface Water," Journal of the American Water Works Association, 82 (12): 76 - 81.

Laîné, Jean-Michel, James P. Hagstrom, Mark M. Clark et al., (1989) "Effects of Ultrafiltration Membrane Composition," Journal AWWA, Nov.: 61 - 67.

Landry, Christopher C., Nina Pappe, Mark R. Mason et al., (1995) "From Minerals to Materials: Synthesis of Alumoxanes from the Reaction of Boehmite with Carboxylic Acids," J. Mater. Chem., 5 (2): 331-341.

Larson, I., C.J. Drummond, D.Y.C. Chan et al., (1997) "Direct Force Measurements betwen Silica and Alumina," Langmuir, 13: 2109-2112.

Lee, C.K. and J. Hong, (1988) "Characterization of Electric Charges in Microporous Membranes," J. Memb. Sci., 39: 79-88.

Leenaars, A.F.M., K. Keizer, and A.J. Burggraaf, (1984) "The Preparation and Characterization of alumina membranes with ultra-fine pores, Part 1: Microstructural investigations on non-supported membranes," J. Mater. Science, 19: 1077-1088.

Lin, Yue-Sheng and A.J. Burggraaf, (1991) "Preparation and Characterization of High-Temperature Thermally Stable Alumina Composite Membrane," J. Am. Ceram. Soc. 74 (1): 219-224.

Lloyd, Douglas R. and Timothy B. Meluch, (1985) "Selection and Evaluation of Membrane Materials for Liquid Separations," Materials Science of Synthetic Membranes , American Chemical Society, Ch. 3, pp. 47 - 79.

Loeb, Sidney, (1981) "Loeb-Sourirajan Membrane: How it came about.," presented at the 2nd Chemical Congress of the North American Continent, Las Vegas, NV, (unpublished).

Mallevialle, J., P.E. Odendaal, and M.R. Wiesner, (1996) Water Treatment: Membrane Processes, McGraw-Hill, New York.

Mikulasek, P. and P. Dolecek, (1994) "Characterization of Ceramic Tubular Membranes by Active Pore-Size Distibution," Separation Science and Technology, 29 (9): 1183-1192.

Munari, S., A. Bottino, P. Moretti et al., (1989) "Permoporometric Study on Ultrafirtration Membranes," J. Membrane Science, 41: 69-86.

Nakao, S-i, (1994) "Determination of pore size and pore size distribution 3. Filtration Membranes," J. Membrane Science, 96: 131-165.

Nanoscope IIIa Multimode Scanning Probe Microscope User Manual, (1995) Digital Instruments, Santa Barbara, CA.

Nazzal, F.F. and M.R. Wiesner, (1994) "pH and ionic strength effects on the performance of ceramic membranes in water filtration," J. Membrane Science 93: 91-103.

Neimark, A.V., (1986) "A Percolation Method for calculating the Pore Size Distribution in Materials of Intermediate Porosity Based on the Adsorption and Desorption Isotherms in The Hysteresis Region.," Russian Journal of Physical Chemistry, 60 (7), 1045-1048.

Odani, M. and G. Schock, (1989) "Characterization of Ultrafiltration Membranes by Infrared Spectroscopy, ESCA, and Contact Angle Measurements," Journal of Membrane Science, 43: 243-258.

Pasynkiewicz, S., (1990) "Alumoxanes: Synthesis, Structures, Complexes and Reactions," Polyhedron, 9 (2/3): 429-453.

Porter, John J. and Grant A. Goodman, (1984) "Recovery of Hot Water, Dyes and Auxiliary Chemicals Form Textile Wastestreams," Desalination, 49: 185 - 192.

Porter, J.J. and R. S. Porter, (1995) "Filtration studies of selected anionic dyes using asymmetric titanium dioxide membranes on porous stainless-steel tubes," J. Memb. Sci., 101: 67 - 81.

Porter, John J. and S. Zhuang, (1996) "Microfiltration of sodium nitrate and Direct Red 2 Dye using asymmetric titanium dioxide membranes on porous ceramic tubes," J. Memb. Sci., 110: 119 - 132.

Pradanos, P., M.L. Rodrigues, J.I. Calvo et al., (1996) "Stuctural Characterization of an UF Membrane by Gas Adsorption-Desorption and AFM Measurements," J. Membrane Science, 117 (1-2): 291-302.

Pugh, Robert J. and Lennart Bergstrom, (1994) Surface and Colloid Chemistry in Advanced Ceramics Processing, in Surfactant Science Series, Marcel Dekker, New York, v. 51, pp. 363.

Rocek, J. and P. Uchytil, (1994) "Evaluation of selected methods for the characterization of ceramic membranes," J. Membrane Science, 89: 119-129.

Sarrade, Stephane, Gilbert M. Rios, and Maurice Carles, (1994) "Dynamic Characterization and Transport Mechanisms of Two Inorganic Membranes For Nanofiltration," J. Membrane Science, 97 (Dec. 27): 155-166.

Seaton, N.A., (1991) "Determination of the Connectivity of Porous Solids From Nitrogen Sorption Measurements," Chemical Engineering Science, 46 (8): 1895-1909.

Sidorova, M.P., L.E. Ermakova, and I.A. Savina, (1993) "Electochemistry of weakly charged membranes," J. Memb. Sci., 79: 159-179.

Storr, Alan, Kenneth Jones, and A.W. Laubengayer, (1968) "The Partial Hydrolysis of Ethylalane Compounds," J. of the Amer. Chem. Soc., 90 (12): 3173-3177.

Tarleton, E.S. and R.J. Wakeman, (1994) "Understanding Flux Decline in Crossflow Microfiltration: Part III - Effects of Membrane Morphology," Chemical Engineering Research & Design, Part A: Transactions of the Institute of Chemical Engineers, 72 (A4): 521-529.

Tartaj, J. and G.L. Messing, (1997) "Effect of the addition of a-Fe2O3 on the microstructural development of boehmite-derived alumina.," J. Mater. Sci. Let., 16: 168 - 170.

Taylor, James S., D.M. Thompson, and K.J. Carswell, (1987) "Applying Membrane Processes to Groundwater Sources for Trihalomethane Precursor Control," J.AWWA, Aug.: 72-82.

Treffry-Goatley, K., C.A. Buckley, and G. R. Groves, (1983) "Reverse Osmosis Treatment and Reuse of Textile Dyehouse Effluents," Desalination, 47: 313 - 320.

Wiesner, Mark R. and Shankararaman Chellam, (1992) "Mass Transport Considerations for Pressure-Driven Membrane Processes," J. AWWA, 88-95.

Wiesner, M.R., J. Hackney, S. Sethi et al., (1994) "Cost Estimates for Membrane Filtration and Conventional Treatment," J. AWWA, Dec.: 33 - 41.

Xomeritakis, G., J. Han, and Y.S. Lin, (1997) "Evolution of Pore Size Distribution and Average pore Size of Porous Ceramic Membranes During Modification By Counter-Diffusion Chemical Vapor Deposition," J. Membrane Science,124 (1): 27- 42.

Zander, A.K., C. Cleveland, and N.K. Curry, (1995) "Measurement of Membrane Surface Hydrophobicity and Charge as affected by solution Characteristics," presented at the 1995 Membrane Technology Conference, Reno, Nevada, (unpublished).

Zaspalis, V.T., W. Van Praag, K. Keizer et al., (1992) "Synthesis and Characterization of primary alumina, titania and binary membranes," Journal of Material Science, 27: 1023-1035.

Zeman, Leos and Lauraine Deanault (1992) "Characterization of microfiltration membranes by image analysis of electron micrographs. Prt I. Method development," J. of Membrane Science, 71 (3): 221 - 231.

Zeman, Leos, (1992) "Characterization of microfiltration membranes by image analysis of electron micrographs. Part II. Functional and morphological parameters," J. of Membrane Science,71 (3): 233-246.

Zeman, Leos J. and Andrew L. Zydney, (1996) Microfiltration and Ultrafiltration, Principles and Applications, Marcel Dekker, Inc., New York.

Zeng, Zhiquang, Xiaoyue Xiao, Zhilun Gui et al., (1997) "AFM study on surface morphology of Al2O3-SiO2-TiO2 composite ceramic membranes," J. Membrane Science, 136: 153-160.

Zhang, L. and J.Y. Ying, (1997) "Synthesis and Characteization of Mesoporous Niobium -Doped Silica Molecular Sieves," AIChE Journal, 43 (11A): 2793 - 2801.

Appendix A: Synthesis of Alumoxane Based Membranes

A.1 Synthesis of A-Alumoxane

Pseudoboehmite (20.0 g, 333mmol) was slowly added to a vigourously stirring mixture of acetic acid (51.0 mL, 667 mmol) in water (200 mL). The resulting slurry was decanted after 10 min. and then centrifuged at 6000 rpm for 1 hour to yield a clear viscous solution. Removal of the volatiles in vacuo (10^{-2} Torr) at 90 °C results in clear, white granules. The granules were dissolved in water and dried for 24 hours at 80 °C to yield a crear glassy material. The acetate-alumoxane is soluble in water and slightly soluble in ethanol. IR (Nujol, cm^{-1}) 3583 (w), 3298 (s), 3088 (s), 2089 (m), 1608 (m), 1557 (m), 1260 (m), 1070 (s), 799 (m), 737 (w), 625 (m), 487 (m). ^{1}H NMR (D$_2$O) δ 1.95 (2H, s, O$_2$CCH$_3$).

A.2 Synthesis of MEA-Alumoxane

Pseudoboehmite (10.0 g, 167mmol) and (methoxyethoxy)acetic acid (38.0 mL, 333 mmol) were refluxed in water (100 mL) for 24 hours, resulting in a clear solution. The solution was centrifuged at 6000 rpm for 1 hour and decanted. The water was removed in vacuo (10^{-2} Torr) at 50 °C results in a gel. The gel was washed with Et$_2$O (3 x 75 mL) and then dissolved in EtOH (50 mL) while stirring (10 min.). The MEA-alumoxane was precipitated via the addition of Et2O (100 mL) as a white powder. After drying overnight at 50 °C the solid yield was approximately 25 g. The MEA-alumoxane is soluble in H$_2$O, CHCL$_3$, and CH$_2$Cl$_2$. IR (Nujol, cm^{-1}) 3493 (s), 3303 (s), 3048 (w), 1649 (m), 1598 (m), 1260 (m), 1024 (w), 799 (m), 727 (w), 625 (m), 476 (m). ^{1}H NMR (D$_2$O) δ 3.90 (2H, s, O$_2$CCH$_3$), 3.56 (4H, m, CH$_2$), 74.1 (CH$_2$), 73.9 (CH$_2$), 62.6 (CH$_3$). ^{27}Al NMR (CDCl$_3$) δ 6 (W$_{1/2}$ = 3800 Hz).

A.3 Physical mixing of MEA-alumoxane

MEA-A (1.0 g) and A-A (1.0 g) were dissolved into about 20 mL of water. After stirring for approximately 0.5 hours, the solutions were poured into drying containers. After approximately 36 hours, the solutions had evaporated to leave a thin membrane which is glass-like.

A.4 Synthesis of mixed ligand MEA/A-alumoxane (Chemically mixed)

Acetic acid (19.0 mL) and methoxy(ethoxy)acetic acid (152.0 mL) was dissolved in 500 mL of water and Vista Captal B boehmite (20 g) was slowly added and refluxed for 72 hours. The white solution was filtered and the filtrate was dissolved under reduced pressure to yield an off-white gel. The gel was dissolved in ethanol (100 mL) and the white powder product was obtained by the addition of diethyl ether. The MEA/A-alumoxane was dissolved in water and allowed to evaporated to a thin glass-like membrane.

A.5 Synthesis of Alumina Membranes

Samples of the carboxylate-alumoxane membranes were subjected to the following firing sequence: (a) heating to 200 °C at 1.5 °C/min., (b) soaking at 200 °C for 2 hours, (c) heating to 1000 °C at 4.5 °C/min., and (d) soaking at 1000 °C for 2 hours.

Sample	Description
30	1;1:1 MEAA-AA (#9, 2/98 batch) chip attatched to Al foil disk w/ 3/8" d hole, reg. epoxy used
31	1;1:1 MEAA-AA (#9, 2/98 batch) chip attatched to Al foil disk w/ 3/8" d hole, reg. epoxy used
32	1;1:1 MEAA-AA (#9, 2/98 batch) chip attatched to Al foil disk w/ 1/2" d hole, reg. epoxy
33	1;1:1 MEAA-AA (#9, 2/98 batch) chip attatched to Al foil disk w/ 1/2" d hole, reg. epoxy
34	1;1:1 MEAA-AA (#9, 2/98 batch) chip attatched to Al foil disk w/ 11/32" d hole, reg. epoxy
	(Epoxy on Samples 30 - 34 never dried)
35	S31 reglued with cement and then again w/ reg. epoxy, new d = 3/8"
36	S32 reglued with cement and then again w/ reg. epoxy, new d = 11/32"
37	S33 reglued with cement and then again w/ reg. epoxy, new d = 11/32"
38	1;0:1 MEAA-AA w/o frit (2/98 batch), Al foil disk w/ 21/64" d hole, reg epoxy used
39	1;0:1 MEAA-AA w/o frit (2/98 batch), Al foil disk w/ 21/64" d hole, reg epoxy used
40	1;0:1 MEAA-AA w/o frit (2/98 batch), Al foil disk w/ 21/64" d hole, reg epoxy used
41	1;0:1 MEAA-AA w/o frit (2/98 batch), Al foil disk w/ 3/8" d hole, reg epoxy used
42	1;0:1 MEAA-AA w/o frit (2/98 batch), Al foil disk w/ 21/64" d hole, reg epoxy used
43	1;0:1 MEAA-AA w/o frit (2/98 batch), Al foil disk w/ 21/64" d hole, reg epoxy used
44	1;1:0.5 MEAA-AA w/o frit (2/98 batch), Al foil disk w/ 21/64" d hole, reg epoxy used
45	1;1:2 MEAA-AA w/o frit (2/98 batch), Al foil disk w/ 13/32" d hole, reg epoxy used
46	1;0:4 MEAA-AA (2/98 batch), Al foil disk w/ 21/64" d hole, reg epoxy used
47	1;1:2 MEAA-AA w/o frit (2/98 batch), Al foil disk w/ 13/32" d hole, reg epoxy used
48	1;0:2 MEAA-AA (2/98 batch), Al foil disk w/ 21/64" d hole, reg epoxy used
49	15 nm PCTE (Nuclepore), Al foil disk w/ 15/32" d hole, reg epoxy used
50	1/2" Al foil piece glued to Al foil disk w/ 1/2" d hole (reg epoxy), control
51	1;1:1 MEAA-AA (3/98 batch), Al foil disk w/ 7/16" d hole, reg epoxy used
52	1;1:2 MEAA-AA (3/98 batch), Al foil disk w/ 13/32" d hole, reg epoxy used
53	1;1:4 MEAA-AA (3/98 batch), Al foil disk w/ 19/64" d hole, reg epoxy used
54	1;1:0.5 MEAA-AA (3/98 batch), Al foil disk w/ 3/8" d hole, reg epoxy used
55	1;0:0.5 MEAA-AA (3/98 batch), Al foil disk w/ 13/32" d hole, reg epoxy used
56	1;1:1 MEAA-AA (3/98 batch), Al foil disk w/ 7/16" d hole, reg epoxy used
57	1;1:2 MEAA-AA (3/98 batch), Al foil disk w/ 13/32" d hole, reg epoxy used
58	1;1:4 MEAA-AA (3/98 batch), Al foil disk w/ 9/32" d hole, reg epoxy used
59	1;1:0.5 MEAA-AA (3/98 batch), Al foil disk w/ 13/32" d hole, reg epoxy used
60	1;0:2 MEAA-AA (3/98 batch), Al foil disk w/ 21/64" d hole, reg epoxy used
61	15 nm PCTE (Nuclepore), Al foil disk w/ 3/8" d hole, Elmer's Contact Cement glue
62	15 nm PCTE (Nuclepore), Al foil disk w/ 3/8" d hole, Elmer's Contact Cement glue
63	1;0:4 MEAA-AA (3/98 batch), Al foil disk w/ 1/4" square hole, reg epoxy used + blue dye
64	1;0:0.5 MEAA-AA (3/98 batch), Al foil disk w/ 5/8" x 3/8" hole, reg epoxy used + blue dye
65	1;0:0.5 MEAA-AA (3/98 batch), Al foil disk w/ 7/32" x 7/8" hole, reg epoxy used + blue dye
66	1;0:2 MEAA-AA (3/98 batch), Al foil disk w/ 3/16" x 3/4" hole, reg epoxy used + blue dye
67	1;1:0 MEAA-AA (3/98 batch), Al foil disk w/ 1/8" x 1/2" hole, reg epoxy used + blue dye
68	1;0:0.5 MEAA-AA (3/98 batch), Al foil disk w/ 1/4" x 5/8" hole, reg epoxy used + red dye
69	1;0:0.5 MEAA-AA (3/98 batch), Al foil disk w/ 5/16" Square hole, reg epoxy used + red dye
70	1;0:2 MEAA-AA (3/98 batch), Al foil disk w/ 5/16" circle hole, reg epoxy used + red dye
71	0;0:1 pure AA (3/98 batch), Al foil disk w/ 13/32" circle hole, reg epoxy used + red dye
72	0;0:1 pure AA (3/98 batch), Al foil disk w/ 13/32" circle hole, reg epoxy used + red dye
73	1;1:0 MEAA-AA (3/98 batch), Al foil disk w/ 1/4" triangle hole, reg epoxy used + green dye
74	1;0:0 pure MEAA (3/98 batch), Al foil disk w/ 1/8" x 1/4" hole, reg epoxy used + green dye
75	1;0:0 pure MEAA (3/98 batch), Al foil disk w/ 3/16" triangle hole, reg epoxy used + green dye
76	1;0:4 MEAA-AA (2/98 batch), Al foil disk w/ 1/4" x 3/8" hole, reg epoxy used + green dye
77	0;0:1 pure AA (3/98 batch), Al foil disk w/ 3/8" triangle hole, reg epoxy used + green dye
78	0;0:1 pure AA (3/98 batch), Al foil disk w/ 5/16" triangle hole, reg epoxy used + yellow dye
79	0;0:1 pure AA (3/98 batch), Al foil disk w/ 5/32" x 3/8" hole, reg epoxy used + yellow dye
80	1;0:0 pure MEAA (3/98 batch), Al foil disk w/ 1/8" x 1/8" hole, reg epoxy used + yellow dye
81	1;0:0.5 MEAA-AA (3/98 batch), Al foil disk w/ 1/4" x 7/16" hole, reg epoxy used + yellow dye

Sample	Description			
82	1;1:0 MEAA-AA (cdj 031), Al foil disk w/ 1/8" x 3/16" hole, reg epoxy used + blue dye			
83	1;1:1 MEAA-AA (3/98 batch), Al foil disk w/ 3/8" x 1/2" hole, reg epoxy used + blue dye			
84	1;1:2 MEAA-AA (3/98 batch), Al foil disk w/ 1/4" x 3/4" hole, reg epoxy used + blue dye			
85	1;1:4 MEAA-AA (3/98 batch), Al foil disk w/ 5/16" x 1/4" hole, reg epoxy used + blue dye			
86	1;1:0.5 MEAA-AA (3/98 batch), Al foil disk w/ 3/8" diam. hole, reg epoxy used + blue dye			
87	0;0:1 pure AA (3/98 batch), Al foil disk w/ 1/4" circle hole, reg epoxy used + purplish dye			
88	1;0:1 MEAA-AA (3/98 batch), Al foil disk w/ 5/8" circle hole, reg epoxy used + purplish dye			
89	1;0:4 MEAA-AA (2/98 batch), Al foil disk w/ 5/16" circle hole, reg epoxy used + purplish dye			
90	1;0:0.5 MEAA-AA (3/98 batch), Al foil disk w/ 3/8" circle hole, reg epoxy used + purplish dye			
91	1;0:0.5 MEAA-AA (3/98 batch), Al foil disk w/ 5/8" x 5/32" hole, reg epoxy used + purplish dye			
92	15 nm PCTE (Nuclepore), Al foil disk w/ 3/8" d hole, Elmer's Contact Cement glue			
93	15 nm PCTE (Nuclepore), Al foil disk w/ 3/8" d hole, Elmer's Contact Cement glue			
94	15 nm PCTE (Nuclepore), Al foil disk w/ 3/8" d hole, Elmer's Contact Cement glue			
95	1;0:1 MEAA-AA (3/98 batch), Al foil disk w/ 7/16" square hole, reg epoxy used + orangish dye			
96	1;1:4 MEAA-AA (3/98 batch), Al foil disk w/ 3/16" x 1/2" hole, reg epoxy used + orangish dye			
97	1;1:2 MEAA-AA (3/98 batch), Al foil disk w/ 3/8" circle hole, reg epoxy used + orangish dye			
98	1;1:1 MEAA-AA (3/98 batch), Al foil disk w/ 3/8" square hole, reg epoxy used + orangish dye			
99	1;1:0.5 MEAA-AA (3/98 batch), Al foil disk w/ 3/8" circle hole, reg epoxy used + orangish dye			
100	0.02 µm Anodisc (as is)			
101	0.02 µm Anodisc (as is)			
102	0.02 µm Anodisc (as is)			

Theoretical Flux: J = 2.708 x 10-20 (ΔPr⁴n/μL)   Units = ml/ cm²-s

Where: ΔP = Pressure accross membrane (psi)
      r = pore size radius (nm)
      n = number of pores per cm²
      μ = viscosity of liquid flowing through memb. (g/cm-s)
      L = membrane thickness (μm)

Theoretical Flux:

Sample	Sample #	ΔP (psi)	r (nm)	n (pores/ cm²)	μ g/cm-s	Tot. thick, L (0.0004 inch)	adjusted L (μm)	J (ml/ cm²-s)	k (theor) nm2
1;1:1 (	35	10	5.8	6.00E+11	0.0096	16	162.67	1.18E-04	2.67
1;1:1 (	36	10	5.8	6.00E+11	0.0096	18	183.00	1.05E-04	2.67
1;1:1 (	36	20	5.8	6.00E+11	0.0096	18	183.00	2.09E-04	2.67
1;0:1 (	39	10	5.8	6.00E+11	0.0096	17	172.83	1.11E-04	2.67
1;0:1	41	10	6.65	5.00E+11	0.0096	13	132.17	2.09E-04	3.84
1;0:1	41	20	6.65	5.00E+11	0.0096	13	132.17	4.17E-04	3.84
1;0:1	41	30	6.65	5.00E+11	0.0096	13	132.17	6.26E-04	3.84
1;0:1	43	10	6.65	5.00E+11	0.0096	13	132.17	2.09E-04	3.84
1;0:1	43	20	6.65	5.00E+11	0.0096	13	132.17	4.17E-04	3.84
1;0:1	43	30	6.65	5.00E+11	0.0096	13	132.17	6.26E-04	3.84
1;1:0.5	44	10	7.65	4.00E+11	0.0096	14.5	147.42	2.62E-04	5.38
1;0:4	46	10	5.25	8.00E+11	0.0096	22	223.67	7.66E-05	2.39
1;0:4	46	20	5.25	8.00E+11	0.0096	22	223.67	1.53E-04	2.39
1;0:4	46	30	5.25	8.00E+11	0.0096	22	223.67	2.30E-04	2.39
1;1:2	47	10	4.75	1.00E+12	0.0096	21	213.50	6.73E-05	2.00
1;0:2	48	10	5.15	8.00E+11	0.0096	19	193.17	8.22E-05	2.21
1;0:2	48	20	5.15	8.00E+11	0.0096	19	193.17	1.64E-04	2.21
1;0:2	48	30	5.15	8.00E+11	0.0096	19	193.17	2.47E-04	2.21
1;1:1	51	10	5.8	6.00E+11	0.0096	23.5	238.92	8.02E-05	2.67
1;1:1	51	20	5.8	6.00E+11	0.0096	23.5	238.92	1.60E-04	2.67
1;1:1	51	30	5.8	6.00E+11	0.0096	23.5	238.92	2.41E-04	2.67
1;1:2	52	10	4.75	1.00E+12	0.0096	21	213.50	6.73E-05	2.00
1;1:4 (	53	10	5.35	7.00E+11	0.0096	18	183.00	8.84E-05	2.25
1;1:4	53	20	5.35	7.00E+11	0.0096	18	183.00	1.77E-04	2.25
1;1:4	53	30	5.35	7.00E+11	0.0096	18	183.00	2.65E-04	2.25
1;1:0.5	54	10	7.65	4.00E+11	0.0096	23.5	238.92	1.62E-04	5.38
1;1:1	56	10	5.8	6.00E+11	0.0096	23	233.83	8.19E-05	2.67
1;1:1	56	20	5.8	6.00E+11	0.0096	23	233.83	1.64E-04	2.67
1;1:2	57	10	4.75	1.00E+12	0.0096	24	244.00	5.89E-05	2.00
1;1:4	58	10	5.35	7.00E+11	0.0096	18	183.00	8.84E-05	2.25
1;1:4	58	20	5.35	7.00E+11	0.0096	18	183.00	1.77E-04	2.25
1;1:4	58	30	5.35	7.00E+11	0.0096	18	183.00	2.65E-04	2.25
1;1:0.5	59	10	7.65	4.00E+11	0.0096	23	233.83	1.65E-04	5.38
1;1:0.5	59	20	7.65	4.00E+11	0.0096	23	233.83	3.31E-04	5.38
1;0:2	60	10	5.15	8.00E+11	0.0096	17	172.83	9.18E-05	2.21
1;0:2	60	20	5.15	8.00E+11	0.0096	17	172.83	1.84E-04	2.21
15nm P	61	10	11	1.50E+09	0.0096	0.75	7.63	8.12E-05	0.09
15nm P	61	20	11	1.50E+09	0.0096	0.75	7.63	1.62E-04	0.09
15nm P	61	30	11	1.50E+09	0.0096	0.75	7.63	2.44E-04	0.09
15nm P	62	10	11	1.50E+09	0.0096	0.75	7.63	8.12E-05	0.09
15nm P	62	20	11	1.50E+09	0.0096	0.75	7.63	1.62E-04	0.09
15nm P	62	30	11	1.50E+09	0.0096	0.75	7.63	2.44E-04	0.09

Theoretical Flux:

Sample	Sample	ΔP (psi)	r (nm)	n (pores/ cm²)		μ g/cm-s	Tot. thicl (0.0004	adjusted L (μm)	J (ml/ cm2-s)	k (theor) nm2
1;0:4 (3	63		10	5.25	8.00E+11	0.0096	23.5	238.92	7.18E-05	2.39
1;0:4 (3	63		20	5.25	8.00E+11	0.0096	23.5	238.92	1.44E-04	2.39
1;0:4 (3	63		30	5.25	8.00E+11	0.0096	23.5	238.92	2.15E-04	2.39
1;1:0 (3	67		10	6.9	5.00E+11	0.0096	14.5	147.42	2.17E-04	4.45
1;1:0 (3	67		20	6.9	5.00E+11	0.0096	14.5	147.42	4.34E-04	4.45
1;1:0 (3	67		30	6.9	5.00E+11	0.0096	14.5	147.42	6.51E-04	4.45
1;0:0.5	69		10	7.3	4.00E+11	0.0096	15.5	157.58	2.03E-04	4.46
1;0:0.5	69		20	7.3	4.00E+11	0.0096	15.5	157.58	4.07E-04	4.46
1;0:0.5	69		30	7.3	4.00E+11	0.0096	15.5	157.58	6.10E-04	4.46
1;0:2 (3	70		10	5.15	8.00E+11	0.0096	20	203.33	7.81E-05	2.21
1;0:2 (3	70		20	5.15	8.00E+11	0.0096	20	203.33	1.56E-04	2.21
1;0:2 (3	70		30	5.15	8.00E+11	0.0096	20	203.33	2.34E-04	2.21
1;0:0 pu	74		10	7.5	4.00E+11	0.0096	22.5	228.75	1.56E-04	4.97
1;0:0 pu	74		20	7.5	4.00E+11	0.0096	22.5	228.75	3.12E-04	4.97
1;0:0 pu	74		30	7.5	4.00E+11	0.0096	22.5	228.75	4.68E-04	4.97
1;0:4 (2	76		10	5.25	8.00E+11	0.0096	17.5	177.92	9.64E-05	2.39
1;0:4 (2	76		20	5.25	8.00E+11	0.0096	17.5	177.92	1.93E-04	2.39
0;0:1 pu	77		10	5.35	6.00E+11	0.0096	25	254.17	5.46E-05	1.93
0;0:1 pu	77		20	5.35	6.00E+11	0.0096	25	254.17	1.09E-04	1.93
0;0:1 pu	78		10	5.35	6.00E+11	0.0096	25	254.17	5.46E-05	1.93
0;0:1 pu	78		20	5.35	6.00E+11	0.0096	25	254.17	1.09E-04	1.93
0;0:1 pu	79		10	5.35	6.00E+11	0.0096	25	254.17	5.46E-05	1.93
0;0:1 pu	79		20	5.35	6.00E+11	0.0096	25	254.17	1.09E-04	1.93
0;0:1 pu	79		30	5.35	6.00E+11	0.0096	25	254.17	1.64E-04	1.93
1;0:0 pu	80		10	7.5	4.00E+11	0.0096	22.5	228.75	1.56E-04	4.97
1;0:0 pu	80		20	7.5	4.00E+11	0.0096	22.5	228.75	3.12E-04	4.97
1;0:0 pu	80		30	7.5	4.00E+11	0.0096	22.5	228.75	4.68E-04	4.97
1;1:1 (3	83		10	5.8	6.00E+11	0.0096	30	305.00	6.28E-05	2.67
1;1:1 (3	83		20	5.8	6.00E+11	0.0096	30	305.00	1.26E-04	2.67
1;1:0.5	86		10	7.65	4.00E+11	0.0096	23	233.83	1.65E-04	5.38
1;1:0.5	86		20	7.65	4.00E+11	0.0096	23	233.83	3.31E-04	5.38
1;1:0.5	86		30	7.65	4.00E+11	0.0096	23	233.83	4.96E-04	5.38
0;0:1 pu	87		10	5.35	6.00E+11	0.0096	25	254.17	5.46E-05	1.93
0;0:1 pu	87		20	5.35	6.00E+11	0.0096	25	254.17	1.09E-04	1.93
0;0:1 pu	87		30	5.35	6.00E+11	0.0096	25	254.17	1.64E-04	1.93
1;0:4 (2	89		10	5.25	8.00E+11	0.0096	16	162.67	1.05E-04	2.39
1;0:4 (2/	89		20	5.25	8.00E+11	0.0096	16	162.67	2.11E-04	2.39
1;0:0.5	90		10	7.3	4.00E+11	0.0096	15.5	157.58	2.03E-04	4.46
1;0:0.5	90		20	7.3	4.00E+11	0.0096	15.5	157.58	4.07E-04	4.46
1;0:0.5	90		30	7.3	4.00E+11	0.0096	15.5	157.58	6.10E-04	4.46
PCTE (1	93		10	11	1.50E+09	0.0096	0.75	7.63	8.12E-05	0.09
PCTE (1	93		20	11	1.50E+09	0.0096	0.75	7.63	1.62E-04	0.09
PCTE (1	93		30	11	1.50E+09	0.0096	0.75	7.63	2.44E-04	0.09
PCTE (1	94		10	11	1.50E+09	0.0096	0.75	7.63	8.12E-05	0.09
PCTE (1	94		20	11	1.50E+09	0.0096	0.75	7.63	1.62E-04	0.09
PCTE (1	94		30	11	1.50E+09	0.0096	0.75	7.63	2.44E-04	0.09
1;1:4 (3	96		10	5.35	7.00E+11	0.0096	18	183.00	8.84E-05	2.25
1;1:4 (3	96		20	5.35	7.00E+11	0.0096	18	183.00	1.77E-04	2.25
1;1:4 (3	96		30	5.35	7.00E+11	0.0096	18	183.00	2.65E-04	2.25
1;1:0.5	99		10	7.65	4.00E+11	0.0096	23	233.83	1.65E-04	5.38
1;1:0.5	99		20	7.65	4.00E+11	0.0096	23	233.83	3.31E-04	5.38
1;1:0.5	99		30	7.65	4.00E+11	0.0096	23	233.83	4.96E-04	5.38
0.02 μm	100		10	15	1.45E+10	0.0096		1.00	2.07E-02	2.88
0.02 μm	100		20	15	1.45E+10	0.0096		1.00	4.14E-02	2.88
0.02 μm	102		10	15	1.45E+10	0.0096		1.00	2.07E-02	2.88

Experimental Flux data:

Sample #	V (DI Water) (ml)	A (cm2)	t (sec.)	J (l/ m2-hr)	Exp Error %	# points used	k (exp.) nm2	k(theor)/ k(exp)
35	6.7	0.713	116388	2.91	4.95	2	1.83	1.46
36	10.2	0.599	90600	6.77	5.88	2	4.79	0.56
36	16.4	0.599	67020	14.71	4.87	4	5.21	0.51
39	3.8	0.502	169560	1.61	4.17	3	1.07	2.48
41	8	0.691	254988	1.63	17.13	6	0.84	4.60
41	14	0.691	210540	3.46	12.44	5	0.89	4.34
41	5.6	0.691	57240	5.10	13.83	3	0.87	4.42
41	10.05	0.691	323700	1.62	10.09	6	0.83	4.65
41	12.8	0.691	201600	3.31	6.37	6	0.85	4.54
41	23.5	0.691	245940	4.98	3.48	5	0.85	4.53
43	5.9	0.535	239832	1.66	34.13	6	0.85	4.54
43	5.45	0.535	115800	3.17	10.65	3	0.81	4.74
43	8.55	0.535	123780	4.65	9.79	4	0.79	4.85
44	5.2	0.546	239832	1.43	34.42	6	0.82	6.60
46	3.9	0.491	209844	1.36	112.55	5	1.18	2.02
46	1.8	0.491	115800	1.14	26.14	3	0.49	4.84
46	14.6	0.491	123780	8.65	1.86	4	2.49	0.96
47	2.2	0.836	239832	0.39	40.69	6	0.33	6.13
48	0.85	0.502	363132	0.17	108.15	8	0.13	17.62
48	2	0.502	173160	0.83	35.60	5	0.31	7.14
48	1.95	0.502	125340	1.12	17.20	3	0.28	7.95
51	5.6	0.970	331992	0.63	17.57	7	0.58	4.61
51	4.8	0.970	146458.8	1.22	4.69	4	0.56	4.74
51	6.25	0.970	125340	1.85	5.98	3	0.57	4.68
52	2.05	0.836	331992	0.27	43.20	7	0.22	9.11
53	0.6	0.447	192168	0.25	49.92	4	0.18	12.64
53	1.65	0.447	146458.8	0.91	11.42	4	0.32	7.01
53	2.75	0.447	125340	1.77	7.35	3	0.42	5.40
54	8.15	0.713	276600	1.49	20.15	6	1.38	3.91
56	3.95	0.970	258600	0.57	15.06	4	0.51	5.20
56	7.25	0.970	201600	1.33	13.54	6	0.60	4.42
57	3.3	0.836	243840	0.58	9.91	5	0.55	3.64
58	1.8	0.393	323700	0.51	77.26	6	0.36	6.24
58	1.9	0.393	201600	0.86	13.62	6	0.31	7.37
58	4.15	0.393	245940	1.55	15.32	5	0.36	6.17
59	7.65	0.819	243840	1.38	6.64	5	1.25	4.32
59	10.2	0.819	128350.8	3.49	19.93	5	1.58	3.41
60	2.3	0.546	188413.2	0.81	34.44	4	0.54	4.10
60	2.75	0.546	175078.8	1.04	18.46	5	0.35	6.38
61	12.2	0.713	168552	3.66	7.28	3	0.11	0.80
61	10	0.713	146458.8	3.45	8.90	4	0.05	1.70
61	8.6	0.713	125340	3.47	2.42	3	0.03	2.53
62	7.6	0.684	258613.2	1.55	7.39	4	0.05	1.89
62	7.2	0.684	175078.8	2.16	8.30	5	0.03	2.70
62	11.7	0.684	245940	2.50	7.80	5	0.02	3.50
63	0.95	0.342741	243840	0.409218	48.95	5	0.3781	6.31256556
63	1.25	0.342741	159780	0.8217197	22.27	6	0.3796	6.28734015
63	1.65	0.342741	173760	0.9974021	11.74	5	0.3072	7.76983284
67	3.75	0.362903	258598.8	1.4385246	48.74	6	0.8202	5.42728221
67	3.8	0.362903	148080	2.5456561	2.68	5	0.7257	6.1338051
67	7.65	0.362903	173760	4.367412	2.95	5	0.83	5.36286414

Experimental Flux data:							
Sample #	V (DI Water) (ml)	A (cm2)	t (sec.)	J (l/ m2-hr)	Exp Error %	# points used	k (exp.) nm²	k(theor)/ k(exp)
69	2.5	0.6300	175920	0.812109	3.8	5	0.49	9.01
69	4.72	0.6300	162120	1.663777	2.05	5	0.51	8.80
69	5.72	0.6300	136800	2.389459	6.93	5	0.49	9.19
70	1.47	0.4849	175920	0.620406	7.54	5	0.49	4.53
70	2.88	0.4849	162120	1.318954	1.93	5	0.52	4.26
70	3.49	0.4849	136800	1.894145	8.19	5	0.50	4.45
74	0.255	0.0397	143520	1.611671	13.2	5	1.43	3.49
74	0.6	0.0397	162120	3.357093	7.5	5	1.49	3.35
74	0.42	0.0397	67440	5.649116	6.4	3	1.67	2.98
76	1.78	0.5867	275040	0.397115	6.28	6	0.27	8.74
76	2.18	0.5867	162120	0.82511	4.31	5	0.28	8.41
77	1.8	0.4536	268452	0.532119	57.04	3	0.52	3.69
77	6.74	0.4536	164520	3.2512	34.16	5	1.60	1.21
78	1.34	0.3087	432792	0.361093	7.79	7	0.35	5.44
78	1.12	0.3087	164520	0.79395	3.83	5	0.39	4.95
79	0.9	0.3477	259308	0.359339	68.97	3	0.35	5.47
79	1.09	0.3477	164520	0.68594	10.01	5	0.34	5.73
79	1.54	0.3477	142800	1.11653	1.41	5	0.37	5.28
80	0.6	0.0078	259308	10.66222	8.51	3	9.43	0.53
80	1.32	0.0078	194400	31.28889	12.61	6	13.84	0.36
80	0.94	0.0078	142800	30.33277	19.59	2	8.95	0.56
83	3.23	1.2097	255240	0.376606	5.32	4	0.44	6.00
83	1.1	1.2097	33480	0.97778	3.08	2	0.58	4.62
86	7.64	0.6983	312900	1.258764	4.27	5	1.14	4.73
86	9.75	0.6983	190800	2.634407	6.5	6	1.19	4.52
86	14	0.6983	169680	4.253574	6.6	6	1.28	4.20
87	1.05	0.2977	312900	0.405808	16.03	5	0.40	4.84
87	1.46	0.2977	190800	0.925362	5.5	5	0.45	4.24
87	1.62	0.2977	136800	1.432077	6.1	4	0.47	4.11
89	1.45	0.4700	312900	0.354927	8.94	5	0.22	10.69
89	6.4	0.4700	190800	2.569081	45.33	6	0.81	2.95
90	4.47	0.6983	312900	0.736476	17.24	5	0.45	9.94
90	5.93	0.6983	190800	1.60226	13.34	6	0.49	9.14
90	7.56	0.6983	151680	2.569508	16.07	5	0.52	8.55
93	51.8	0.6983	170280	15.68277	19.28	6	0.46	0.19
93	21.66	0.6983	108000	10.3393	47.78	5	0.15	0.57
93	10.98	0.6983	87300	6.484025	23.94	5	0.06	1.35
94	7.07	0.7126	155040	2.303872	11.45	5	0.07	1.27
94	9.04	0.7126	108000	4.228899	21.89	5	0.06	1.38
94	10.66	0.7126	87300	6.169154	8.93	5	0.06	1.42
96	1.04	0.5685	154740	0.42561	5.24	5	0.30	7.48
96	1.71	0.5685	108000	1.00266	5.28	5	0.35	6.35
96	2.04	0.5685	87300	1.479781	5.26	5	0.35	6.45
99	2.94	0.6556	140040	1.152896	4.41	5	1.04	5.16
99	4.82	0.6556	108000	2.450858	17.95	5	1.11	4.86
99	6.07	0.6556	87300	3.818293	8.06	5	1.15	4.67
100	200	17.3494	541	767.0959	4.53	4	2.97	0.97
100	200	17.3494	283.3333	1464.702	5.13	4	2.83	1.02
102	200	17.3494	537	772.8098	8.85	4	2.99	0.96

IMAGE EVALUATION
TEST TARGET (QA-3)

1.0
1.1
1.25
1.4
1.6
1.8
2.0
2.2
2.5
2.8
3.2
3.6
4.0
4.5
5.0

1.0
1.1
1.25
1.4
1.6
1.8
2.0
2.2
2.5
2.8
3.2
3.6
4.0
4.5
5.0

1.0
1.1
1.25
1.4
1.6
1.8
2.0
2.2
2.5
2.8
3.2
3.6
4.0
4.5
5.0

1.0
1.1
1.25
1.4
1.6
1.8
2.0
2.2
2.5
2.8
3.2
3.6
4.0
4.5
5.0

1.0
1.1
1.25
1.4
1.6
1.8
2.0
2.2
2.5
2.8
3.2
3.6
4.0
4.5
5.0

|◄———————— 150mm ————————►|

|◄———————— 6″ ————————►|
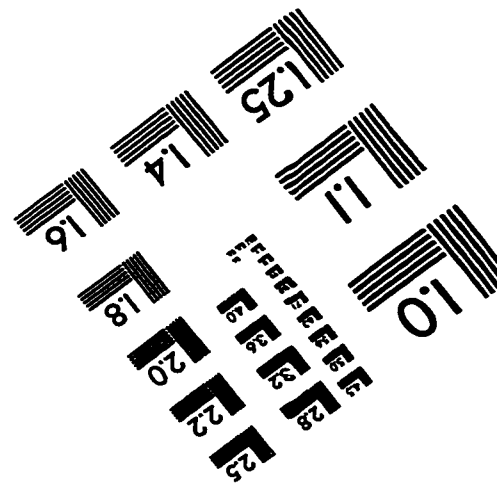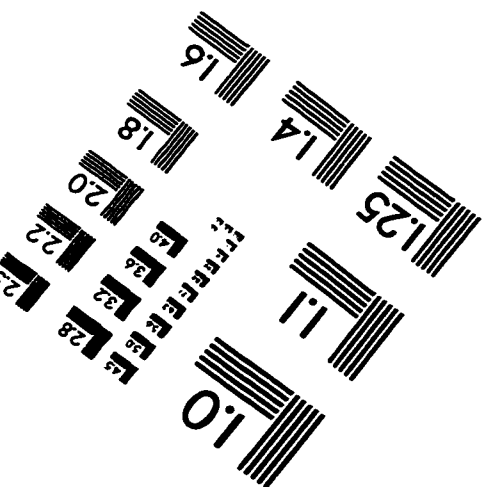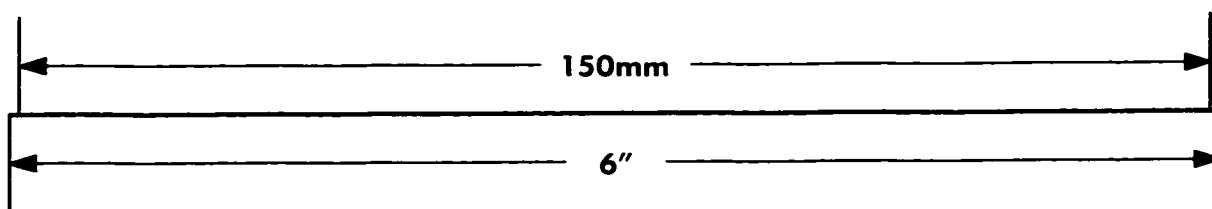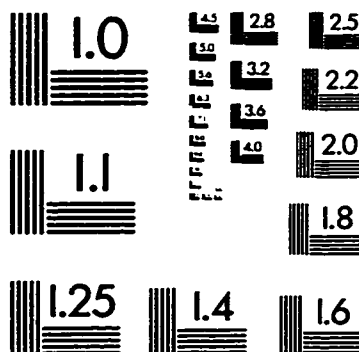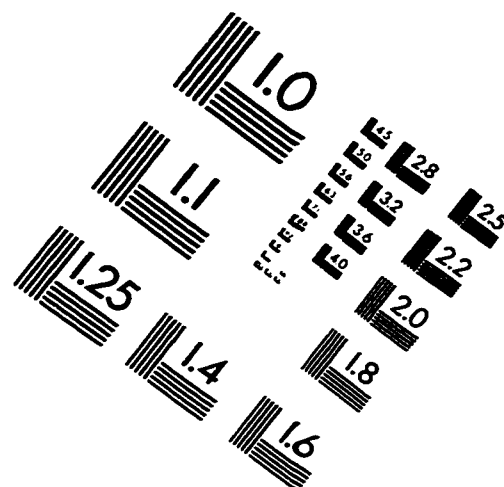
APPLIED IMAGE . Inc
1653 East Main Street
Rochester, NY 14609 USA
Phone: 716/482-0300
Fax: 716/288-5989